MODELLING OF SEDIMENTATION DYNAMICS IN AN UNDERGROUND CANAL IN SOUTHWEST KANO IRRIGATION SCHEME - KENYA

Henry Ochieng Ochiere

A thesis submitted to the Graduate School in partial fulfilment for the requirement of the Master of Science Degree in Agricultural Engineering of Egerton University

EGERTON UNIVERSITY

October, 2016

DECLARATION AND RECOMMENDATION

DECLARATION

I solemnly declare that this thesis my original work and that it has not been presented before in any other Institution known to me for the award of any Degree or Diploma.

Signature: ……. Date: ……

Henry Ochieng Ochiere

BM11/2428/09

RECOMMENDATION

This thesis is the candidate's original work and has been prepared with our guidance and assistance as supervisors. It is submitted for examination with our approval as official University Supervisors.

Signature: ……. Date: ……

Prof. Japheth O. Onyando

Department of Agricultural Engineering,

Egerton University.

Signature: ……. Date: ……

Dr. David N. Kamau

Department of Civil and Environmental Engineering,

Egerton University.

DEDICATION

This work is dedicated to my wife and children to reassure them that, with God's grace and hard work, our abilities dwarf all mountains. Special dedication is owed to my late son, Hillary, who inspired me by his attitude of "things being easy".

ACKNOWLEDGEMENTS

I would like to thank God for giving me wisdom and strength to carry out this research. Egerton University played a pivotal role in admitting me for the course geared to improving irrigation systems in Kenya. I owe my appreciation to Kenya's Ministry of Water and Irrigation for granting me study leave and sponsoring my study. I am grateful to my supervisors, Prof. Japheth O. Onyando and Dr. David N. Kamau for the effort they put in consistently providing me with academic support and guidance throughout my research and thesis writing. Thanks also go to Prof. G. M. N. Ngunjiri, Prof. B. M. Mutua, Prof. D. M. Nyaanga for having equipped me with relevant skills and the necessary knowledge for carrying out the research.

I am indebted to Faculty of Engineering and Technology Staff and fellow students for having facilitated my soil analysis and being resourceful during research proposal and thesis presentations. Finally, I would like to thank Water Resource Management Authority office in Kakamega for providing personnel and equipment used for hydraulic measurements.

ABSTRACT

The design of an irrigation canal is intended to ensure that water is conveyed with minimal erosion and sedimentation. The underground canal in Southwest Kano Irrigation scheme was designed to meet these conditions but over time it has been silted up to the extent that its conveyance capacity has significantly dropped. The sediment control structure at the inlet can only prevent bedload, consisting of large sediments, from entering the canal but cannot prevent entry of fine suspended particles. Deposition of a particle a canal starts when the vertical components of the bed-level turbulence are less than the fall velocity of a particle. Sediment transport capacity depends on the magnitude of these vertical components as they oppose the settling process in which the weight of the particle causes it to descend. This study was based on modelling sediment transport within the underground canal in Southwest Kano Irrigation Scheme using Hydrologic Engineering Centre – River Analysis System (HEC-RAS) model. This model includes Ackers-White sediment transport equation, which was used to estimate sediment transport capacity, discharge and deposition. The conceptual and physical parameters required in the HEC-RAS model were determined through calibration and direct measurement in the field respectively. The conceptual parameters for the Ackers-White equation were optimised using algorithms in the HEC-RAS model. The model was calibrated based on the current operational conditions of the canal followed by simulation using the calibrated model to determine the sediment discharge and deposition rates at different levels of flow in the canal. The simulation results showed that the calibrated HEC-RAS Model could predict the sediment sizes which were deposited at specific sections of the canal at different flow rates. Deposition occurred since the prevailing flowrates were below the critical velocity. Grain classes 8, 9, 10 and 11 should be screened from entering the canal, to ensure that sediment entering the canal is transported to the canal outlet without deposition. The scheme needs to improve on sediment control management to minimise deposition.

TABLE OF CONTENTS

DECLARATION AND RECOMMENDATION ..... **ii**

COPYRIGHT ..... **iii**

DEDICATION ..... **iv**

ACKNOWLEDGEMENTS ..... **v**

ABSTRACT ..... **vi**

LIST OF TABLES ..... **x**

LIST OF FIGURES ..... **xi**

LIST OF APPENDICES ..... **xii**

LIST OF ABBREVIATIONS ..... **xiv**

CHAPTER ONE **1**

INTRODUCTION **1**

1.1 Background 1

1.2 Statement of the Problem 2

1.3 Justification 3

1.4 Objectives 4

1.4.1 Specific objectives 4

1.4.2 Research Questions 4

1.5 Scope and Limitations 4

CHAPTER TWO **6**

LITERATURE REVIEW **6**

2.1 Canal Sedimentation 6

2.2 Natural Channel Hydraulics and Sediment Transport 7

2.3 Sediment Sampling in Rivers and Canals 9

2.4 Canal Flow Velocity and Discharge 10

2.5 Fall Velocity 11

2.6 Erosion and Sediment Transport Equations 13
2.7 Sediment Transport Models 17
2.8 Determination of Sediment Deposition Rate using HEC-RAS Model 18
2.9 Calibration and Validation of HEC-RAS Model 21
CHAPTER THREE 24
METHODOLOGY 24
3.1 Study Area 24
3.2 Primary Data Collection 25
3.2.1 Bed Material Sampling and Gradation 26
3.2.2 Determination of Flow Velocity in the Canal 28
3.3 Determination of Critical Velocity for No Deposition 30
3.4 Calibration and Validation of HEC-RAS Model Based on Current Flow Conditions 31
3.4.1 Determination of Input Parameters into HEC – RAS model 31
3.4.2 Determination of Sediment Deposition Rate using HEC-RAS Model 33
3.4.3 Manual Computation of Sediment Deposition Rate 33
3.4.4 Calibration of HEC-RAS Model for Sediment Deposition Rate 34
3.5 Simulation Using HEC-RAS Model for 0.25, 0.50, 0.75, and Full Flow Scenarios 34
3.6 Sensitivity Analysis 36
CHAPTER FOUR 37
RESULTS AND DISCUSSION 37
4.1 Determination of Critical Velocity for No Deposition 37
4.2 Calibration and Validation of HEC-RAS Model Based on Current Flow Conditions 39
4.2.1 Calibration and Validation of Mannings n 39
4.2.2 Calibration and Validation of Coefficients (A and C) and Exponent (n) 46
4.3 Simulation Using HEC-RAS Model for 0.25, 0.50, 0.75 and Full Flow Scenarios 51
CHAPTER FIVE 58
CONCLUSION AND RECOMMENDATION 58

5.1 Conclusion 58

5.2 Recommendation 59

REFERENCES 60

LIST OF TABLES

Table 2. 1: Range of input values used for development of Ackers-White equation 7
Table 2. 2: Maddock's classification for estimation of the bed load..... 10
Table 2. 3: Commonly used sediment transport equations based on sediment size 14
Table 2. 4: Coefficients for the 1973 and 1990 versions of the Ackers-White formula..... 17
Table 2. 5: Maximum and minimum values of coefficients 17
Table 2. 6: HEC-RAS input parameters 19
Table 3. 1: Equipment used for data collection 26
Table 3. 2: Sampled particle size distribution..... 27
Table 3. 3: Measured discharge using Seba F1 current meter 29
Table 3. 4: HEC-RAS input parameters and how they were determined 31
Table 4. 1: Calibration and Validation of Manning's n 41
Table 4. 2: Calibration and validation results for water surface levels..... 43
Table 4. 3: Calibration and validation results for cumulative sediment discharge 48
Table 4. 4: Discharge values for different flow scenarios 52
Table 4. 5: Cumulative sediment discharge for different discharge scenarios 53
Table 4. 6: Grain size classification..... 56

LIST OF FIGURES

Figure 2. 1: Hjulstrom Diagram 12
Figure 3. 1: Nyando Basin 24
Figure 3. 2: Underground Intake Canal 25
Figure 3. 3: Sketch of Southwest Kano underground canal 27
Figure 3. 4: Sketch of Southwest Kano underground canal cross section 28
Figure 3. 5: Canal cross section 35
Figure 4. 1: Critical velocity from Hjulstrom Diagram 37
Figure 4. 2: Sediment rating curve 39
Figure 4. 3: Calibration curve for profile PF2 44
Figure 4. 4: Calibration curve for profile PF3 44
Figure 4. 5: Calibration curve for profile PF4 45
Figure 4. 6: Validation curve for profile PF1 45
Figure 4. 7: Validation curve for profile PF5 46
Figure 4. 8: Calibration cumulative sediment discharge curve (Mh1) 49
Figure 4. 9: Validation cumulative sediment discharge curve (Mh3) 50
Figure 4. 10: Validation cumulative sediment discharge curve (Mh5) 50
Figure 4. 11: Simulated sediment discharge at inlet and outlet. 55

LIST OF APPENDICES

Appendix 1: Grain size Classification (American Geophysical Union) 65
Appendix 2: HEC-RAS calibration water profile output for profile PF2 66
Appendix 3: HEC-RAS calibration water profile output for profile PF3 67
Appendix 4: HEC-RAS calibration water profile output for profile PF4 68
Appendix 5: HEC-RAS validation water profile output for profile PF1 69
Appendix 6: HEC-RAS validation water profile output for profile PF5 70
Appendix 7: Table of simulated transport capacity for discharge of 0.366 m^3/s at Manhole 1 (Mh1) 71
Appendix 8: Graph of simulated transport capacity for discharge of 0.366 m^3/s at Manhole 1 (Mh1) 72
Appendix 9: Table of simulated transport capacity for discharge of 0.366 m^3/s at Manhole 3 (Mh3) 73
Appendix 10: Graph of simulated transport capacity for discharge of 0.366 m^3/s at Manhole 3 (Mh3) 74
Appendix 11: Table of simulated transport capacity for discharge of 0.366 m3/s at Manhole 5 (Mh5) 75
Appendix 12: Graph of simulated transport capacity for discharge of 0.366 m3/s at Manhole 5 (Mh5) 76
Appendix 13: Table of simulated transport capacity for discharge of 1.337 m3/s at Manhole 1 (Mh1) 77
Appendix 14: Graph of simulated transport capacity for discharge of 1.337 m3/s at Manhole 1 (Mh1) 78
Appendix 15: Table of simulated transport capacity for discharge of 1.337 m3/s at Manhole 3 (Mh3) 79
Appendix 16: Graph of simulated transport capacity for discharge of 1.337 m3/s at Manhole 3 (Mh3) 80
Appendix 17: Table of simulated transport capacity for discharge of 1.337 m3/s at Manhole 5 (Mh5) 81
Appendix 18: Graph of simulated transport capacity for discharge of 1.337 m3/s at Manhole 5 (Mh5) 82

Appendix 19: Table of simulated transport capacity for discharge of 2.438 m3/s at Manhole 1 (Mh1) 83
Appendix 20: Graph of simulated transport capacity for discharge of 2.438 m3/s at Manhole 1 (Mh1) 84
Appendix 21: Table of simulated transport capacity for discharge of 2.438 m3/s at Manhole 3 (Mh3) 85
Appendix 22: Graph of simulated transport capacity for discharge of 2.438 m3/s at Manhole 3 (Mh3) 86
Appendix 23: Table of simulated transport capacity for discharge of 2.438 m3/s at Manhole 5 (Mh5) 87
Appendix 24: Graph of simulated transport capacity for discharge of 2.438 m3/s at Manhole 5 (Mh5) 88
Appendix 25: Table of simulated transport capacity for discharge of 2.674 m3/s at Manhole 1 (Mh1) 89
Appendix 26: Graph of simulated transport capacity for discharge of 2.674 m3/s at Manhole 1 (Mh1) 90
Appendix 27: Table of simulated transport capacity for discharge of 2.674 m3/s at Manhole 3 (Mh3) 91
Appendix 28: Graph of simulated transport capacity for discharge of 2.674 m3/s at Manhole 3 (Mh3) 92
Appendix 29: Table of simulated transport capacity for discharge of 2.674 m3/s at Manhole 5 (Mh5) 93
Appendix 30: Graph of simulated transport capacity for discharge of 2.674 m3/s at Manhole 5 (Mh5) 94
Appendix 31: Data Collected 95
Appendix 32: List of publications 97

LIST OF ABBREVIATIONS

ASCE	- American Society of Civil Engineers
Crit PF	- Critical Velocity Profile
EG PF	- Energy Gradient Profile
FAO	- Food and Agriculture Organisation
GSTARS	- Generalised Sediment Transport Model for Alluvial Rivers and Reservoirs
HEC-RAS	- Hydrologic Engineering Centres - River Analysis System
IAH	- International Association of Hydrogeologists
Mh	- Manhole of width 1.5m across underground canal
MOWI	- Ministry of Water and Irrigation
OWS PF	- Observed Water Surface Profile
PF	- Profile
PPM	- Parts per Million
SRH-Capacity	- Sedimentation and River Hydraulic-Capacity
SWAT	- Soil and Water Assessment Tool
US	-United States
USA	-United States of America
W	-Water width across the channel cross section
WS PF	- Water Surface Profile

CHAPTER ONE
INTRODUCTION

1.1 Background

All rivers and canals conveying water contain eroded sediments. Increase of soil erosion due to catchment degradation especially in developing countries has resulted into increased siltation problems in rivers as reported by Onyando *et al.* (2004). Studies by McCully (1996) consider a river or canal, as a body of flowing sediments as much as one of flowing water. When the velocity of water in the canal is below the fall velocity of a given sediment size, the sediment would be deposited. As the sediments accumulate in the canal, the canal gradually loses its ability to transport water. Such canals lose water conveyance capacity due to sedimentation although the rate at which this happens varies widely. Sometimes the rate of sedimentation is higher than the rate at which revenue required for maintenance of the canal is remitted by the farmers. Sedimentation problems therefore is an impediment to crop production. Canal sedimentation is the most serious technical problem facing irrigation systems (Depeweg and Mendez, 2006).

The proportion of sediments entering a diversion canal depends on the sediment load in the river source. Transport capacity is compared to the sediment load to determine whether detachment or deposition will occur (Finkner *et al.,* 1989). Deposition occurs when the sediment transport capacity of flow is less than the sediment load carried by the flow. The sediment deposited in the canal can be flushed out only if the sediment transport capacity of the canal flow is increased. The sediments transported through flushing should be discharged at non-erosive velocity at the end of the canal.

The underground canal, which is the subject of this study, was constructed in Southwest Kano Irrigation Scheme to convey water to rice fields through gravity flow. The water is abstracted from river Nyando through a 200-meter long bypass canal before eventually getting channelled through an underground circular concrete-lined canal of diameter 1500 mm and 730 m long. The rest of the main water intake system consists of open trapezoidal canal with earth lining. After irrigation water has been distributed to the rice fields, excess water is discharged into Miriu stream 2.5 km away. The farmers have been in charge of the scheme operation and maintenance since it was commissioned in 1993. The scheme has been operating on design discharge unless the main canal is not well maintained.

Southwest Kano intake canal was designed to convey irrigation water but due to continual siltation the capacity of the canal to convey water has been reduced. As mentioned earlier, deposition is a product of sediment load supplied from upstream. Not all sediment supplied from upstream is deposited in the canal section under study as evidenced by periodical dredging further downstream. Maintenance of the open canal downstream is usually carried out by a bucket excavator but the underground section, being enclosed, is not accessible by the excavator. The underground canal section though accessible by humans, use of human labour for manual removal of the deposited sediment has not been attempted since it is expensive. The small scale irrigation farmers in Southwest Kano Irrigation Scheme have been overwhelmed by the cost of maintaining the scheme in the recent past and they had to seek government intervention through "Kazi Kwa Vijana" Programme as reported by Ministry of Water and Irrigation Office, Nyando District (MOWI, 2009). Farmers' attempt to flush out sediment after manually removing sediment at inlet and outlet, results in flushing out a small fraction of the deposits as was observed by the researcher. This maintenance strategy is not effective since the original canal's design discharge capacity is not restored. It was therefore necessary to further understand the dynamics of sedimentation in the underground canal.

Design of most irrigation canals are based on flow regime principle. The South West Kano Irrigation Scheme was designed on this same principle. Ayibotele and Tuffour-Darko, (1979) found out that information on long-term sediment load, concentration and particle size distribution is important in the design of canals, and in the evaluation of quality of water. Therefore, study on sediment transport dynamics along the underground canal in Southwest Kano Irrigation Scheme is important for planning and management of the scheme hence the essence of this study.

1.2 Statement of the Problem

Southwest Kano underground intake canal is increasingly getting silted. This issue has been cited by studies done by Ong and Orego (2002), in which the scholars recommended that the sedimentation problem could be addressed by managing the sediment source, the Nyando Basin. Since then, no documented study has provided as a viable solution. It is important to identify which sediment sizes contribute to siltation and the nature of sedimentation dynamics involved so that efforts could be concentrated on selective elimination of these sediments from the canal flow. Even after flushing operations, there remains a sediment depth of up to 700 mm towards the outlet end

of the canal, as witnessed by the researcher. The problem is aggravated by the fact that desilting the underground section of the canal is extremely technical and expensive to the farmers. After maintenance, it takes just a few storms to build up the sediment depth upstream of the inlet weir to level up with the weir crest thereby enabling bed load entry into the underground canal. Therefore, intake is frequently desilted to avoid this scenario. The farmers have been constrained in terms of reduced water supply and rising cost of maintenance thus reducing the profit margin of their produce.

Sedimentation reduces the underground canal's capacity and efficiency to convey water for irrigation. This could be due to several reasons which include water flow velocity being inadequate to enable transport of total sediment load through the canal. Inflow from canal headworks being higher sediment load than the canal transport capacity. Continued deposition eventually modifies the canal bedslope, enhances further deposition and may block the canal. There is increased amount of sediments getting into the canal from the river at the inlet that cannot be conveyed to the outlet without deposition. This is because of the increased sediment load in the river caused by catchment degradation upstream. The increased sediment load into the canal results in increased deposition within the canal and hence reduces the canal water discharge capacity. The water distribution has been affected and canal maintenance costs increased as a result.

1.3 Justification

Sediment accumulation in the underground canal has reduced the canal's water conveyance capacity. The study is intended to identify and quantify the sediments to be screened off from entering the underground canal so that deposition may be reduced. The quantification is done in such a way that the sediments with potential for deposition would be screened off and those that flow in would mainly be the suspended ones which are carried through to the outlet.

The flow in the canal is subjected to frictional resistance and change of slope which is likely to cause reduction in flow velocity, transport capacity and eventual deposition even if the transport capacity at the inlet is higher than the sediment load. The management practice is that the farmers are to wait until the canal is substantially blocked before they could undertake desiltation. This practice has a higher potential for economic losses as the crops might be water stressed during

desiltation especially when it had to be done during on-season. A systematic strategy is inevitable as envisaged to be developed from the outcome of this study for the canal to be optimally utilised.

A priori determination of sediments to be screened off would enable economic selection of screening materials and reduce the cost and frequency of desiltation as and when this occurs. Essentially this would enable the management of the canal to be more effective and achieve timely delivery of water to the rice fields.

Analysis of sedimentation dynamics enables determination of canal discharge which results in minimal siltation. This will enable further improvement of the structural design of the canal to be precisely determined for effective conveyance of water.

1.4 Objectives

The broad objective of the study was to model sediment transport and deposition dynamics within Southwest Kano underground intake canal to improve effectiveness of the canal in conveying water.

1.4.1 Specific objectives

(i) Determine the flow velocity at which no deposition occurs in the canal.

(ii) Calibrate the HEC-RAS (Hydrologic Engineering Centre - River Analysis System), sediment transport simulation model for estimating sediment flow dynamics.

(iii) Simulate sediment transport in the canal using the HEC-RAS model under varied discharge conditions for effective screen selection.

1.4.2 Research Questions

(i) At what flow velocities does the canal siltation occur?

(ii) Can HEC-RAS model predict sediment transport in the canal?

(iii) What is the sediment load which can be carried through the canal without deposition?

1.5 Scope and Limitations

(i) The area of study was limited to the 730 m long underground canal section where the deposition in the canal is critical.

(ii) Data collection was done for a period of one month during peak flows and low flows in the year.

The following assumptions have been made in order to accomplish the study

(i) Only suspended particles are allowed into the canal.

(ii) The suspended sediments are incoherent or non-cohesive.

(iii) There is continuous steady flow in the canal.

(iv) The velocity of suspended particles is equal to the water flow velocity.

CHAPTER TWO
LITERATURE REVIEW

2.1 Canal Sedimentation

Total sediment load is transported by running water in different ways; namely dissolved load, wash load, suspended load, saltation load and bed load. The different phases of sediment transportation generally occur simultaneously in a stream, and there can be no sharp line of demarcation between them. However, total sediment load is usually divided into two categories, namely, suspended load and bed load. Studies by Rijn (2007) stated that suspended load is composed of fine particles and is predominantly a wash load; it is almost continually in suspension and is transported rapidly through the stream system. Bed load may be further divided into contact load and saltation load: the former slides or rolls, whereas the latter bounces and hopes along the bed (Yang and Simoes, 2002). This is because fall velocity of bed load is below the prevailing stream flow velocity, while for particles under saltation the flow velocity is more or less equal to the particle fall velocity. The size and concentration of sediment in a flowing stream generally increases from surface to bed, but also varies transversely in a river section due to gradual decrease of flow velocity. The magnitude of variation depends on the size and shape of the cross section, the stage of flow, and other stream characteristics. In turbulent flow, the direction of the current at a given point changes rapidly and haphazardly. Raju and Kothyari (2004) found out that the presence of suspended sediments in a flow may increase or decrease resistance to flow depending on the nature of canal boundary. The resistance

Bed load sediment concentration in the water entering a canal is usually higher than the concentration in the parent river. This is due to secondary currents generated at the offtake. The extent of this phenomenon depends on the orientation, location and structure of the intake works (Lawrence, 1986). Findings by Depeweg and Mendez, (2002) indicated that sediment transport in irrigation canals is always under changing flow conditions unlike the assumption of uniform and steady flow condition, which forms the basis of canal design. They further recommended the Ackers-White and Brownlie sediment transport equations for computation of sediment transport under equilibrium conditions and a numerical solution of Galappatti's depth integrated model for non-equilibrium state computations. Ackers-White equation was developed under conditions expressed by parameters given in Table 2.1.

Table 2. 1: Range of input values used for development of Ackers-White equation

Function	Overall Particle diameter (mm)	Median particle diameter (mm)	Sediment specific gravity	Average channel velocity (m/s)	Channel depth (m)	Energy gradient	Channel width (m)	Water temperature (^{o}C)
Ackers-White	0.04 – 7.0	NA	1.0 – 2.7	0.021– 0.82	0.0031– 0.43	0.00006 – 0.037	0.07– 1.22	7.8 – 31.7

Source: Hydraulic Engineering Centre (2010).

The overall particle diameter is the size of the particle range for which the Ackers-White sediment transport equations are applicable. For this study the particle diameter was determined by using different sieves stacked in a vibrator, with the topmost sieve having the largest mesh followed by a comparatively smaller mesh; in that sequence. The sediment specific gravity is the ratio of average density of sediment to density of fresh water. This value is usually assumed to be 2.65 for sand and silt. Average channel velocity is the average velocity of water flowing in the channel. This value is measured at 0.6 times the depth of flow. Channel depth is the longest distance measured perpendicularly from the flow surface to the deepest point on the channel bed. Energy gradient is change in total energy per unit length of flow. The channel width is the width of the channel at the water surface. Water temperature is the average temperature of flowing water. These parameters are applicable in Ackers-White sediment transport equation for open canals and are suited for irrigation canals.

2.2 Natural Channel Hydraulics and Sediment Transport

A study of the processes involved in the movement of sediment within a river system is fundamental to understanding the form and behaviour of stream channels. Knowledge of natural channel hydraulics is necessary for understanding sediment transport and fluvial geomorphology (Chang, 1988). The characteristics of flow in river systems are the driving force for sediment movement and channel morphological transformations. River systems are characterized as open-channel flow systems, bounded by a free-surface. The shape of the free water surface must be established to allow the determination of hydraulic parameters needed for open-channel flow calculations. This water surface profile is often determined using an energy balance approach. Flow velocity, hydraulic radius, depth, roughness, sediment size, and other hydraulic parameters may then be used to predict the magnitude of sediment transport processes.

Assumptions are a necessary part of modelling natural channel flow systems since the natural channel properties are not homogeneous but vary with distance along the direction of flow. Uniform, gradually varied, and rapidly varied flow are common classifications for open channel flow regimes. The uniform flow assumption is valid in areas with constant physical properties along the flow path (Chang, 1988). Man-made or significantly altered river channels may reasonably meet this assumption, but uniform flow is not valid for natural river channels due to the constant variation in channel shape and composition. Uniform flow equations are, however, often applied to natural flow systems when the area simulated is an individual channel cross-section over whose length parameters can be said to remain constant.

Changes in flow properties must be considered with respect to distance and time. Systems are described as steady flow systems if physical properties can be said to remain constant over the time scale to which flow equations are being applied. Most natural channel flow systems are considered unsteady as discharge, velocity, and depth change over time. The assumption of steady or unsteady flow is important in establishing the flow routing methods and equations to be applied to a river system.

The classification of flow as laminar or turbulent is also important in determining the equations which are applicable for a given system. Laminar flow is characterized by a velocity profile that can be assumed to vary linearly with depth (Chang, 1988). Flow may be considered laminar when the Reynolds number, Re, is sufficiently small (Re < 11.6). Reynolds number is calculated as follows:

$$Re = {}^{\mathrm{v}z}/_{\psi} \tag{1}$$

where v is the velocity, z the distance from the boundary, and ψ the kinematic viscosity.

Flow adjacent to boundaries is considered to have three layers. The laminar sublayer is a thin layer in contact with the boundary surface. The transition layer encompasses the flow zone separated from the boundary layer only by the laminar region. This zone is characterized by Reynolds numbers between 5 and 70. The turbulent flow zone, most distant from the boundary layer, is characterized by Reynolds numbers greater than 70. This zone exhibits a greater flow resistance due to eddy formation and the velocity distribution with depth which is non-linear. The rough

boundary conditions of many natural channels have a roughness coefficient too great to allow the formation of a laminar sub layer.

The combination of increased washload supply and decreased channel slope creates an environment where the washload component of the total load becomes more dominant. The high supply and reduced transport capacity in streams allows fine sediments to accumulate through sedimentation on the bed. This build-up of particles then provides a steady supply of washload particles, even between runoff events.

2.3 Sediment Sampling in Rivers and Canals

The first stage of sediment sampling in a river or canal as illustrated by Signal *et al.* (1981) is the selection of a suitable sampling site. The site should satisfy the following criteria: The chosen sampling station should be in a straight reach of length at least 4 times the width of the channel, but not less than 150 m for uniform and steady flow; the chosen reach should be stable, thus neither silting nor scouring for steady flow; a normal section should be located in the middle of the selected reach; the station should not be adjacent to hydraulic structures where flow is not steady; and it should be accessible, and preferably located near a village or town to ease data collection. These conditions represent a nearly laminar flow which can give better measurement results and sites which are easily accessible can still be accessed and data read at short notice such as unexpected storm.

Different organizations have recommended different procedures and techniques for sampling. In the case of suspended sediment load or bed load, the latest instructions of the Central Board of Irrigation and Power, New Delhi, are that it should be measured only at three verticals or points, 1W/6, 3W/6 and 5W/6, respectively (Garde and Ranga, 2000)x.

Attempts have been made to estimate bed load based on more easily measured parameters but these methods are not widely used since there is still much debate on their accuracy and reliability (Hudson, 1994). However, a simple method, using suspended sediment concentration and texture of both suspended sediments and bed material, is shown in Table 2.2. Reliable bed load measurement is difficult to obtain because sampling devices affect the flow and bed load movement (Spillios, 1999). Measured bed load data appear to be random in nature and large

fluctuations are experienced during relatively stable hydraulic and supply conditions (Xiaoqing, 2003).

Table 2. 2: Maddock's classification for estimation of the bed load

Suspended sediment concentration (parts per million)	River bed material	Suspended elements texture	Bed load discharge expressed as % of suspended sediment discharge
less than 1000	sand	similar to the river bed	25-150
less than 1000	gravel, rocks, hard clay	low sand content	5-12
1000 - 7500	sand	similar to the river bed	10-35
1000 - 7500	gravel, rocks, hard clay	25% sand or less	5-12
more than 7500	sand	similar to the river bed	5-15
more than 7500	gravel, rocks, hard clay	25% sand or less	2-8

Source: Hudson, 1994.

The distribution of suspended sediment concentrations has been investigated for selected verticals in a number of canals and rivers at different discharges. It has been found that the mean value of suspended sediment concentration lies at 0.5 D in the case of rivers and at 0.54 D in the case of canals, where D is depth of flow in a vertical (Signal *et al.*, 1981). Therefore, average silt concentration may be determined from sampling at these depths rather than from many points along the whole vertical. The silt content reaches a maximum during floods, and it is these periods which are of most interest for sediment sampling. A sediment bottle sampler can be sufficiently used at 0.54D during periods of high and low flows in the canal.

2.4 Canal Flow Velocity and Discharge

Flow velocity is an important parameter to be considered while sampling suspended sediments. Flow velocity is not constant but varies with depth. It increases from zero at the invert of the canal to a maximum value close to the water surface. The velocity difference is due to the resistance to flow at the bottom and sides of the canal. In order to determine the value of flow, it can be directed through a measurement device and measured directly or measurement carried out indirectly through the use of appropriate measurements and mathematical models. Current meters provide a

translation of flow energy of moving water into a flow velocity and, if used correctly, can measure velocity accurately. For small canals, a current meter can be used to determine flow velocity at three different verticals at 1W/6, 3W/6 and 5W/6, where W is the water width across the channel section (see Figure 3.4). The depth of each flow measurement point is taken at 0.6 times the flow depth (Signal *et al.,* 1981) since this point represents mean velocity of flow.

The discharge, *Q,* can be determined using several methods but in consideration of the practical situation in the field and for the whole cross section to be accounted for, the mean-section method is preferred due to differences in computed discharge components and uncertainty components are almost always negligible (Coz *et al.,* 2012). The velocities(v_{i-1} and v_i) and depths (d_{i-1} and d_i) of each successive verticals are averaged and their products multiplied by the distance between the segments to get discharge.

$$Q = \sum_{i=1}^{n} q_i = \sum_{i=1}^{n} \left(\frac{v_{i-1}+v_i}{2}\right)\left(\frac{d_{i-1}+d_i}{2}\right)(b_i - b_{i-1}) \quad (2)$$

where b_i = horizontal distance of the measurement vertical *i* from the bank of canal and there being *n* measurement verticals.

2.5 Fall Velocity

This is the velocity of flow at which sedimentation starts. If the flow velocity is more than fall velocity, transportation of suspended particles occurs but if it falls below fall velocity deposition occurs. Therefore, for no deposition to occur, fall velocities of sediments deposited at the bed of a canal must be below the prevailing flow velocities. Hjulstrom (1935) diagram (named after Swedish geographer, Filip Hjulstrom) in Figure 2.1 shows the relationship between grain size, erosion, transportation and deposition of various grain sizes (Morgan, 1986). The minimum critical velocity necessary for erosion, transportation, and deposition for each particle can be derived from this diagram. Given the stream flow velocity, it is possible to determine particle sizes likely to settle at the stream bed, since bed formation is dependent on fall velocity.

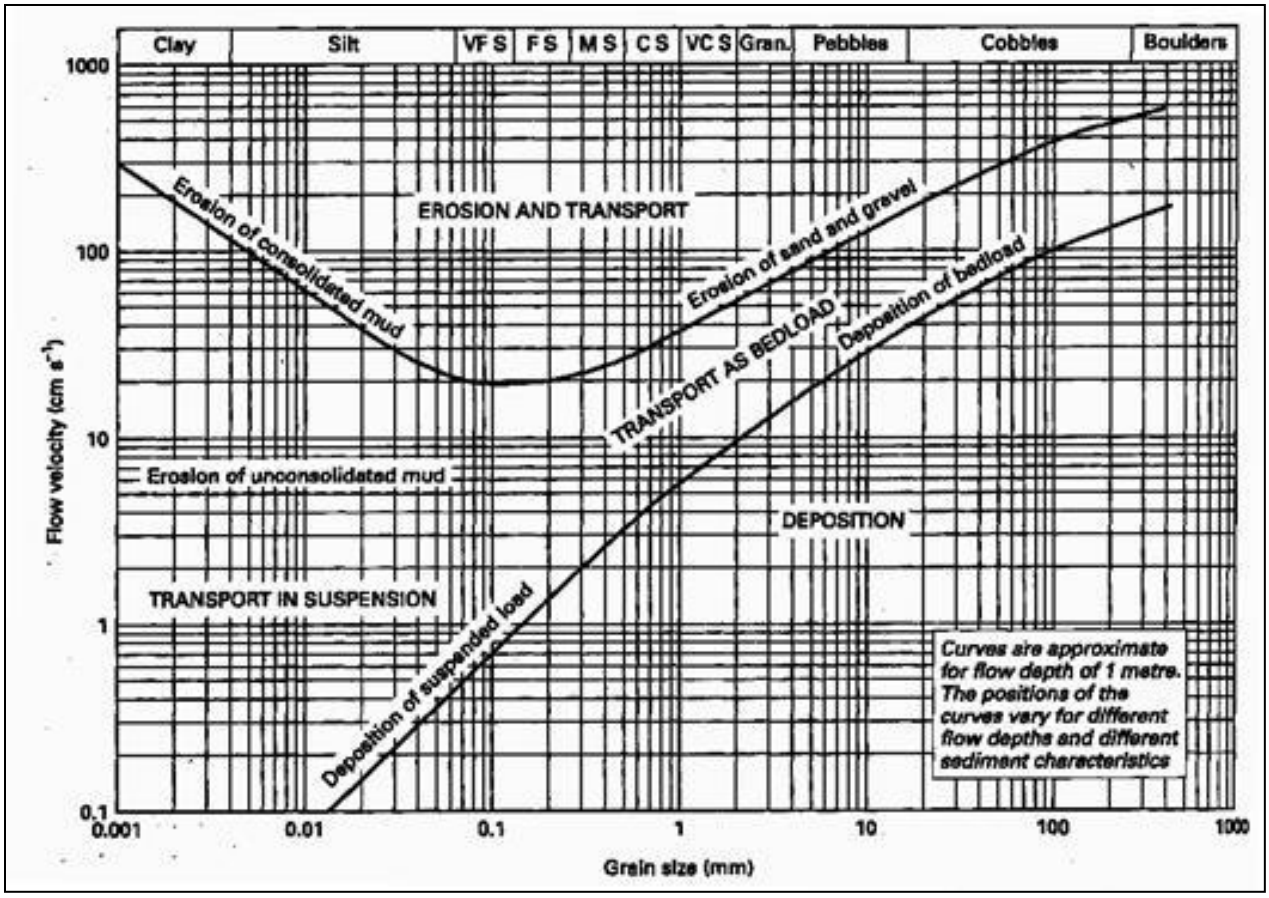

Figure 2. 1: Hjulstrom Diagram

Other studies conducted by Gerard Kennedy, concluded that the silt supporting power in a channel cross section is mainly dependent upon the generation of eddies from the bottom width of the channel section. Later studies done by Lacey (1930), on whose concept most canal designs are hinged, improved on Kennedy's equation and concluded that suspension of sediments transported by a flow is due to vertical components of turbulence generated not only on the channel bed but also on the sides of the channel (Garde and Ranga, 2000). Lacey Theory is used for design of stable channels. Lacey noted that the material forming the channel is also an important factor, referred to as silt factor (f) in the equation below:

$$f = 1.76\sqrt{d_m} \tag{3}$$

Where, d_m = diameter of particle size in mm

Velocity of flow for no deposition of this particle is given by:

$$V = \left\lfloor \frac{Qf^2}{140} \right\rfloor^{1/6} \quad (4)$$

where Q is discharge

For steady, continuous flow

$$Q = AV \quad (5)$$

where A is cross section of flow

Therefore

$$V = \left\lfloor \frac{Af^2}{140} \right\rfloor^{1/5} \quad (6)$$

2.6 Erosion and Sediment Transport Equations

A number of sediment transport relationships have been developed to predict the movement of sediment through watersheds (Wilcock 2001). These equations are dependent on particle size and are often combined in watershed and stream modelling algorithms to increase prediction accuracy and to improve the scope of software applicability.

Sediment transport equations are related to the way sediment is transported, namely equilibrium or non-equilibrium. The equilibrium condition means that the amount of sediment for a certain flow condition can be transported without deposition or erosion. The non-equilibrium condition describes how the flow conveys a certain amount of sediment as well as the erosion and deposition processes. For the flow conditions and sediment sizes usually encountered in irrigation canals, the sediment is transported both as bed load and suspended load. Therefore, any sediment transport predictor to be used should compute either the total transport load (bed load and suspended load) or the bed load and suspended load separately. Many methods have been proposed to predict sediment transport under a large range of flow conditions and sediment characteristics. (Wilcock 2001)

Due to the complexity of instream sediment transport processes no single equation has yet been developed to simulate the movement of particles from all size classes. The sediment transport capacity of individual size class must be analysed separately. This requirement demands watershed

and stream modelling algorithm to employ a suite of transport equations to simulate the movement of all sediment within the canal. A framework of concepts, including tractive force theory and stream power, help relate channel transport equations to one another. The choice of sediment transport equation depends on the sediment size range. Huang and Bountry (2009) suggested applicability of some of the most widely used methods to compute sediment transport based on sediment size as in Table 2.3.

Table 2. 3: Commonly used sediment transport equations based on sediment size

Sediment size		
Sand	**Gravel and sand**	**Gravel**
Engelund and Hansen (1972)	Parker (1990)	Wilcock and Crowe (2003)
Ackers and White (1973)	Wilcock and Crowe	Parker (1990)
Yang (1973)	(2003)	Meyer-Peter and Muller (1948)
Yang (1979)	Wu (2004)	Yang (1984)

Source: Huang and Bountry, 2009

According to studies by Depeweg and Mendez (2002), prediction of the sediment transport in irrigation canals within an percentage error smaller than ±100% is hardly possible. Even in the case of the most reliable method, only 61% of the values are predicted with a tolerance of error of ±100% compared to the measured values. The performance of sediment transport equations was reviewed by Vanoni (1975a) and study findings showed that the mean ratio of observed to predicted transport rate was between 0.5 and 2 for only 64% percent of the comparisons for the best method that was tested. Some of the sediment transport methods are mentioned below with more emphasis on Ackers-White for the purposes of this study.

Duboys' Method for Non-cohesive Sediment transport, as cited by Graf (1984), is based on the excess shear stress approach and the concept that non-cohesive sediment moves as independent layers sliding over one another. Although interactions between sediment layers do occur, the equation is useful in estimating bed load movement. Meyer-Peter and Muller formula as cited by Martin(2003) is based on experimental data using coarse, well-graded sediment with diameters of 0.4 mm to 29 mm and specific gravities of 1.25 to over 4.0. It is applicable to gravel range of particles and under predicts fine particles. Laursen's Formula (1958) predicts total bed-material

load transport. It was developed based on qualitative analysis and original data. The formula outperforms other transport equations in the silt range as per recent studies at Colorado State. Yalin's bed load formula developed in 1963 is appropriate for sand and smaller particle sizes but not suited for gravel (Strelkoff and Bjorneberg, 1999). Einstein's Deposition Model (1968) developed a deposition model for sediment based on the principal that sediment discharge can be determined from the product of sediment concentration and flow discharge. Toffaletti's Method (1969) was based on work presented by Einstein (1950) as cited by Simons and Senturk (1992). Toffaletti's method provided a simplified total load transport equation based on extensive field and flume data (Hydrologic Engineering Centre, 2002a). The method is applicable to sediment with a size range of 0.095 mm to 0.93 mm. The method has successfully been applied on large systems like Mississippi and Arkansas. Engelund and Hansen's (1972) method was developed to calculate total sediment load in sandy streams with a large suspended load. They developed a dimensionally homogeneous transport function. The method was developed using flume experiments with sand of grain diameters between 0.19 mm and 0.93 mm. Extensive field testing has shown this method provides consistent estimates (Hydrologic Engineering Centre, 2002b). Brownlie (1981) derived a method with uniform dimensionality and best approximates sand transport. The equation gives sediment concentration (ppm/weight). Yang's sand transport equation was developed to predict total bed-material load movement for sand sized particles. The model is based on the concept that sediment transport is related to unit stream power. The method is applicable to sediments with diameters in the range of 0.062 mm to 7.0 mm (Yang, 1973). The equation, for particles larger than two millimetres (Yang, 1984), takes the same form but the coefficients were adjusted through the collection of data from more than 150 laboratory flume studies. Ackers and White (1973) formula determines total load, assuming that fine sediment transport is correlated with turbulent fluctuations in the water column and coarse sediment transport is related to particle shear stress.

Not all sediment transport equations are applicable for irrigation canals. Each equation was developed within a specific range of class of sediments and hydrologic conditions. To minimise computation errors, each equation should be applied to conditions which closely resemble the environment under which it was developed. Depeweg and Mendez (2002) found out that based on the overall performance of each method, the Ackers-White and Brownlie methods best predict sediment transport in irrigation canals. This study prefers Ackers-White for its flexibility, wide

sediment class range and ability to compute total sediment load. Mean velocity is used as the representative parameter (Hydrologic Engineering Centre, 2002c). Ackers and White developed a dimensionless mobility number, F_{gr}, to approximate the transport of sediment from channel bed as:

$$F_{gr} = U^{*n}\left[gd\left(\frac{\gamma_s}{\gamma}-1\right)\right]^{-1/2}\left[\frac{V}{\sqrt{32}log(\alpha D/d)}\right]^{1-n} \quad (7)$$

where U^* is the shear velocity (m/s) given by:

$$U^* = \sqrt{gRS} \quad (8)$$

R is the hydraulic radius, S the bed slope, g the gravitational acceleration (m/s^2), γ_s the sediment specific weight (Kg/m^{2}s^2), γ the water specific weight (Kg/m^{2}s^2), V the average flow velocity (m/s), d the sediment particle size (m), D the water depth (m), n the transition exponent coefficient dependent on d_{gr}, and α the coefficient usually taken as 10 for turbulent flow.

Sediment size is also defined through a dimensionless grain diameter, d_{gr}, equation:

$$d_{gr} = d\left[\frac{g}{\psi^2}\left(\frac{\gamma_s}{\gamma}-1\right)\right]^{1/3} \quad (9)$$

where ψ is the kinematic viscosity of water (m^2/s).

The generalized dimensionless sediment transport function can be expressed as:

$$G_{gr} = \frac{q_s D}{qd}\left[\frac{U^*}{V}\right]^n = C\left[\left(\frac{F_{gr}}{A}-1\right)\right]^m \quad (10)$$

where q_s and q are sediment discharge and water discharge respectively, the coefficients A, C, m, and n are conceptual parameters dependent on d or d_{gr} and were derived from best-fit curves of laboratory data for sediment sizes larger than 0.04 mm and Froude numbers below 0.8, a condition for subcritical flow; in 1973 version of Ackers-White formula. The boundary condition for each coefficient is developed from boundary conditions in Table 2.4 and tabulated in Table 2.5.

This formula is known to over predict transport rates for coarse sediments and fine sediment smaller than 0.02 mm. Modifications to the equations have been made to compensate for these errors. Table 2.5. shows the coefficients and corrections in the 1990 version of Ackers-White formula, which is suitable for study of a wide range of finer suspended sediments.

Table 2. 4: Coefficients for the 1973 and 1990 versions of the Ackers-White formula.

Boundary condition	1973	1990
$1 < d_{gr} \leq 60$	$A = 0.23 d_{gr}^{-1/2} + 0.14$	$A = 0.23 d_{gr}^{-1/2} + 0.14$
	$\log C = -3.53 + 2.86 \log d_{gr} - (\log d_{gr})^2$	$\log C = -3.46 + 2.79 \log d_{gr} - 0.98 (\log d_{gr})^2$
	$m = 9.66 d_{gr}^{-1} + 1.34$	$m = 6.83 d_{gr}^{-1} + 1.67$
	$n = 1.00 - 0.56 \log d_{gr}$	$n = 1.00 - 0.56 \log d_{gr}$
$d_{gr} > 60$	$A = 0.17$	$A = 0.17$
	$C = 0.025$	$C = 0.025$
	$m = 1.50$	$m = 1.78$
	$n = 0$	$n = 0$

Source: Ackers and White, 1973; USDI, 2005

Table 2. 5: Maximum and minimum values of coefficients

Coefficient	1973		1990	
	max	min	max	min
A	0.37	0.17	0.37	0.17
C	0.033	0.00029	0.033	0.00034
m	11	1.50	8.56	1.78
n	1.00	0.0052	1.00	0.0052

2.7 Sediment Transport Models

InfoWorks RS Model software models the key elements in river and channel systems. (Mountz and Crowley, 2009). It includes full solution modelling of open channels, floodplains, embankments and hydraulic structures. Rainfall-runoff simulation is available using both event-based and conceptual hydrological methods. InfoWorks is comprehensive, easy-to-use and flexible. Data can be imported from a wide range of sources or created within the system; source and model data are stored in a master database and may be edited at any time. The system provides full model management, allowing for maintenance of a complete audit trail of the modelling process from source data to final outputs.

Sedimentation and River Hydraulic – Capacity (SRH – Capacity) Model was developed by Jianchun Victor Huang and Blair P. Greimann (2009) at the Sedimentation and River Hydraulics Group, Technical Service Centre, United States Bureau of Reclamation. The purpose of the model is to compute sediment transport capacity for a given set of hydraulics and flow value. Several different transport equations are used in the model. Each transport equation was developed for a certain range of sediment size and flow conditions. Most sediment transport equations predict transport capacity for each grain size separately. Like other computer models, SRH-Capacity is potentially fallible. All results obtained from the use of the model should be carefully examined to determine if they are reasonable and accurate. However, the model cannot handle full pipe flows.

Hydrologic Engineering Centre – River Analysis System (HEC – RAS) Model was developed by U. S. Army Corps of Engineers as reported in the user manual, version 4.1 by Hydrologic Engineering Centre (2010). The purpose of the model is to perform one-dimensional hydraulic calculations for a full network of natural and constructed channels. The basic computational procedure is based on one-dimensional energy equation. Energy loses are by friction and cross section expansion or contraction. The momentum equation is used where the water surface profile is rapidly varied. The model computes one-dimensional sediment transport or movable boundaries calculations due to deposition or scour over moderate time periods. Sediment transport potential is determined by grain size fraction, thereby allowing simulation of hydraulic scouring and armouring. Sediment transport equations used within the model include; Ackers-White, Engelund-Hansen, Laursen, Meyer-Peter Muller, Toffaleti, and Yang sediment transport equations. HEC-RAS model is flexible to use, allows for calibration of the conceptual parameters in the equations and can handle full pipe flow computations and hence preferred for this study.

2.8 Determination of Sediment Deposition Rate using HEC-RAS Model

The HEC-RAS model uses both physical and conceptual parameters outlined in Table 2.6. for application of Ackers-White sediment transport equation. The algorithms required to calculate the sediment deposition rate as follows:

Table 2. 6: HEC-RAS input parameters

Physical variables/ Parameters	
Symbol/unit	Description
d (m)	Particle diameter
D(m)	Water depth
V(m/s)	Average flow velocity
ψ(m^2/s),	Kinematic viscosity
g(m/s^2)	Acceleration due to gravity
γ_s(Kg/m^2s^2)	Sediment specific weight
γ(Kg/m^2s^2)	Water specific weight
R(m)	Hydraulic radius
S(m/m)	Slope
$T(^oC)$	Water temperature
Conceptual Parameters	
Symbol (dimensionless)	Description
m	Exponent
n	Transition exponent
C	Coefficient
A	Critical mobility parameter
α	Coefficient

The value of grain diameter is used to calculate dimensionless grain diameter, d_{gr}, as shown in equation 9, where ψ is kinematic viscosity and is dependent on temperature as shown in equation 12 below;

$$\psi = \left[1.14 - 0.31(T - 15) + 0.00068(T - 15)^2\right]10^{-6} \quad (12)$$

The transition exponent, n, the critical mobility factor, A, the coefficient, C, and the exponent, m, are determined by running the model based on sediment transport functions in Table 2.4. Water temperature, T, is measured using a thermometer in ^oC.

The particle mobility number, F_{gr}, is calculated as shown in equations 7 and 8.

The generalised dimensionless sediment transport rate is expressed as:

$$G_{gr} = \frac{q_s D}{qd}\left[\frac{U^*}{V}\right]^n = C\left[\left(\frac{F_{gr}}{A} - 1\right)\right]^m \quad \text{if } A<F_{gr} \tag{13}$$

Otherwise,

$$G_{gr} = 0 \quad \text{if } A \geq F_{gr} \tag{14}$$

Sediment flux X, in parts per part, which is the ratio of weight of sediment to weight of water transporting it, is given by:

$$X = \frac{q_s}{q} = \frac{G_{gr} d}{D\left(\frac{U^*}{V}\right)^n} \tag{15}$$

where q_s and q are sediment discharge and water discharge respectively.

Potential sediment discharge G, in kg/s

$$G = \frac{\gamma q X}{g} \tag{16}$$

This output is a product of the model for various segments within the canal for each grain class outlined in Figure 3.2. The total transport capacity, T_c, for n number of grain classes with β_i percentage composition of class i and G_i transport potential for class i is given by:

$$T_c = \sum_{i=1}^{n} \beta_i G_i \tag{17}$$

Transport potential is used to determine whether there is a deficit or surplus sediments in supply resulting into erosion or deposition respectively.

Deposition efficiency, C_d, is used to determine the boundary condition for erosion or deposition;

$$C_d = \frac{V_s(i)\Delta t}{D_e(i)} \tag{18}$$

where $V_s(i)$ is the settling velocity of particle class i at time step Δt and D_e effective depth of water. For irregular section divided into subsections;

$$D_e = \frac{\sum_{i=1}^{n} D_{avg} a_i D_{avg}^{2/3}}{\sum_{i=1}^{n} a_i D_{avg}^{2/3}} \tag{19}$$

where a_i is the area of subsection i, D_{avg} the average depth of subsection i and n the number of subsections. Similarly, effective width W_e is given by,

$$W_e = \frac{\sum_{i=1}^{n} a_i D_{avg}^{2/3}}{D_e^{5/3}} \tag{20}$$

Settling velocity V_s is computed using the Van Rijn equation as recommended by Depeweg and Mendez (2002). Thus,

$$V_s = \begin{cases} \frac{(s_s-1)gd}{18\psi}; & 0.001 < d < 0.1mm \\ \frac{10\psi}{d}\left[\left(\frac{1+0.001(s_s-1)gd^3}{\psi^2}\right)^{0.5} - 1\right]; & 0.1 < d < 1mm \\ 1.1[(s_s-1)gd]^{0.5}; & d \geq 1mm \end{cases} \tag{21}$$

where s_s is the specific gravity of particles, ψ the kinematic viscosity, d particle diameter in millimetres and g the acceleration due to gravity.

Deposition occurs for $C_d < 1$ but for erosion $C_d > 1$. At $C_d = 1$ neither deposition nor erosion occurs. This is a check for whether erosion or deposition processes need to occur.

The difference between sediment discharge at the inlet segment, q_1, and the adjacent segment, q_2, gives the sediment deposition rate. Therefore, deposition rate D_r in Kg/s between sections 1 and 2 was given by:

$$D_r = G_1 - G_2 \tag{22}$$

$$D_r = \frac{\gamma q X}{g}(q_1 - q_2) \tag{23}$$

Where q_1 and q_2 are sediment discharge at the beginning of flow segment and end of flow segment respectively.

2.9 Calibration and Validation of HEC-RAS Model

Calibration process involves adjustment of the model conceptual parameters within the margins of the uncertainties to obtain a model representation of sediment transport within the canal. The assessment can be done using regression analysis. If the simulated and the measured values do not closely relate, then the model would be calibrated by optimising the conceptual parameters *A*, *C*, *m* and *n*. The starting value of the parameter to be determined is based on documented guidelines and experience. This value is optimised until an optimisation parameter, *P*, is minimised. The equation for determination of P is given by;

$$P = (\sum_{i=1}^{t}(X_i - X_{ci})^2)^{1/2} \quad (24)$$

Where X is the measured value, X_c is the computed value for each data set i and t is the total number of data sets. The computed value will eventually be accepted as given by the model if the optimisation P is at its minimum.

In addition, an average difference, D_a, in the simulated and measured values is computed for N stations using,

$$D_a = \left(\sum_{i=1}^{t} \frac{(X_i - X_{ci})^2}{N}\right)^{1/2} \quad (25)$$

This represents the average error, over the study reach, where the computed value is above or below the measured value and provides an intuitive measure of the accuracy.

Validation process involves evaluation of processed data to establish scientific evidence that the model is capable of consistently delivering quality products whereby values obtained from the model simulation are compared with directly measured values. The assessment can be done using regression analysis.

The regression curve is used to estimate a variable *Y* by means of a variable *X*. The line can show whether there is a pronounced relationship between *X* and *Y* (Hoel, 1984). The closeness of the two variables is known as the correlation coefficient, *r*, given by

$$r = \frac{\sum_{i=1}^{n}(x_i - \bar{x})(y_i - \bar{y})}{(n-1)S_x S_y} \quad (26)$$

where *i* has values of 1, 2, 3,..., *n; x_i* the *i*th sediment load direct measurement; y_i the *i*th sediment load value from model output; *n* the sample size; S_x the variance of *x*; S_y the variance of *y*; $\bar{x}$ the mean value of *x*; and $\bar{y}$ the mean value of *y*.

The correlation coefficient, which ranges from −1 to 1, is an index denoting how closely related the observed and simulated data are. Value of $r = 0$, shows no linear relationship exists but for $r = 1$ or $r = -1$, a perfect positive or negative linear relationship exists respectively. The coefficient of determination, R^2, measures the variance of the measured data. High values of R^2 indicate comparatively less error and values higher than 0.5 are considered acceptable for sedimentation

studies (Santhi *et al.*, 2001a). The fact that only the dispersion is quantified, it follows that if R^2 is considered alone there could be errors of over-prediction or under-prediction even with values of R^2 close to 1.0.

If R^2 is used for model validation it is therefore advisable to consider additional information which can cope with that problem. Such information is provided by the gradient, *b*, and the intercept, *a*, of the regression on which R^2 is based. For a good agreement, the intercept *a* should be close to zero which means that an observed value of zero would also result in a prediction near zero and the gradient *b* should be close to one. For a proper model assessment, the gradient *b* should always be discussed together with R^2. To do this in a more operational way the two parameters can be combined to provide a weighted version (wR^2) of R^2 (Krause, *et al.*, 2005). Such a weighting can be performed by:

$$wR^2 = \begin{cases} |b| \cdot R^2 & for\ b \leq 1 \\ |b|^{-1} \cdot R^2 & for\ b > 1 \end{cases} \tag{27}$$

By weighting R^2 under-prediction or over-predictions are quantified together with the dynamics which results in a more comprehensive reflection of model results. When the value of wR^2 is less than 1 there is under-prediction but when it is more than 1 there is over-prediction.

CHAPTER THREE
METHODOLOGY

3.1 Study Area

The area of study is Southwest Kano Irrigation Scheme located in Nyando Division, Nyando Sub-county, Kisumu County, Kenya. The Southwest Kano Irrigation Scheme has one of the unique irrigation canal systems in Kenya since part of it is constructed underground to ensure minimum interference with the operations in Ahero Town. The water source for the diversion canal is from Nyando River, located in the Nyando basin is shown in Figure 3.1 (Gathenya, 2009).

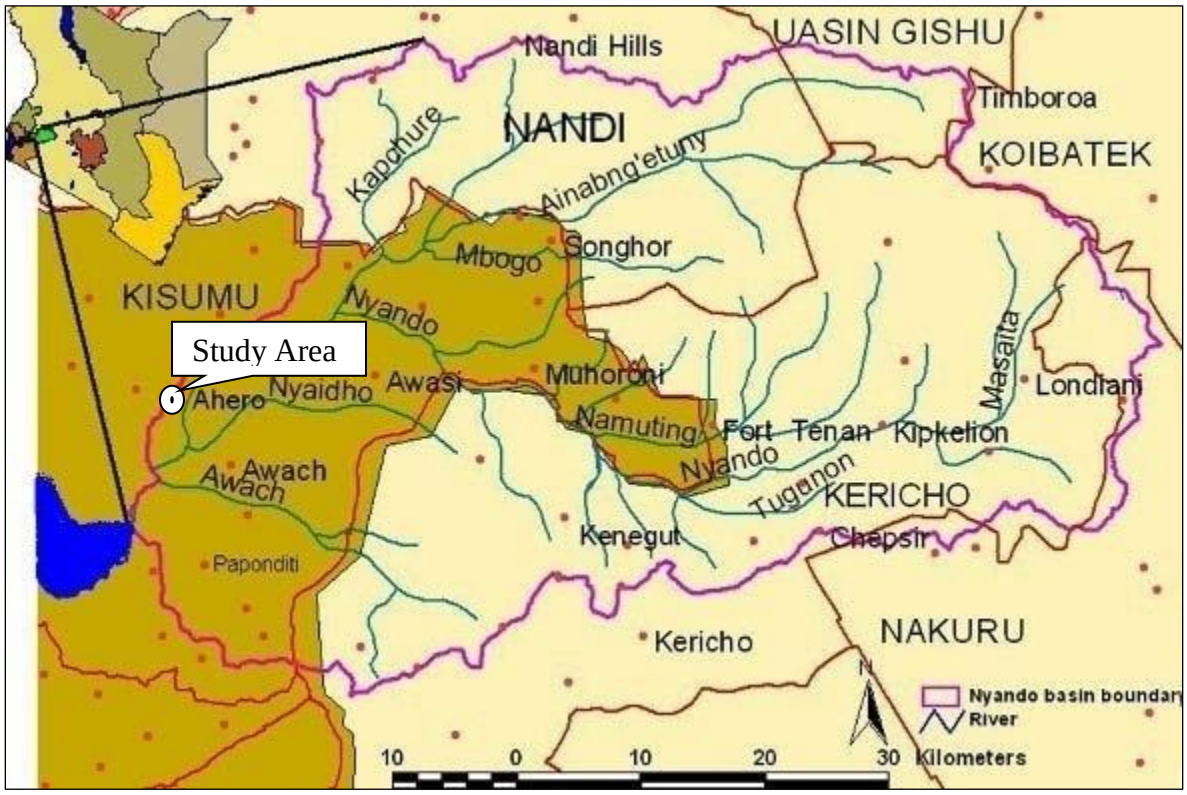

Figure 3. 1: Nyando Basin

The section of the scheme canal which was studied by the author is the underground intake canal is shown in Figure 3.2 running from the intake, A, to outlet, B. The canal is 730 m long of concrete pipe of internal diameter of 1.5 m. The underground section has 5 manholes. The canal supplies irrigation water for production of paddy rice. The scheme covers an area of 540 hectares.

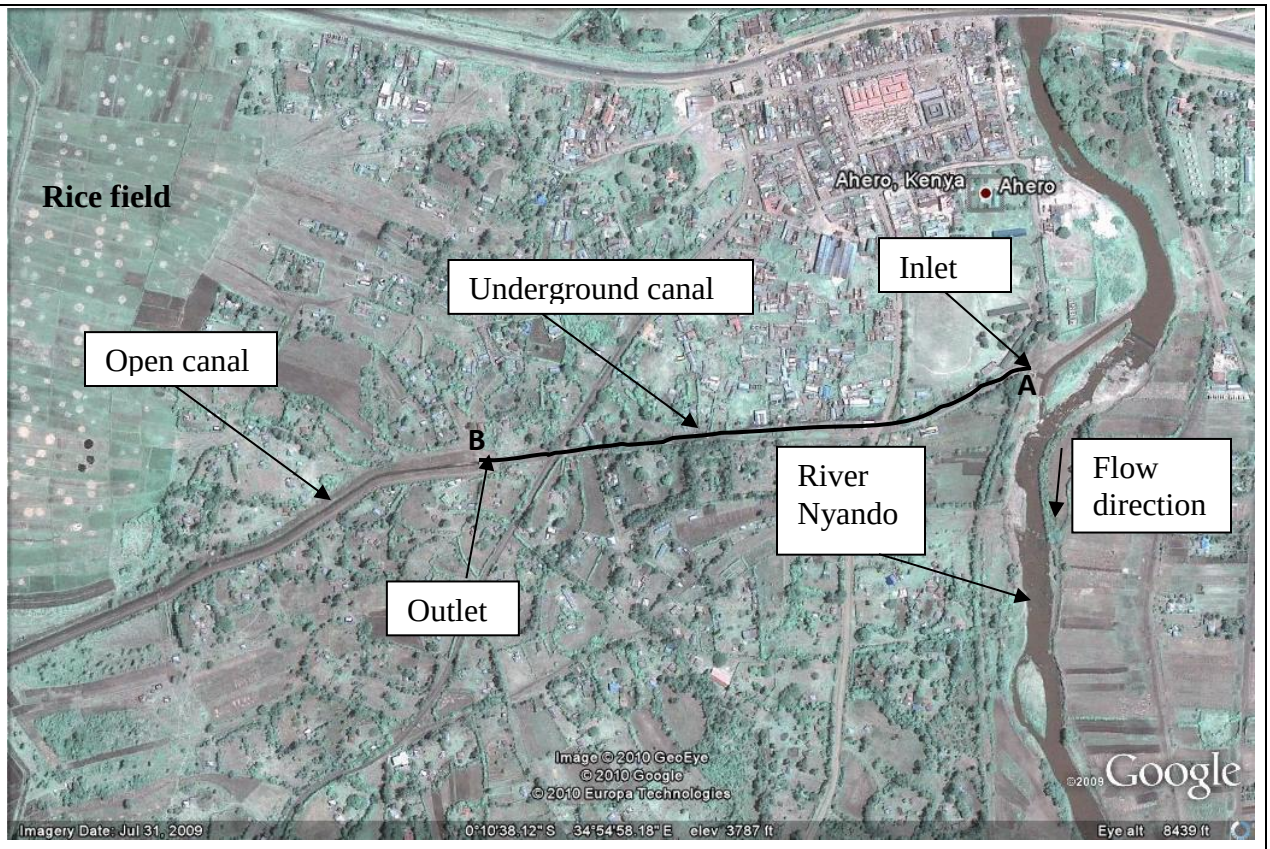

A - Inlet of underground canal

B - Outlet of underground canal

Source: Google Earth Imagery (2009)

Figure 3. 2: Underground Intake Canal

3.2 Primary Data Collection

Data was collected to meet the specific objectives and enable determination of input parameters required for running of HEC-RAS model. Profile survey was carried out to determine the geometry of the canal and its profile using a dumpy level and tape measure, as shown in Figure 3.3 Field data was further collected along the underground canal at three stations; identified as Manhole 1 (Mh1), Manhole 3 (Mh3) and Manhole 5 (Mh5) as shown in Figure 3.3. The data was collected during the short rainy season, on the 15th, 16th and 26th days of September 2011. The data included flow samples from integrated sediment sampler, US D-59, scooped deposited particles sampled from canal bed, flow temperature and flow velocity determined by current meter, SEBA F1. At each station, there were three verticals along which readings of velocity; flow depth; temperature

and time were taken. Velocity readings were taken three times at a distance 0.6 times the canal depth and a final average recorded for each vertical. The data collected is shown in appendix 31.

Table 3. 1: Equipment used for data collection

Equipment	Purpose
Dumpy level (Pentax AP-224)	Taking levels to determine the slope
Current meter (Seba F1)	Measuring flow velocity
Depth integrated sampler (US DH-59)	Measuring suspended sample concentration
Tape measure	Determining width and depth of canal, distance between measurement stations and manholes
Navigation rod	Determination of level of canal bed and depth of sediment deposit.
Metallic scoop	Scooping sediment deposits samples from the canal bed
Stop watch	Determination of time at which measurements and samples were being taken.
Thermometer (100^0C scale)	Measurement of water temperature
Sieves	Grading of sediment particles in the laboratory
Filter paper	Separating fine suspended particles from water
Drying oven	Drying sediment samples in the laboratory
Vibrator	Enhance sieving of dry sediment samples in the laboratory
Weighing scale	Measure weight of dry sediment samples

3.2.1 Bed Material Sampling and Gradation

The composition of canal bed material was used to estimate the critical velocity for no deposition. The bed material samples were scooped from the channel bed at three verticals, 1W/6, 3W/6 and 5W/6 using metallic scoop for each of the 3 stations between A and B (see Figure 3.2, Figure 3.3 and Figure 3.4). Only 3 manholes were chosen out of 5 for data collection since the 5 manholes were closely spaced and measurements taken from 3 manholes would be representative. Samples were taken to Egerton University soil laboratory for gradation where the researcher mixed together the sediment samples collected from the canal bed at the three measurement verticals; poured the sediment sample over a 0.5µm sieve to separate the silt and sand particles, and washed the silt and sand sample with distilled water to remove dissolved solids (salt). The silt and sand particles from

the mixed sample were left to settle for 24 hours in a can of water, the water decanted to free both sediment samples of fluid. The silt and sand sample were put into evaporating dishes (reweighed) and the samples dried in an oven (at 90 °C) until all visible moisture was evaporated. Further drying was done in an oven (at 105 °C) for one hour, cooled in a desiccator, weighed (using a balance accurate to 0.1 mg). The dry sediment weights were determined and a vibrator mounted with different sieve sizes used to classify the soil particles based on American Geophysical Union (AGU) standard in Appendix 1, as per each particles size. The weight of each class was used to calculate the percent distribution for each sediment size. Total average grading for all the samples from the three cross stations mixed together is shown in Table 3.2.

Table 3. 2: Sampled particle size distribution

Sediment Material	Grain class	Grain diameter range (mm)	Geometric median (mm)	% finer
Very fine sand	6	0.0625-0.125	0.088	1.98
Fine sand	7	0.125-0.25	0.177	19.12
Medium sand	8	0.25-0.5	0.354	29.97
Coarse sand	9	0.5-1	0.707	62.12
Very coarse sand	10	1-2	1.410	90.54
Very fine gravel	11	2-4	2.83	90.54
Fine gravel	12	4.0000-8.0000	5.66	98.21
Medium gravel	13	8.0000-16.0000	11.3	100

The grains classified under very fine gravel to medium gravel were not true grains but soft mudstones and therefore the largest sized grain was taken as 2 mm. This was the grain size below which 90.54% would be transported if the grain formed an armouring layer at the canal bed. A sediment rating curve was plotted as shown in Figure 4.1.

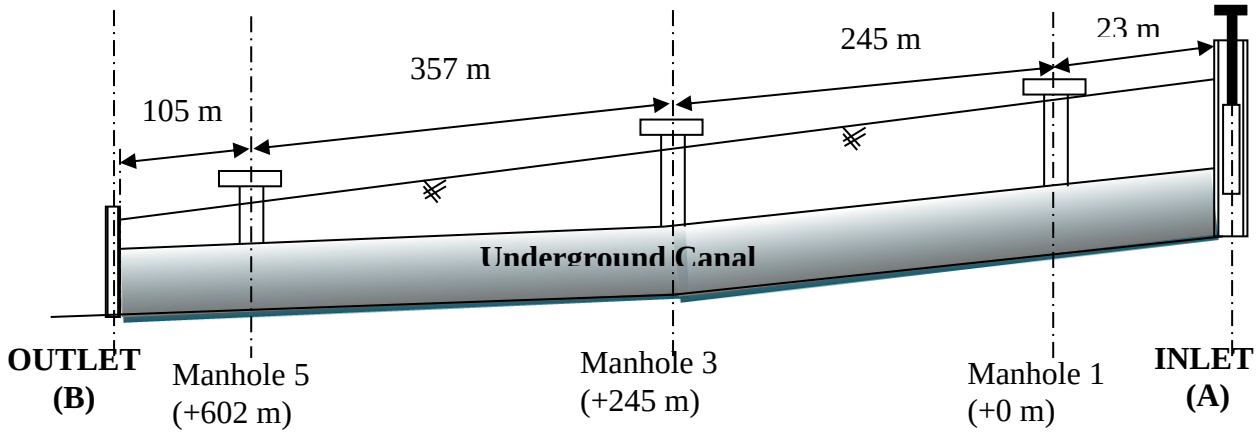

Figure 3. 3: Sketch of Southwest Kano underground canal

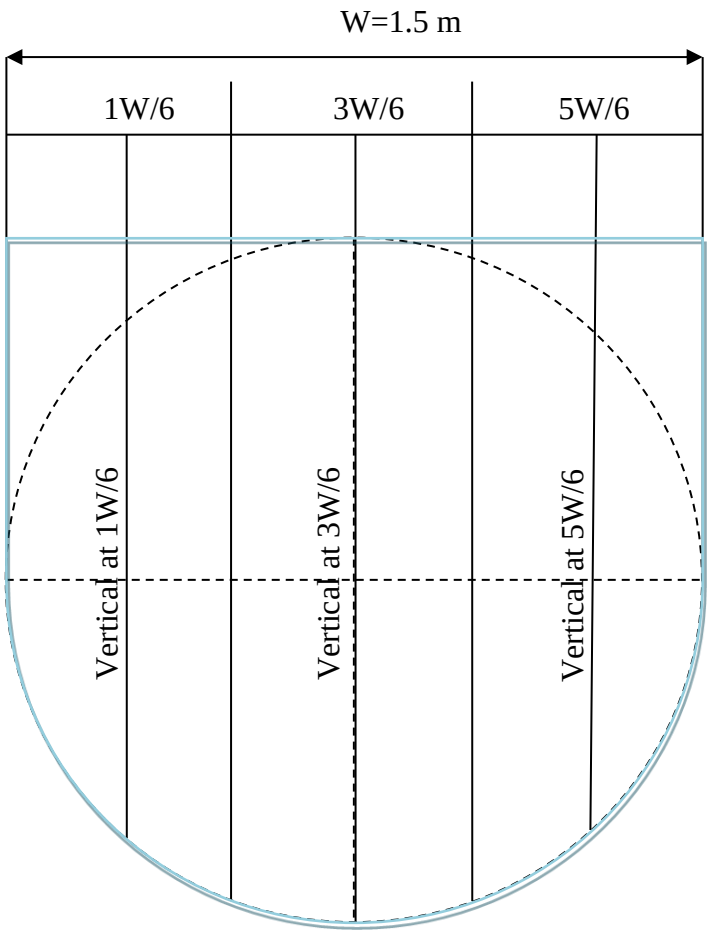

Figure 3. 4: Sketch of Southwest Kano underground canal cross section

3.2.2 Determination of Flow Velocity in the Canal

Current meter, Seba F1 was used to determine flow velocity at three different verticals at 1W/6, 3W/6 and 5W/6 as in Figure 3.4. The depth of suspension of the current meter was maintained at 0.6 times the flow depth at each vertical as recommended by Signal *et al.*, 1981. The discharge, *Q*, was determined by using mean section method. Averages of mean velocities in the verticals and of the depths at the boundaries of the section subdivision were taken and multiplied by the width of the subdivision as shown in equation 28.

$$Q = \sum_{i=1}^{n} q_i = \sum_{i=1}^{n} \left(\frac{v_{i-1}+v_i}{2}\right)\left(\frac{d_{i-1}+d_i}{2}\right)(b_i - b_{i-1}) \quad (28)$$

where b_i = horizontal distance of the measuring point *i* from the bank of canal and *n* being the number of sub-areas. Table 3.3 shows the water discharge measured using Seba F1 current meter.

Table 3. 3: Measured discharge using Seba F1 current meter

Day	Station	Distance (m)	Depth flow (m)	Velocity (m/s)	Discharge (m^3/s)	Total water Discharge (m^3/s)	Average water discharge (m^3/s)
1	1st Manhole (Mh1)	0.25	1.42	0.265	0.063	0.585	0.711
		0.75	1.35	0.505	0.157		
		1.25	1.42	0.255	0.061		
	3rd Manhole (Mh3)	0.25	1.06	0.675	0.128	0.782	
		0.75	1.03	0.705	0.170		
		1.25	1.06	0.365	0.069		
	5th Manhole (Mh5)	0.25	0.99	0.455	0.086	0.766	
		0.75	0.80	0.715	0.139		
		1.25	0.92	0.735	0.133		
2	1st Manhole (Mh1)	0.25	0.84	0.505	0.086	0.490	0.507
		0.75	0.68	0.545	0.087		
		1.25	0.48	0.525	0.058		
	3rd Manhole (Mh3)	0.25	0.82	0.425	0.072	0.521	
		0.75	0.86	0.475	0.095		
		1.25	0.78	0.495	0.079		
	5th Manhole (Mh5)	0.25	0.74	0.495	0.078	0.510	
		0.75	0.69	0.545	0.089		
		1.25	0.67	0.495	0.073		
3	1st Manhole (Mh1)	0.25	0.80	0.555	0.087	0.494	0.499
		0.75	0.58	0.635	0.089		
		1.25	0.40	0.535	0.055		
	3rd Manhole (Mh3)	0.25	0.78	0.545	0.090	0.557	
		0.75	0.77	0.635	0.114		
		1.25	0.75	0.355	0.058		
	5th Manhole (Mh5)	0.25	0.72	0.495	0.074	0.446	
		0.75	0.64	0.495	0.077		
		1.25	0.68	0.425	0.060		
4	1st Manhole (Mh1)	0.25	0.58	0.395	0.049	0.302	0.445

		0.75	0.50	0.425	0.050		
		1.25	0.38	0.505	0.044		
	3rd Manhole (Mh3)	0.25	0.60	0.355	0.048	0.336	
		0.75	0.60	0.395	0.057		
		1.25	0.61	0.405	0.055		
	5th Manhole (Mh5)	0.25	0.80	0.605	0.082	0.697	
		0.75	0.90	0.745	0.152		
		1.25	0.80	0.675	0.092		
5	1st Manhole (Mh1)	0.25	0.97	0.495	0.091	0.654	0.590
		0.75	0.87	0.635	0.129		
		1.25	0.76	0.605	0.087		
	3rd Manhole (Mh3)	0.25	0.79	0.425	0.072	0.547	
		0.75	0.82	0.595	0.113		
		1.25	0.75	0.455	0.074		
	5th Manhole (Mh5)	0.25	0.83	0.575	0.096	0.568	
		0.75	0.67	0.575	0.093		
		1.25	0.68	0.535	0.078		

From discharge, Q, and channel cross sectional area, *A*, the flow velocity, v, was computed using the relation in equation 5 as below:

$$V = Q/A \tag{29}$$

3.3 Determination of Critical Velocity for No Deposition

Critical velocity is the minimum velocity of flow which would result in no deposition of sediments in the canal. Fall velocities of sediments deposited at the bottom of the canal must be lower than the velocity of water flowing in the canal for deposition to occur. Canal bed material composition was therefore used to estimate the flow velocity in the canal under which there would be no deposition. Bed material sample obtained and classified, as in section 3.2.1, was used to estimate the critical velocity, being the value of erosive velocity corresponding to the upper grain size in Hjulstrom diagram as shown in Figure 2.1. Erosive velocity was used to estimate critical velocity. Since water discharge in the canal is dependent on the irrigation water requirement, there is bound to exist varied discharge of water at different times. Varied discharge of water has different flow velocities. Therefore, the critical velocity should be the velocity of water flow which has a potential

of eroding previously deposited sediments during low velocities. These sediments must be dislodged and transported for the canal to be non-silting.

The critical velocity was also estimated based on maximum particle size as per equations 4 and 6 developed by Lacey for no deposition nor erosion. If the velocity of flow was maintained above the critical velocity from Lacey Theory, then there would be no deposition.

3.4 Calibration and Validation of HEC-RAS Model Based on Current Flow Conditions

Sediment deposition rate was simulated using the HEC–RAS model under various input variables. The output of the model was sediment discharge at different sections. The rate of sediment deposition in a segment between manholes was obtained from the difference in the sediment discharge observed at the successive manholes. A temporal deposition limiter was used by the HEC-RAS model as per the equations 18, 19, 20 for settling velocity to determine conditions for deposition and erosion. Sediment deposition rate was also computed from direct measurements of sediment load and a graph of simulated versus measured values was plotted and analysed.

3.4.1 Determination of Input Parameters into HEC – RAS model

The input parameters were both physical and conceptual as shown in Table 3.4. The value of each parameter was either measured directly or computed from hydrologic equations or was already determined in the model.

Table 3. 4: HEC-RAS input parameters and how they were determined

Physical Parameters		**Means of determination**
Symbol/unit	Description	
d (m)	Particle diameter	Determined from sieving sediment sample
D(m)	Water depth	Measured using tape measure and navigation rod
V(m/s)	Average flow velocity	Measured using the current meter and then computed
ψ(m^2/s),	Kinematic viscosity	HEC-RAS user manual at measured water temperature
g(m/s^2)	Acceleration due to gravity	Constant provided in HEC-RAS user manual (10 m/s^2)

γ_s(Kg/m^{2}s^2)	Sediment specific weight	Constant provided in HEC-RAS user manual (2.65 Kg/m^{2}s^2)
γ(Kg/m^{2}s^2)	Water specific weight	HEC-RAS user manual at measured water temperature
R(m)	Hydraulic radius	Computed from effective depth and effective width
S(m/m)	Slope	Computed from elevation determined using the dumpy level
T(°C)	Water temperature	Measured using a thermometer
Conceptual Parameters		
Symbol (dimensionless)	Description	
m	Exponent	Calibration
n	Transition exponent	Calibration
C	Coefficient	Calibration
A	Critical mobility parameter	Calibration
α	Coefficient	Constant provided in HEC-RAS user manual (10) for turbulent flow

The sets of input data were determined for each station where the three manholes were positioned; between points A and B as shown in Figure 3.2 and Figure 3.3. Samples for determination of sediment size and percent composition were obtained from the bed of the channel reach and gradation done in the laboratory. During gradation, the particles were screened using different sieves into various grain classes (see Figure 4.1) to determine the sediment size (diameter) distribution. Canal flow velocity, water depth, and water temperature were measured using current meter, tape measure and thermometer respectively. Bed slope was determined using dumpy level.

The HEC-RAS model used the input water discharge values as shown in Table 3.3 among other parameters to produce the outputs of sediment discharge for each sediment size.

3.4.2 Determination of Sediment Deposition Rate using HEC-RAS Model

After gradation of deposited layer, all the input parameters required for running the model shown in Table 3.4 were then available having been obtained from algorithms discussed in section 2.8, direct measurements and computations. These parameters were input into the model and simulations carried out to give sediment deposition rate. The sediment deposition rate is computed from the amount of sediment entering and leaving the sediment control volume. The sediment control volume is starts midway from the next cross section upstream and ends midway to the next cross section downstream.

3.4.3 Manual Computation of Sediment Deposition Rate

Suspended sediment samples were taken at 3 stations, corresponding to the manholes, between A and B for suspended particles using depth integrated sampler at three different verticals thus; 1W/6, 3W/6 and 5W/6, where W was the water width across the channel cross section. The depth of each measurement point was estimated as being equivalent to 0.54 times the flow depth, being the point at which the sediment concentration has an average value (Signal *et al.,* 1981). The samples were taken for analysis at the Egerton University soil laboratory.

The following procedures were followed for suspended load: The researcher weighed a filter paper and poured the sediment sample over the filter paper to separate the sediment with water then dried the samples in an oven (at 90 °C) until all visible moisture had evaporated. The samples were further dried in an oven (at 105 °C) for one hour, cooled in a desiccator and weighed the samples and filter paper (using balance accurate to 0.1 mg). The dry sediment weights were determined and the particle concentration calculated based on the bottle volume for each sample. The steps were repeated for all the samples sets. The average concentration of sediment in the flow for each station between A and B in Kg/m^3 was determined. The researcher estimated the bed load concentration based on the suspended sediment concentration as shown in Table 2.2.

Assuming the total sediment transport rate is the same as water flow rate in channel, total sediment transport rate at point *i*, T_{Si}(kg/s), of the canal was determined from data sets of sample volume and channel discharge for the successive flow segments.

$$T_{Si} = C_i \, a_i v_i \tag{28}$$

where C_i (kg/m^3) was the sediment concentration at measuring point as determined in the

laboratory; a_i (m^2) the cross section area represented by sampling point *i*; v_i (m/s) the average velocity at point *i*.

The sediment deposition rate, S_{di}, at each sampling point *j* along the channel was determined by changes in the suspended sediment transport rate between the successive sampling points. Sediment deposition rate was computed for all the 3 sampling points along the canal.

$$S_{di} = T_{S(i-1)} - T_{Si} \tag{29}$$

where *i* values are 1, 2, 3.

3.4.4 Calibration of HEC-RAS Model for Sediment Deposition Rate

HEC-RAS model was calibrated in two steps. First step was to calibrate the Manning's roughness coefficient (n-value) using the measured water surface elevation data. An n-value was first estimated based on documented guidelines based on work done by Chow (1959a). Using this as a starting point the n-value was progressively varied until the optimisation parameter, *P*, was minimised as discussed in section 2.9.

The second step was the calibration of the conceptual parameters in HEC-RAS model, where a sediment transport equation Ackers and White was chosen for analysis. This was achieved by comparing the simulated transport potential, T_c and actual measured transport rate, T_S. The conceptual parameters were optimised using the criteria that the simulated values must be as close as possible to the measured values. The weighted value of correlation coefficient from a graph of simulated versus measured sediment transport rates gave an indication of the degree of how close the model predicted sediment deposition.

3.5 Simulation Using HEC-RAS Model for 0.25, 0.50, 0.75, and Full Flow Scenarios.

Simulations were done for the selected scenarios for the purposes of plotting the sediment rating curve. The calibrated model, with conceptual parameters already determined, was used to simulate different canal flow scenarios assuming the canal had no initial deposited sediments. This meant that the ensuing flow velocity would change after some time due to change in bedslope. The depths derived from 0.25, 0.50, 0.75, and full flow scenarios were used to compute corresponding velocities using the Manning's equation:

$$V = \frac{1}{n} R^{2/3} S^{1/2} \tag{30}$$

where *V* is the velocity, *n* the Manning's roughness coefficient, *R* the hydraulic radius and *S* the bed slope. *S* was obtained from elevation measurements using the dumpy level and a navigation rod and *n*, for the concrete lined pipe, from the HEC - RAS manuals. *R* was determined using geometrical relation for circles as in equation 31. Angle *Ø* (radians) was computed from the flow surface width, *B*, and flow depth, *D*, using the relation in equation 32 (see Figure 3.5).

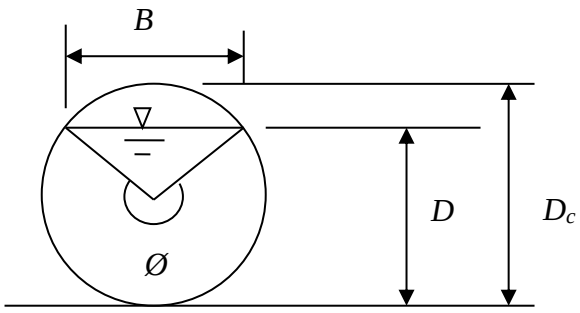

Figure 3. 5: Canal cross section

$$R = \frac{1}{4}\left(1 - \frac{sin\,\emptyset}{\emptyset}\right) D_c \tag{31}$$

where Ø was the angle subtended by the water surface from the centre of the canal and D_c the canal diameter.

$$\emptyset = 2\,sin^{-1}\left(\frac{B}{D}\right) \tag{32}$$

The HEC-RAS model was run with sets of input data for the specified scenarios to give respective outputs of sediment discharge and deposition rate at any time step, Δt. From these simulations, it was possible to tell which scenario had minimum deposition rate. It was also possible to predict how much sediment would be deposited after a given duration.

The permissible intake sediment load, which should be equal to or less than the sediment discharge at underground canal outlet was computed using the HEC-RAS model through Ackers-White sediment transport equation, after having been calibrated and sediment rating curve plotted on a logarithmic scale as shown in Figure 4.15.

3.6 Sensitivity Analysis

The choice of input variables is a fundamental in identifying the optimal functional form of statistical models. HEC-RAS has both physical and conceptual parameters. The conceptual parameters depend on environment in which the model operates and can be determined through calibration, unlike the physical parameters which were determined through direct measurements. Since the output of the model, sediment discharge, was physically measured and was therefore known, the conceptual parameters had to be carefully chosen to best represent the output when the model is simulated. The conceptual parameters A, C and m values were initially calculated with particle size of 0.69 mm at d_{50} using Ackers-White sediment transport equations thus Mobility parameter A = 0.17, coefficient, C = 0.025 and exponent, m = 1.78. (see equations 9 and 12, and Table 2.4)

To identify the most sensitive parameter the researcher decided to use input variable selection method. This involved selection of each variable through forward selection. This selection method involved linear incremental search strategy that selected individual candidate parameters one at a time, test their importance in influencing output and initially use the most influential parameter to estimate the known sediment discharge. (Tikka, 2008). Using this process, the most influential parameter turned out to be Mobility parameter, A. The value of A was selected stepwise towards a known output of sediment discharge until the best prediction was achieved. Similar process was followed for the less influential parameters C and m to give the best representation of the actual output. All these increments were done within the acceptable range as shown in Table 2.6.

The conceptual parameters A, C and m values were finally determined as Mobility parameter A = 0.2, coefficient, C = 0.004 and exponent, m = 4. The value of n was automatically determined by the algorithms in the model.

CHAPTER FOUR
RESULTS AND DISCUSSION

4.1 Determination of Critical Velocity for No Deposition

The samples for particle size distribution analysis were obtained from three stations in the canal bed. Total average grading for all the samples from the three stations mixed together is shown in Table 3.2.

The grains classified under very fine gravel to medium gravel were not true grains but soft mudstones and therefore the largest sized grain was taken as 2 mm. A sediment rating curve was plotted as shown in Figure 4.1. From the figure, $d_{90.54}$ (the grain size at which 90.54% of the grains are finer) was 2 mm. This grain size was used to estimate critical velocity from Hjulstrom diagram in Figure 2.1 as 0.54 m/s, as summarised in Figure 4.1 below. This is the erosive velocity for particle size of 2mm.

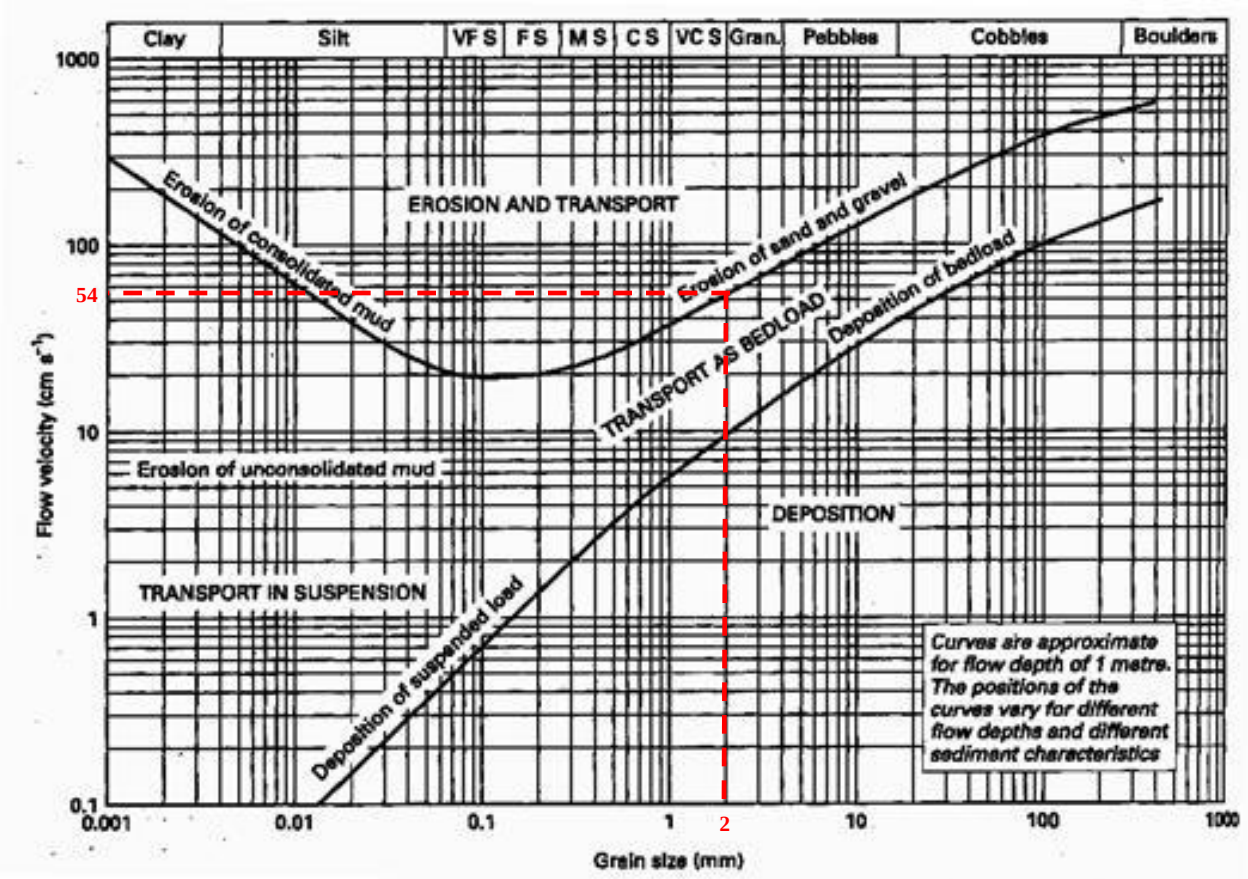

Figure 4. 1: Critical velocity from Hjulstrom Diagram

Discharge in irrigation canals is not constant due to varying water demands at different times. Velocity also varies with discharge as shown in Table 4.4. In canals where discharge is not constant, erosive velocity is preferred to fall velocity as a means of estimating the critical velocity for no deposition since more power would be required to dislodge previously deposited particles during low velocities. The erosive velocity is believed to vary with depth and sediment characteristics according to Hjulstrom. The maximum depth attained during Hjulstroms experimentation was 1 m. The actual depth of flow in the canal was found to be, in some instances, above 1 m depending on water demand. Hence the critical velocity derived using this method would not be appropriate for higher flow depths.

Lacey Theory was also used to calculate critical velocity by applying equations 3, 4, 5 and 6 (pages 12-13) for grain size of 2 mm (d_m = 2mm) at full flow as follows:

$$f = 2.49 \tag{33}$$

and the critical velocity of flow for no deposition of this particle is given by:

$$V = \left[\frac{\pi r^2 V f^2}{140}\right]^{1/6} \tag{34}$$

where r is the radius of canal

Or

$$V^5 = \frac{\pi r^2 f^2}{140} \tag{35}$$

$$V^5 = \frac{3.14X0.75^2X2.49^2}{140} \tag{36}$$

$$V = 0.60 \text{ m/s} \tag{37}$$

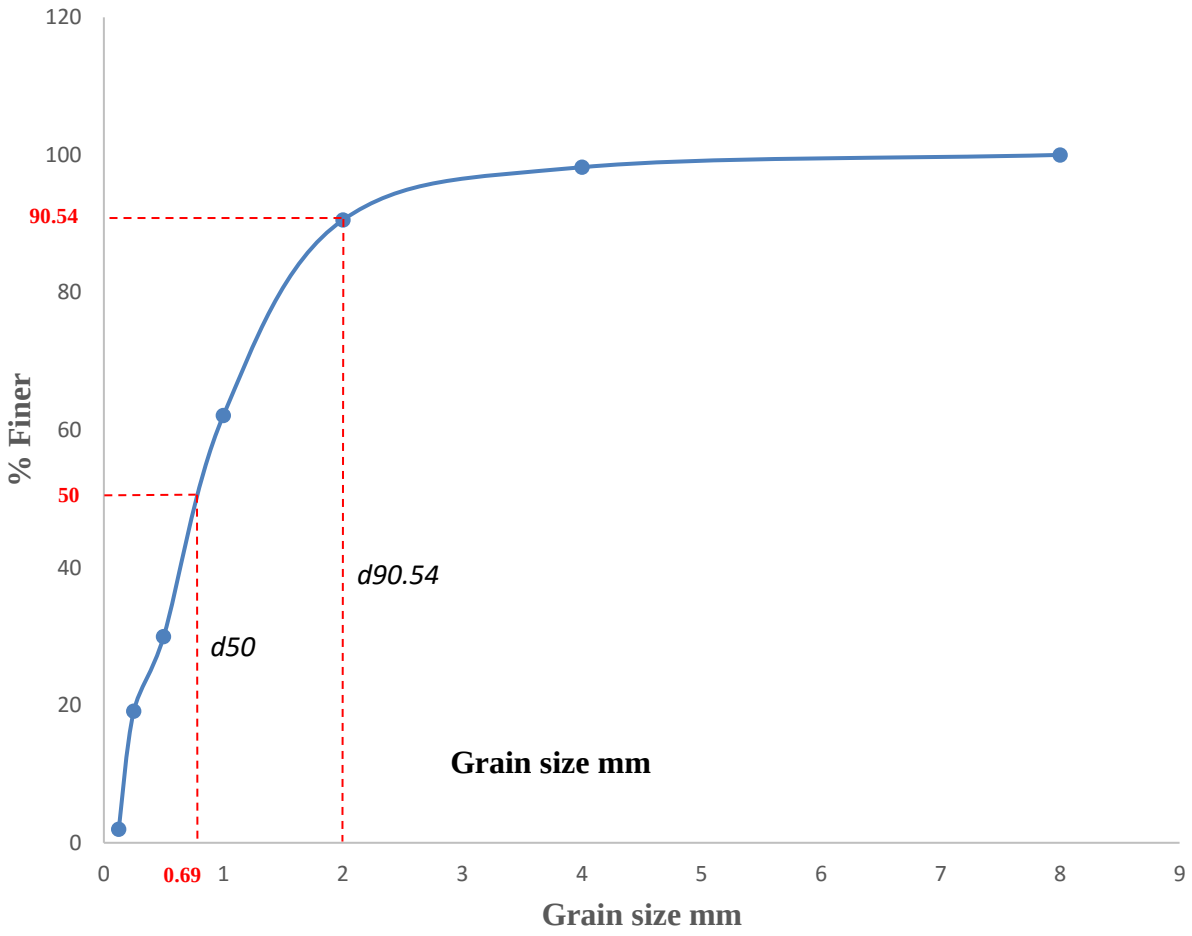

Figure 4. 2: Sediment rating curve

This velocity is almost the same as the value from the Hjulstrom diagram. Lacey Theory is empirically developed and is based on field observations. Hjulstrom diagram is also based on field observations but limited to one-meter depth and hence not quite applicable to the canal under study (maximum depth 1.5 m). Therefore, the critical velocity derived from Lacey's method was adopted for no deposition. It follows that at least 90% of deposition occurred when the channel velocity was below the critical velocity of 0.60m/s. This means that at this velocity most of sediment entering the canal would not be deposited at the canal bed.

4.2 Calibration and Validation of HEC-RAS Model Based on Current Flow Conditions

4.2.1 Calibration and Validation of Mannings n

The first phase of calibration involved the determination of Manning's roughness coefficient, n. The HEC-RAS model was run for steady flow state using the concept of stream flow energy

balance with a known water surface elevation downstream. The value of Manning's n was varied until the resulting surface elevation of water in the canal best fitted the actual measured surface elevations. Low flow values of flow profile-PF2, profile-PF3 and profile-PF4 were used for calibration while higher flow values of profile-PF1 and profile-PF5 were used for validation since the calibrated Manning's roughness coefficient works best for high flow as observed by Parhi *et al.*,2012 (see Table 4.1). The initial value of n was taken to be 0.013 for the whole canal as was recommended by Chow (1959b) for concrete lined canals. The final calibrated values of Manning's n varied from one canal station to the next; with first manhole, Mh1, having n=0.032, third manhole Mh3, having n=0.011 and fifth manhole, Mh5, having n=0.011. These values were arrived at using optimisation method as described in equation 24 and 25. Calibration, which involved the variation of value of Manning roughness coefficient reduced the values of average difference, D_a, hence reducing the error factor for profiles PF2, PF3 and PF4 to 2.06%, 6.58%, 0.38% respectively as shown on Table 4.1. The error factors encountered during calibration using low flows compared closely. This is an indication that the flow in the canal represented that of an open canal and the Manning's equation is applicable. Error factors for high flows were comparatively high. These high error values could have arisen from confinement of flow by the pipe boundaries thereby creating partly pressurised flow, where open flow conditions cease to apply. For this reason, measured water level may not then reflect the true level of water expected in open channel flows. The characteristic of the water flow in the canal therefore would oscillate between open flow and pressurised flow.

Table 4. 1: Calibration and Validation of Manning's n

Profile and Flowrate (m^3/s)	Average observed depth of flow (m)	Calibrated n-value			Model Validation		
		n	D_a (m)	Error %	n	D_a (m)	Error %
PF2 0.507	0.81	0.032, 0.011, 0.011	0.18	2.06	-	-	-
PF3 0.499	0.81	0.032, 0.011, 0.011	0.20	6.58	-	-	-
PF4 0.445	0.70	0.032, 0.011, 0.011	0.1467	0.38	-	-	-
PF1 0.711	1.12	-	-	-	0.032, 0.011, 0.011	0.12	21.4
PF5 0.590	0.87	-	-	-	0.032, 0.011, 0.011	0.39	44.2

[1]Error is computed as the average difference D_a, being a percent of the flow depth.

The percentage weighted correlation coefficient, wR^2, ranged from 0.67 to 0.99 for both calibration and validation data as shown in Table 4.2, Figure 4.3, Figure 4.4, Figure 4.5, Figure 4.6 and Figure 4.7 with profile PF4 value of wR^2 being 0.67. The other values of wR^2 for calibration and validation were within the acceptable range of 0.5 (Santhi *et al.*, 2001b). The calibrated value of n being 0.032 at Manhole Mh1 was above the recommended value for concrete lined canal, but suited a lined canal with gravel bottom and sides of dry rubble or riprap according to Chow (1959c). This value was higher than expected meaning that there could be other factors contributing to drop in velocity head but not necessarily attributable to Mannings' n such as intermittent pressurised flow between manhole (Mh1) and manhole (Mh3) because of higher bedslope. Nevertheless, at Manhole, Mh5 of n being 0.011 is for lined canal with neat cement surface. This description fitted the condition of channel under investigation for it had deposits but

no growth or trash in it. The gentle slope between manhole (Mh3) and manhole (Mh5) made the simulation process produce the reasonable value of Manning's n mentioned above.

The simulated water surface elevation from the bottom of the canal, generated by the HEC-RAS Model, was plotted against the measured value from results tabulated in Table 4.2 as shown in the Appendices 2, 3, 4, 5 and 6. In all cases, the simulated water surface level for manhole (Mh3), was above the observed values as indicated in Table 4.2 and Appendices 2, 3, 4, 5 and 6. This indicates that there is a likelihood of pooled water at that station under normal circumstances of open channel flow. The low value of measured water level could be due to restriction of free surface flow by the canal walls.

The variation in profile could have been affected by changes in discharge during data collection. Each profile was built with data from all the three manholes with an assumption that the discharge remained constant. This condition could be altered by rising or falling water levels in the river or trash screen at the inlet getting partly clogged by trash.

Table 4. 2: Calibration and validation results for water surface levels

Model Run	Profile	Discharge (m^3/s)	Station*/ Manhole	Measured water level		Simulated water level n=0.011				
				Measured Surface Elevation (m)	Invert Level (m)	Simulated Surface Elevation (m)	a	b	R^2	wR^2
Calibration	PF2	0.507	602/Mh1	1148.91	1148.07	1148.91	-118.5	1.10	1.00	0.91
			245/Mh3	1147.92	1147.06	1148.33				
			0/Mh5	1147.38	1146.64	1147.38				
	PF3	0.499	602/Mh1	1148.91	1148.11	1148.90	112.88	0.90	0.97	0.87
			245/Mh3	1147.83	1147.05	1148.32				
			0/Mh5	1147.47	1146.75	1147.47				
	PF4	0.445	602/Mh1	1148.72	1148.14	1148.80	261.23	0.77	0.87	0.67
			245/Mh3	1147.66	1147.05	1148.29				
			0/Mh5	1147.73	1146.83	1147.73				
Validation	PF1	0.711	602/Mh1	1149.23	1147.88	1149.15	9.58	0.99	1.00	0.99
			245/Mh3	1148.08	1147.02	1148.48				
			0/Mh5	1147.53	1146.57	1147.53				
	PF5	0.590	602/Mh1	1149.12	1148.15	1149.03	268.34	0.77	0.93	0.72
			245/Mh3	1147.83	1147.02	1148.39				
			0/Mh5	1147.45	1146.62	1147.45				

*The station name is represented by the distance along the canal axis, in meters, between the station and the farthest downstream station.

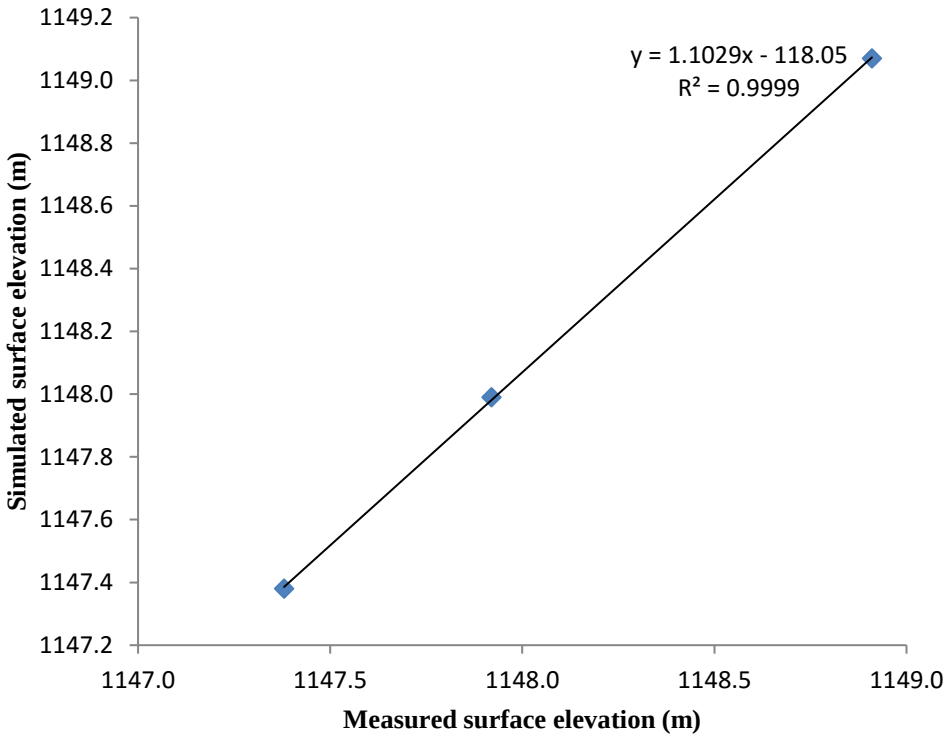

Figure 4. 3: Calibration curve for profile PF2

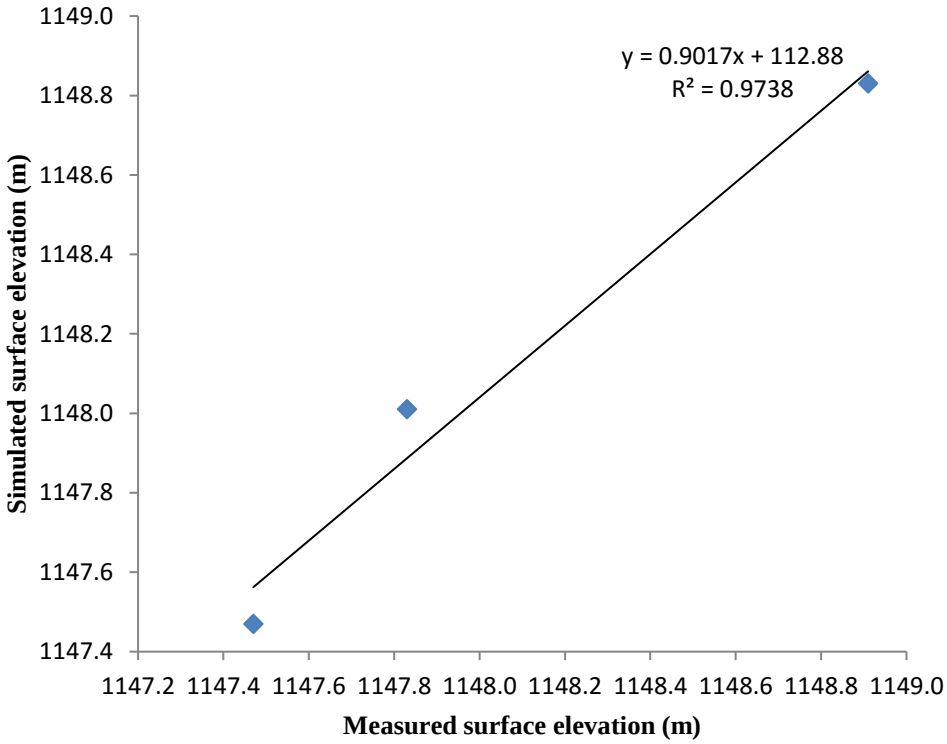

Figure 4. 4: Calibration curve for profile PF3

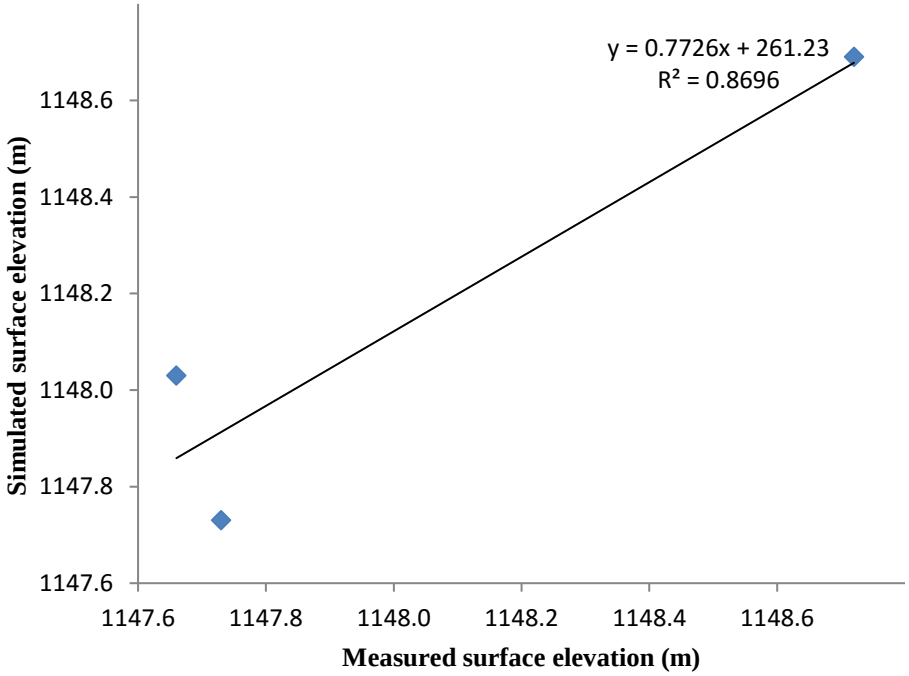

Figure 4. 5: Calibration curve for profile PF4

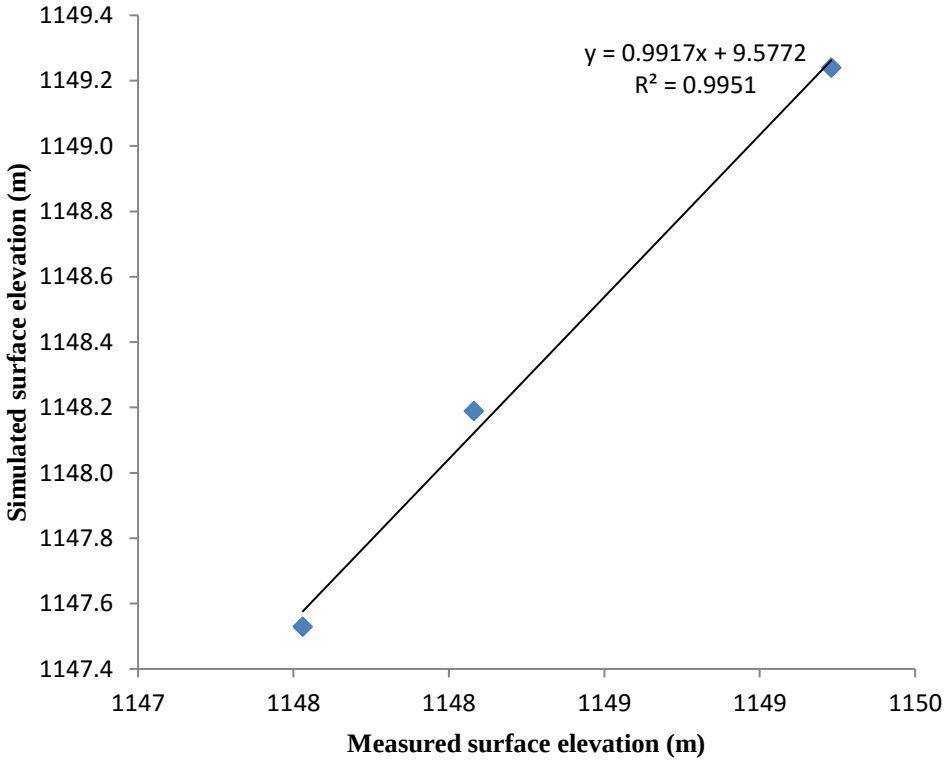

Figure 4. 6: Validation curve for profile PF1

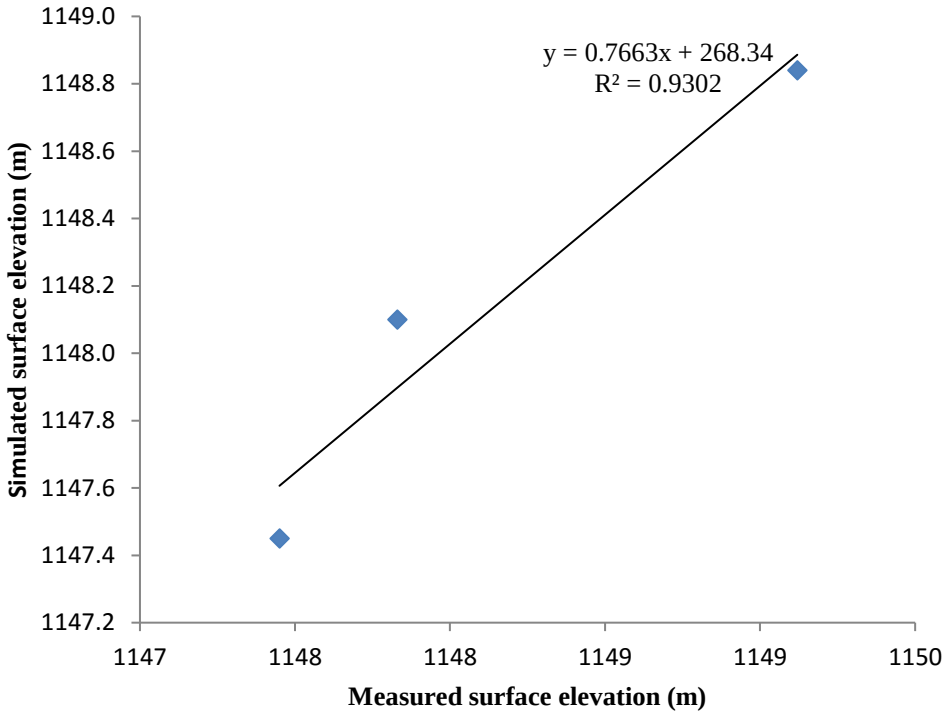

Figure 4. 7: Validation curve for profile PF5

4.2.2 Calibration and Validation of Coefficients (A and C) and Exponent (n)

The second phase of HEC-RAS model calibration for sediment transport was done after running simulations using steady flow state. The calibration to obtain sediment erosion parameters, coefficients and exponents in HEC-RAS model were done through parameter optimisation. The simulated sediment discharge at measurement stations assumed that the flow entering the canal was at equilibrium sediment load. The hydraulic data for the first manhole (Mh1) was used for calibration. All manholes were assumed to have similar canal bed sediment characteristics for each simulation. The hydraulic data for the third manhole (Mh3) and fifth manhole (Mh5) were used for validation. The model input parameters for calibration of the HEC-RAS model were determined through physical measurement, derivation from steady flow equations or generated from inbuilt algorithms of HEC-RAS model. The revised Ackers-White sediment transport equation of 1990 shown in Table 2.4 used the average sediment size d_{50}. The initial conceptual parameter values used for simulation were determined from sediment particle, d_{50}, size below which 50% of the particles are finer. From Figure 4.1, the value of d_{50} was 0.69 mm. These initial parameters were: critical mobility parameter A = 0.17, coefficient, C = 0.025 and exponent, m =

1.78. The critical mobility parameter was the most sensitive parameter in Ackers and White sediment transport equation.

The obtained values obtained after optimisation were A equals 0.20, C equals 0.004 and m equals 4. However, there were other conceptual parameters which were not calibratable in the model by the researcher. These were the exponent, n, and constant, α. The value of α was taken to be equivalent to 10 as provided for in the model and the transition exponent, n, being a function of sediment properties, never needed calibration, and were computed by the inbuilt algorithms in HEC-RAS model. Tabulated in Table 4.3 and graphically represented in Figure 4.8, Figure 4.9 and Figure 4.10 are the simulated and measured sediment discharge values at each manhole during calibration and validation processes.

The calibration curve in Figure 4.8 was arrived at after simulation runs giving values of R^2 and wR^2 of 0.5109 and 0.3922 respectively. There was an over-prediction of sediment discharge by 30.27%. The over-prediction characteristic of Ackers and White sediment transport equation was confirmed by Hassanzadeh *et.al.,* (2011) where it was concluded that the equation overestimated total sediment load. The validation results showed a drop in the error factor from 63.28% to 60.78%. The weighted correlation error was within the error factor of ± 100% documented as the finding from application of "more reliable methods" of sediment transport prediction. (Depeweg and Mendez, 2002).

The validation of the model as shown in Figure 4.9 and Figure 4.10, indicated that the discharge for manhole 3 (Mh3) and manhole 5 (Mh5) had correlation errors of 49.85% and 38.09% respectively. However, their respective weighted correlation coefficient wR^2 stood at 0.1454 and 0.5342, signifying that there was more under-prediction in manhole 3 (Mh3) than Manhole 5 (Mh5) as shown in the validation graph in Figure 4.9 and Figure 4.10. The under-prediction phenomenon was due to formation of armoured sediment layer on the canal bed for continuous flow. The armoured layer is the topmost layer of particles which cannot be eroded by a given flow velocity. This layer was, in practice, interfered with by periodical temporary canal closure for maintenance. Previously suspended particles could have settled on the bed thereby covering the armoured layer. The settled particles increased the quantity of sediment available for transport.

Table 4. 3: Calibration and validation results for cumulative sediment discharge

Model run type and properties	Date	Time	Discharge (m^3/s)	Simulated (ton)	Measured (ton)	Description of line of best fit			
						a	b	R^2	wR^2
Calibration Manhole 1 (Mh1) A=0.2, C=0.004, m=4	15/9/2011	11.28am	0.711	1.72	158.09	-174.21	1.3027	0.5109	0.3922
	16/9/2011	09.23am	0.507	94.99	167.84				
	16/9/2011	12.45pm	0.499	106.82	703.58				
	26/9/2011	11.09am	0.445	1068.19	705.68				
	26/9/2011	01.47pm	0.590	1078.95	737.97				
Validation Manhole 3 (Mh3) A=0.2, C=0.004, m=4	15/9/2011	11.28am	0.711	3.24	296.59	21.113	0.2899	0.5015	0.1454
	16/9/2011	09.23am	0.507	219.29	306.61				
	16/9/2011	12.45pm	0.499	182.52	871.39				
	26/9/2011	11.09am	0.445	322.57	873.85				
	26/9/2011	01.47pm	0.590	326.13	922.87				
Validation Manhole 5 (Mh5) A=0.2, C=0.004, m=4	15/9/2011	11.28am	0.711	8.93	283.19	-116.63	0.8628	0.6191	0.5342
	16/9/2011	09.23am	0.507	272.67	294.80				
	16/9/2011	12.45pm	0.499	277.77	768.59				
	26/9/2011	11.09am	0.445	693.58	775.44				
	26/9/2011	01.47pm	0.590	699.06	816.39				

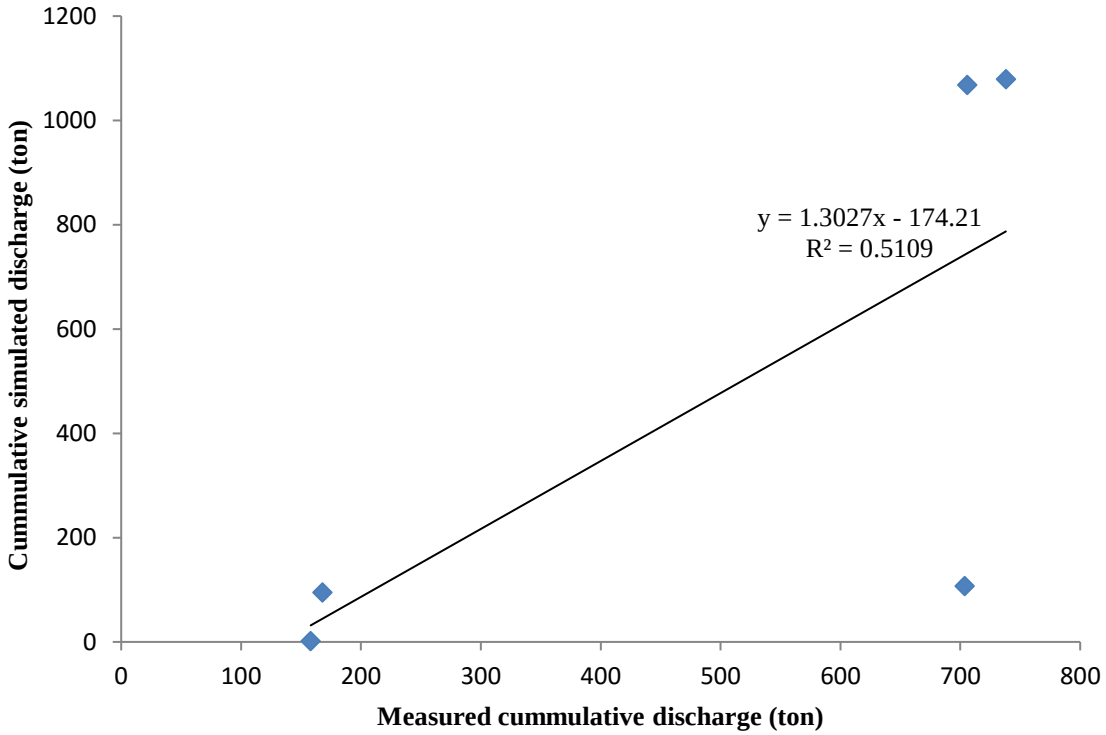

Figure 4. 8: Calibration cumulative sediment discharge curve (Mh1)

All the curves plotted for calibration and validation seem to be scattered. This is due to the nature of unpredictability surrounding sediment transport. 64% of Sediment transport equations tested have a mean ratio of observed to predicted values between 0.5 to 2 (Vanoni, 1975b). This means the equations have a general trend but with a wider dispersion space. This shown in the low values of R^2 falling between 0.5015 and 0.6191.

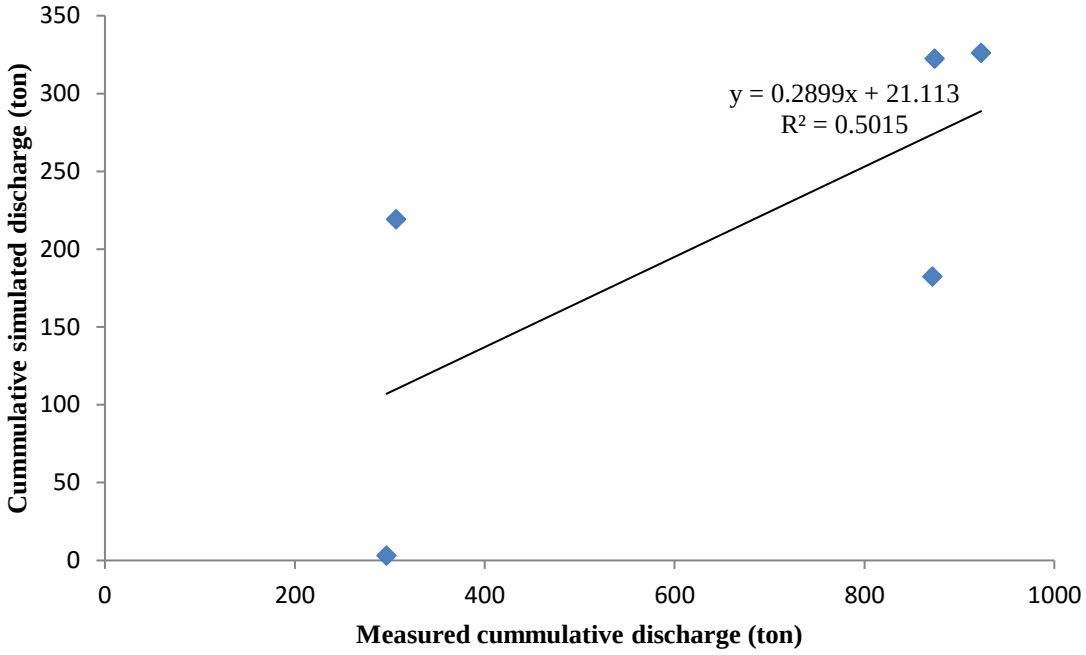

Figure 4. 9: Validation cumulative sediment discharge curve (Mh3)

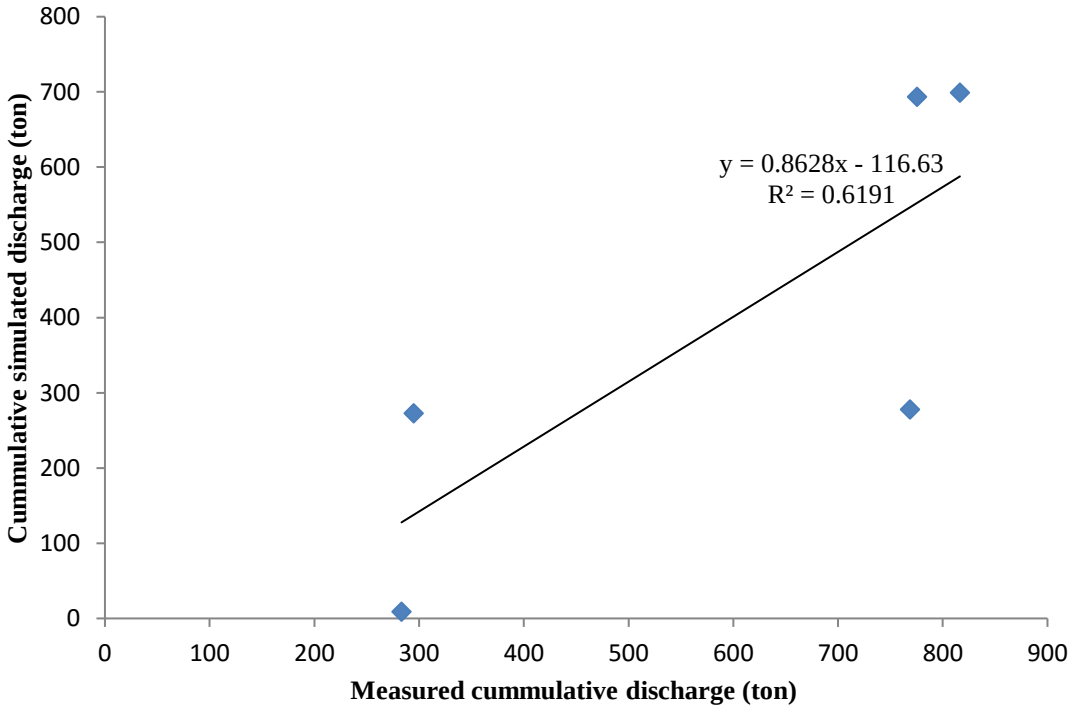

Figure 4. 10: Validation cumulative sediment discharge curve (Mh5)

4.3 Simulation Using HEC-RAS Model for 0.25, 0.50, 0.75 and Full Flow Scenarios.

Simulations were done for the selected scenarios for the purposes of plotting sediment rating curve from which other flow scenarios could be predicted. The conceptual parameters remained as calibrated in earlier simulation except the value on Manning's roughness coefficient which was set at finished concrete surface, with gravel on bottom, n=0.017 (Chow 1959). The Manning's coefficients obtained earlier at the current canal status, were not used due to change in canal characteristic arising from deposition of sediments along the canal bed. The discharge and respective water surface elevations, as derived from equations 30, 31 and 32 and tabulated in Table 4.4, were used in the simulation.

Table 4. 4: Discharge values for different flow scenarios

Flow scenario	Depth D (m)	Water Surface Elevation (m)	Slope S	Hydraulic radius R (m)	Velocity v (m/s)	Angle Ø (radians)	Cross section area (m^2)	Discharge Q (m^3/s)
0.25	0.375	1146.63	0.002447	0.2199	1.06	2.09	0.350	0.366
0.50	0.750	1147.01	0.002447	0.3750	1.51	3.14	0.883	1.337
0.75	1.125	1147.38	0.002447	0.4525	1.72	4.19	1.420	2.438
1.00	1.500	1147.76	0.002447	0.3750	1.51	6.28	1.770	2.674

The HEC-RAS model was run with sets of input data for the specified scenarios to give respective outputs of cumulative sediment discharge at a time step of 30 days. The sediment load input into the model was 0.5 kg/s, being the average load over the observation period. Observed storm load of 2.0 kg/s, input into the model, blocked the canal before the end of simulation time of 30 days. This means that continuous storms containing sediment load of 2.0 Kg/s can block the canal within a period of less than 30 days and therefore the farmers need to prevent such flows from entering the canal. The discharge for each scenario is shown in Table 4.5 below.

Table 4. 5: Cumulative sediment discharge for different discharge scenarios

Flow scenario water discharge		**Total cumulative sediment discharge at inlet A**		**Total cumulative sediment discharge at outlet B**	
m^3/s	**Log(m^3/s)**	**kg/s**	**Log(kg/s)**	**kg/s**	**Log(kg/s)**
0.366	-0.436520	18.4653	1.266357	11.4931	1.060437
1.337	0.126131	87.2522	1.940777	85.5752	1.932348
2.438	0.387034	198.9619	2.298770	191.659	2.282528
2.764	0.441538	216.4992	2.335456	208.5372	2.319184

The sediment discharge at inlet was much higher than the sediment discharge at outlet in all flow scenarios. This is an indication of net deposition for all flow scenarios but at different rates. Water discharge increased linearly with the cumulative sediment discharge plotted on a logarithmic scale at both canal inlet and outlet as shown in Figure 4.13. Inlet and outlet sediment curves converge with increase in discharge meaning that higher percentage of sediment entering the canal got transported to the outlet without deposition with increase in discharge. The farmers need to operate the canal at full discharge to minimise deposition.

Ideally, for no deposition, inlet sediment load should be equal to the sediment discharge at underground canal outlet. However, this may not be the case since the bed gradient is not uniform in the canal. There may appear that the sediment entering the canal is equivalent to sediment outflow and still the canal would get blocked due to temporal deposition and erosion taking place at different points along the canal. Simulation of sediment transport capacity for each class (see Table 4.6) was necessary to evaluate which particles were predominantly discharged through each manhole.

Each flow scenario was simulated for a time step of 30 days to determine sediment transport capacity at each manhole to evaluate whether all classes of sediment particles entering an observation station are transported through. The classes ranged from class 5 to 11 as in Table 4.6 adopted from grain size classification by American Geophysical Union. These were the grain classes sampled from canal bed at each manhole. The simulation results are shown in Appendix 7 to Appendix 30 in both tabular and graphical forms. It is seen from the Tables in the appendices that the transport capacity for the first day of measurement was nil. This is because the first measurement was taken before the sediment control volume and the flow is assumed to enter the first station at equilibrium sediment load where no deposition nor erosion takes place.

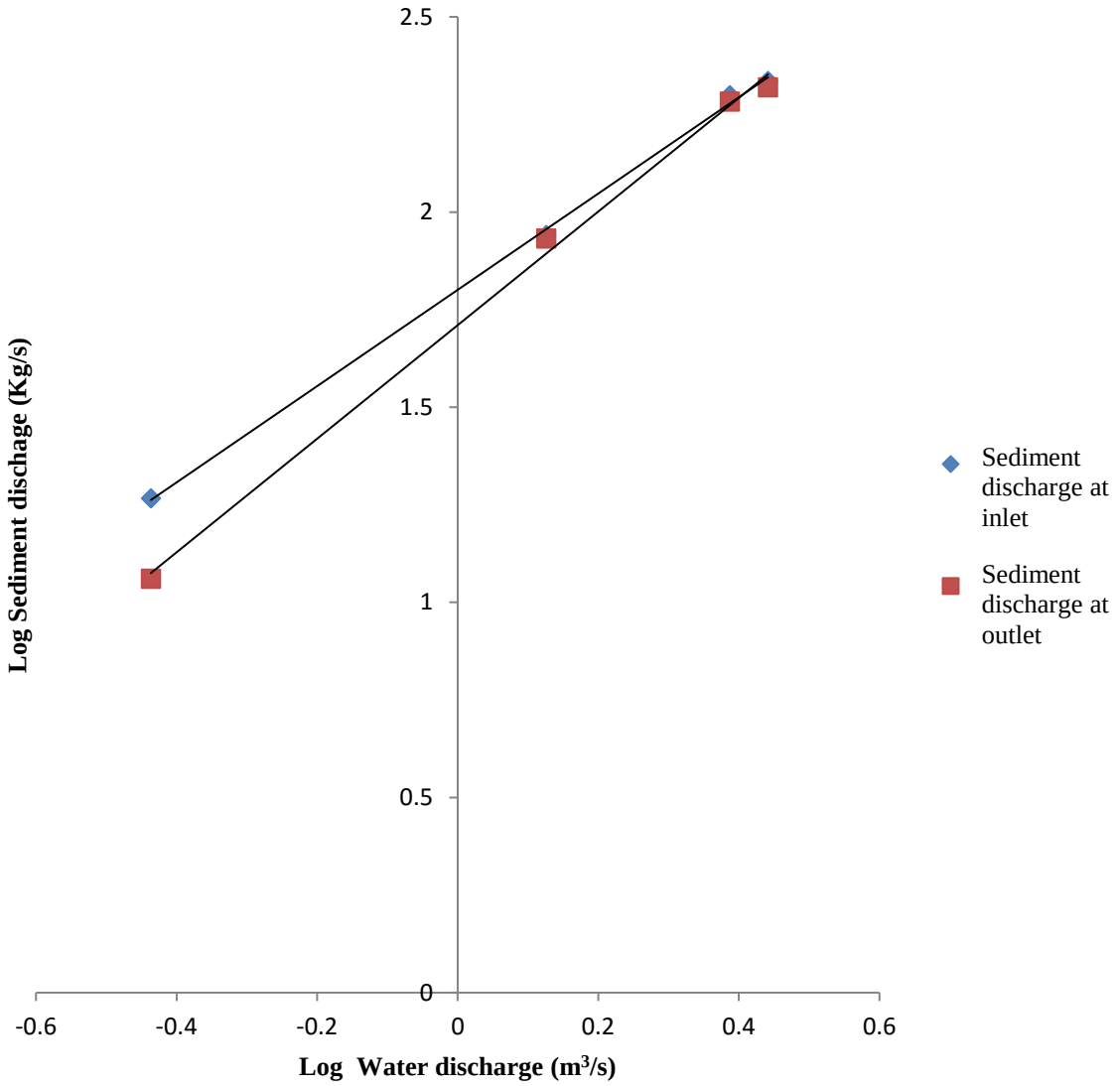

Figure 4. 11: Simulated sediment discharge at inlet and outlet.

For all flow scenarios transport capacity at manhole 1 dropped with time after entering the sediment control volume. The drop can be attributed to gradual decrease in bed slope and flow velocity thereby triggering deposition between manhole 3 and manhole 5 where the bed lope is more gentle.

The transport capacity at manhole 3 increased gradually at flow scenario of 0.366 m^3/s since at low flows the formation of an armoured layer occurs faster thereby sealing the would-be source of

sediment from previously deposited bed. Therefore, limited sediment supply does not meet the potential transport capacity. Higher flows of 1.337 m^3/s, 2.438 m^3/s and 2.674 m^3/s have higher velocities which can erode the previously deposited sediments creating more sediment supply and hence reducing the transport capacity.

The main source of sediments in manhole 5 is the canal length between manhole 3 and manhole 5 where the bedslope becomes gentler and the segment composed of previously deposited sediments. The availability of deposits balances the deficit in sediment supply making the change in transport capacity in this manhole more or less stable with time for all flow scenarios.

Table 4. 6: Grain size classification

Grain Class	Description	Grain diameter range (mm)
5	Coarse silt	0.032-0.0625
6	Very fine sand	0.0625-0.125
7	Fine sand	0.125-0.250
8	Medium sand	0.250-0.5
9	Coarse sand	0.5-1.0
10	Very coarse sand	1-2
11	Very fine gravel	2-4

SOURCE: Hydrologic Engineering Centre (2002).

Simulated total transport capacity increased with discharge at each manhole. Manhole 5 (Mh5) had the highest transport capacity followed by Manhole 1 (Mh1) and Manhole 3 (Mh3) in that order for different water discharge values of 1.337 m^3/s, 2.438 m^3/s and 2.674 m^3/s. Manhole 5 (Mh5) had the lowest transport capacity followed by Manhole 3 (Mh3) and Manhole 1 (Mh1) in that order for water discharge value of 0.366 m^3/s. Transport capacity depended on flow velocity and Mh5, having the highest bedslope, exhibited the highest transport capacity. Change of bedslope at Mh3 drastically reduced its transport capacity. At Mh1 the flow velocity was higher than at Mh3 due to uniform bedslope and lack of pooled water at the station. This showed that there is net deposition at Mh3 while further erosion of previously deposited particles occurred at Mh5, which was also dependent upon the supply of sediment available from upstream sources. The erosion phenomena may be misleading since sediment transport is limited by sediment availability. This case is referred to as sediment supply-limited (Julien, 1998). At flow scenario of 0.366 m^3/s transport capacity decreased gradually from Mh1, through Mh3 to Mh5; implying there was net deposition at Mh3 and Mh5.

Transport capacity at Manhole 1 (Mh1) could accommodate all grain classes sampled from the canal bed for all flow scenarios except for grain classes 10 and 11 whose capacity was comparatively low. At Manhole 3 (Mh3) transport capacity could not accommodate both grain classes 10 and 11 for all flow scenarios. This shows that previously transported grain classes 10 and 11 via Manhole 1 would be deposited at Manhole 3. Canal section at Manhole 3 is most likely to get blocked from piling deposits of grains 10 and 11 for all flow scenarios. Flow scenario discharge, 0.366 m^3/s, recorded zero transport capacity at Manhole 5 (Mh5) for grain classes 8, 9 and 11. The canal is likely to get blocked at Manhole 5 during low flows due to piled deposits of grain classes 8, 9 and 11. Change in bed slope may eventually give rise to deposits piling at Manhole 1 as well.

CHAPTER FIVE
CONCLUSION AND RECOMMENDATION

5.1 Conclusion

The critical velocity for no deposition determined by two different methods; Hjulstrom diagram and Lacey Theory were 0.54 m/s and 0.60 m/s respectively. Since Lacey Theory applies to greater depths than 1 m, then the theory can apply to the conditions in the canal. The varying depth of flow in the canal below 1 m made Hjulstrom method less reliable in determination of critical velocity as it was developed under conditions of 1 m flow depth. At discharge velocity of 0.60 m/s and full canal discharge, no sediment of the range sampled from the canal bed would be deposited. The velocities in the canal calculated using Mannings equation with n = 0.017 were much higher than critical velocity; ranging between 1.06 m/s to 1.71 m/s. The stream power depends on velocity of flow and therefore for deposition to occur, as was the situation then, there must have been factors contributing to reduction of velocity such as entrance loss due to contraction, exit loss due to expansion at the five manholes, formation of dunes at the bed and friction loss. Dunes alone can increase the Manning's n to between 0.02 to 0.04 (Schall *et al.*, 2008) and reduce velocity as much as between 0.4 m/s to 0.6 m/s. The velocity measurements done by the researcher were between 0.21 m/s - 0.34 m/s, almost half the critical velocity. The measured velocities could have been reduced further by existence of flattened bedslope developed after deposition in the canal.

During calibration of the HEC-RAS model, the manning's roughness coefficient, n, at Manhole 1 was 0.032 but 0.011 for Manhole 3 and Manhole 5. This was because the reduced slope induced much finer grains to settle at the bed hence reducing the value of Manning's roughness coefficient downstream. The conceptual parameters in the Ackers-White sediment transport equation were calibrated as A=0.20, C=0.004 and m=4. These calibration values can be used to predict sediment transport within the canal since the deviation of predicted from measured values were within the acceptable range of ± 100%.

HEC-RAS model simulation indicated a selective grain size sediment transport. This varied from one observation point to the other and would vary with canal discharge. The sediment load that can be carried through the canal without deposition therefore does not depend entirely on sediment concentration but also on grain size percent composition and the prevailing bed slope. The grain

classes 8, 9, 10 and 11 should be screened from entering the canal to avoid sediment deposition within the canal. Equilibrium sediment transport in the river becomes source of sediment deposits as soon as it enters the canal. This problem is aggravated by reduction of slope further downstream of irrigation canal. Piped flows are more likely to block where the bed slope reduces. This is due to reduction of transport capacity of flow. Sediment transport capacity increases with increase in flow discharge a higher proportion of sediment entering the canal is discharged at the outlet. Higher flow discharge is necessary to minimise deposition.

5.2 Recommendation

Further to research findings on this work the researcher recommended that further studies on the underground canal to collect more sets of data to improve accuracy in prediction of sediment discharge by HEC-RAS model and investigate the high values of n of 0.032 between manholes Mh1 and Mh3. The n value, this high, is not recommended for such a canal as documented by Chow (1959e). Future irrigation canal designs should avoid sudden reduction of bed slope even if the average slope is acceptable since the water discharge to the irrigation fields is never constant in practice. The HEC-RAS model can be used as a tool to design and evaluate irrigation canals' sediment transport capacity. Since the deposition has modified the canal bed slope and reduced its capacity to convey water, the underground canal should be dredged of all deposits, intake design improved and the farmers advised to observe sustainable operation and maintenance practices. To improve intake design to screen off sediment sizes as simulated by the model, the intake structure should be redesigned to include options such as installation of silt deflectors, raising of the height of the weir at inlet and construction of sedimentation basin. Deposition in the canal should be minimised by operating at high flows but not during flood flows, which usually contain high sediment load. This can be achieved through use of the flow control sluice gates already installed at the inlet. The gates should be closed temporarily during flood flows.

REFERENCES

Ackers, P. and White, W. R. (1973). Sediment transport: new approach and analysis. *ASCE Journal of Hydraulic Division, 99*(11), 2041-2060.

Ayibotele, N. B. and Tuffour-Darko , T. (1979). *Sediment Loads in the Southern Rivers of Ghana*. Accra, Ghana: Water Resources Research Unit.

Brownlie, W. R. (1981). *Prediction of flow depth and sediment discharge in open channels* (Tech. Rep. No. KH-R-43A). California Institute of Technology, Asadena, CA: W.M. Keck Laboratory of Hydraulics and Water Resources, Division of Engineering and Applied Science.

Chang, H. H. (1988). *Fluvial processes in river engineering*. Malabar, Florida: Krieger Publishing Company.

Chanson, H. (1999). *The Hydraulics of Open Channel Flow.* Arnold, 338 Euston Road, London, UK.

Chow, V.T. (1959). *Open-channel hydraulics*. New York, McGraw-Hill.

Coz, J. L., Camenen, B, Peyrard, X. and Dramais, G. (2012). Uncertainty in open-channel discharges measured with the velocity-area method. *Journal of Flow Measurement and Instrumentation, 26,* 18 - 29.

Daryl, B. S. and Century, F. (1992). *Sediment transport technology: water and sediment dynamics*: Michigan, USA: BookCrafters.

Depeweg, H. and Mendez, N. V. (2002). Sediment transport applications in irrigation canals. *Wiley InterScience Journal, Irrigation and Drainage, 51,* 167–179.

Depeweg, H. and Mendez, N. V. (2006). *A new approach to sediment Transport in the design and operation of Irrigation Canals*. USA: Routledge.

Einstein, H.A. (1950). The Bed-Load Function for Sediment Transportation in Open Channel Flows, *Technical Bulletin of the U.S. Department of Agriculture, Soil Conservation Service, Washington D.C., 1026.*

Einstein, H.A. (1968). Deposition of suspended particles in a gravel bed. *ASCE Journal of the Hydraulics Division, 94*(5), 1197-1205.

Engelund, F. and Hansen, E. (1972). *A monograph on sediment transport in alluvial streams*. Copenhagen, Denmark: Teknish Forlag Technical Press.

Finkner, F. C., Nearing, M. A., Foster, G. R., Gilley, J. E. (1989). A Simplified Equation for Modelling Sediment Transport Capacity. *Journal of ASAE* 32(5), 1545-1550.

Garde R. J., Ranga Raju K. G. (2000). *Mechanics of Sediment Transportation and Alluvial Stream Problems*, New Age International (P) Ltd Publishers, Daryaganj, New Delhi.

Gathenya, J. M. (2005). *Flood disaster management in Lake Victoria basin*. Paper presented at the Workshop of University Network for Disaster Risk Reduction in Africa, Makerere University, Kampala, Uganda.

Graf, W. H. (1984). *Hydraulics of Sediment Transport*. Water Resources Publications

Hassanzadeh, H., Faiznia, S., Bajestan, M., and Motamed, A. (2011). Estimate of Sediment Transport Rate at Karkheh River in Iran Using Selected Transport Formulas. *Journal of World Applied Sciences Journal 13*(2), 376-384.

Hjulstrom, F. (1935). Studies of the morphological activity of rivers as illustrated by the River Fyris. *Bulletin of the Geological Institute University of Uppsala, 25,* 221-527.

Hoel, P. G. (1984). *Introduction to mathematical statistics*. Canada: John Wiley and Sons.

Huang, J.V. and Bountry, J. (2009) DRAFT SRH-Capacity User Manual Version 1.37, U.S. Dept. of the Interior, Bureau of Reclamation, Technical Service Center, Denver CO.

Hudson, N. W. (1994). Field measurement of soil erosion and runoff. *FAO Soils Bulletin (FAO), 68,* 153.

Hydrologic Engineering Centre (2002). *HEC-RAS Hydraulic Reference Manual, Version 3.1, November 2002, CPD-69*. Davis, CA: U.S. Army Corps of Engineers.

Hydrologic Engineering Centre (2010). *HEC-RAS River Analysis System, Users' Manual, Version 4.1, November 2010, CPD-68*. Davis, CA: U.S. Army Corps of Engineers.

zsaJulien, P. Y. (1998). *Erosion and Sedimentation.* Cambridge, United Kingdom: Cambridge University Press.

Krause, P., Boyle, D. P. and Base, F. (2005). Comparison of different efficiency criteria for hydrological model Assessment. *Journal of Advances in Geosciences, 5,* 89-97.

Lacey, G. (1930). *Stable Channels in Alluvium.* Paper 4736, Proceedings of The Institution of Civil Engineers, Vol. 229, William Clowes & Sons Ltd., London, U.K. P. 259-292.

Laursen, E.M. (1958). The Total Sediment Load of Streams, *ASCE Journal of the Hydraulics Division, 84*(1), 1-36.

Lawrence, P. (1986). Sediment control in wadi irrigation systems. *Journal of Technical Background Papers: International, 4*, 91-101.

Martin, Y. (2003). Evaluation of bed load transport formulae using field evidence from the Vedder River, British Columbia. *Journal of Geomorphology, 53*, 75–95

McCully, P. (1996). *The Ecology and Politics of Large Dams.* London: Zed Books.

Meyer-Peter, E. and Mueller, R. (1948). *Formula for bed-load transport*. Paper presented at the International Association for Hydraulic Research, 2nd Meeting, Stockholm.

Morgan, R. P. C. (1986). *Soil Erosion and Conservation.* New York: John Wiley and Sons.

MOWI (2009). *District Irrigation Annual Report*, Nyando District.

Mountz, T. and Crowley, J. (2009) Comparison of HEC-RAS and InfoWorks RS: A Case Study in Grand Prairie, Texas. *World Environmental and Water Resources Congress 2009*, 1-10

Ong, C. and Orego, F. (2002). Links between land management, sedimentation, nutrient flows and smallholder irrigation in the Lake Victoria Basin. *The Changing Face of Irrigation in Kenya: Opportunities for Anticipating Change in Eastern and Southern Africa*. International Water Management Institute, Colombo, Sri Lanka, 135–154.

Onyando, J. O., Kisoyan, P. and Chemelil, M. C. (2004). Estimation of potential soil erosion of river Perkerra catchment in Kenya. *Journal of Water Resources Management, 19,* 133–143.

Parhi, P. K., Sankhua, R. N., Roy G. P. (2012). Calibration of Channel Roughness for Mahanadi River, (India) Using HEC-RAS Model, *Journal of Water Resource and Protection, 4,* 847-850

Parker, G. (1990). Surface based bed load transport relationship for gravel rivers. *Journal of Hydraulic Research*, *28*(4), 417–436.

Raju, K. G. R. and Kothyari, U. C. (2004). *Sediment management in hydroelectric projects.* Paper presented at the Ninth International Symposium on River Sedimentation, Yichang, China.

Rijn, V. (2007). *Manual Sediment Transport Measurements*. Amsterdam: Aqua Publications.

Schall, J. D., Richardson, E. V., Morris J. L. (2008), Introduction to Highway Hydraulics, *Journal of Hydraulic Design Series Number 4,* Ayres Associates Inc, Colorado, USA.

Santhi, C., Arnold, J. G., Williams, J. R., Dugas, W. A., Srinivasan, R. and Hauck, L. M. (2001) Validation of the SWAT model on a large river basin with point and nonpoint sources. *Journal of American Water Resources Assoc*. *37*(5), 1169-1188.

Signal, H. S. S., Joshi, G. C. and Verma, R. S. (1981). Sediment sampling in rivers and canals. *Erosion and Sediment Transport Measurement.* Paper presented at the Florence Symposium, India.

Simons, D. B. and Senturk, F. (1992). *Sediment Transport Technology: Water and Sediment Dynamics.* BookCrafters, Inc., Chelsea, Michigan, U.S.A.

Spillios, L. C. (1999). *Sediment intrusion and deposition near road crossings.* Unpublished master's thesis, University of Alberta, Alberta, Canada.

Strelkoff, T. S. and Bjorneberg, D. L. (1999). Hydraulic Modeling of Irrigation-Induced Furrow Erosion. *Selected paper from the 10th International Soil Conservation Organization Meeting held May 24-29, 1999 at Purdue University and the USDA-ARS National Soil Erosion Research Laboratory.*

Tikka, J. (2008). *Input variable selection methods for construction of interpretable regression models.* Doctoral thesis, Helsinki University of Technology, Dissertations in Information and Computer Science, Espoo, Finland.

Toffaletti, F. B. (1969). Definitive Computation of Sand Discharge in Rivers. *ASCE Journal of Hydraulics Division, 51*(1), 6357.

Vanoni, V.A. (1975). Sedimentation Engineering. *American Society of Civil Engineers, Manuals and Reports on Engineering Practice, 54*, 745.

Wilcock, P. R. and Crowe, J. C. (2003). Surface-based Transport Model for Mixed-Size Sediment. *ASCE Journal of Hydraulic Engineering, 129*(2), 120-128.

Wilcock, P. R. (2001). Toward a Practical Method for Estimating Sediment-Transport Rates in Gravel-Bed Rivers. *Journal of Earth Surface Processes and Landforms, 26*, 1395 – 1408.

Wu, W. (2004). Depth-Averaged Two-Dimensional Numerical Modeling of Unsteady Flow and Nonuniform Sediment Transport in Open Channels. *Journal of Hydraulic Engineering, 130*(10), 1013-1024.

Xiaoqing, Y. (2003). Manual on sediment Management and Measurement. *Operational Hydrology Report, 47.*

Yalin, Y. S. (1963). An expression for bed-load transportation. *ASCE Journal of the Hydraulics Division*, *89*(3), 221-250.

Yang, C. T. (1973). Incipient motion and sediment transport. *ASCE Journal of the Hydraulics Division*, *99*(7), 919 – 934.

Yang, C. T. (1979). Unit Stream Power Equations for Total Load. *Journal of Hydrology*, *40,* 123–138.

Yang, C. T. (1984). Unit stream power equation for gravel, *ASCE Journal of Hydraulics Division*, *110*(12), 1783-1797.

Yang, C. T. (1996). *Sediment Transport: Theory and Practice*. New York: McGraw-Hill Companies.

Yang C. T. and Simões F. J. M. (2002). *User's Manual for GSTARS3 (Generalized Sediment Transport model for Alluvial River Simulation version 3.0).* Technical Service Center, U.S. Bureau of Reclamation, Denver, Colorado.

Yang, C. T. and Song, C. C. S. (1979). Theory of minimum rate of energy dissipation. *ASCE Journal of the Hydraulics Division*, *105*(7), 769 – 784.

APPENDICES

Appendix 1: Grain size Classification (American Geophysical Union)

Sediment Material	Grain class	Grain diameter range (mm)	Geometric median (mm)
Clay	1	0.002-0.004	0.003
Very fine silt	2	0.004-0.008	0.006
Fine silt	3	0.008-0.016	0.011
Medium silt	4	0.016-0.032	0.023
Coarse silt	5	0.032-0.0625	0.045
Very fine sand	6	0.0625-0.125	0.088
Fine sand	7	0.125-0.250	0.177
Medium sand	8	0.250-0.5	0.354
Coarse sand	9	0.5-1.0	0.707
Very coarse sand	10	1-2	1.41
Very fine gravel	11	2-4	2.83
Fine gravel	12	4-8	5.66
Medium gravel	13	8-16	11.3
Coarse gravel	14	16-32	22.6
Very coarse gravel	15	32-64	45.3
Small cobble	16	64-128	90.5
Large cobble	17	128-256	181
Small boulders	18	256-512	362
Medium boulders	19	512-1024	724
Large boulders	20	1024-2048	1448

SOURCE: Hydraulic Engineering Centre (2002)

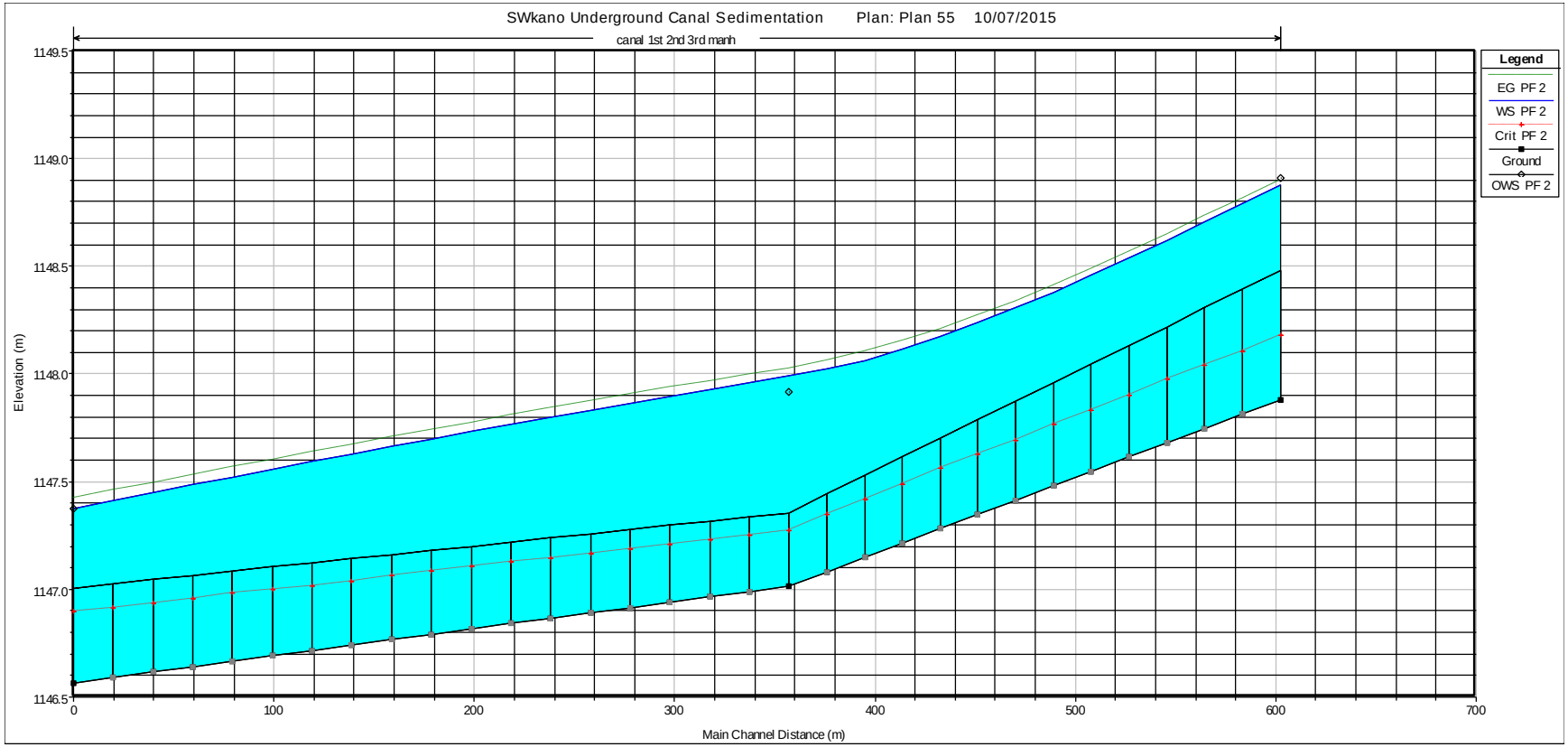

Appendix 2: HEC-RAS calibration water profile output for profile PF2

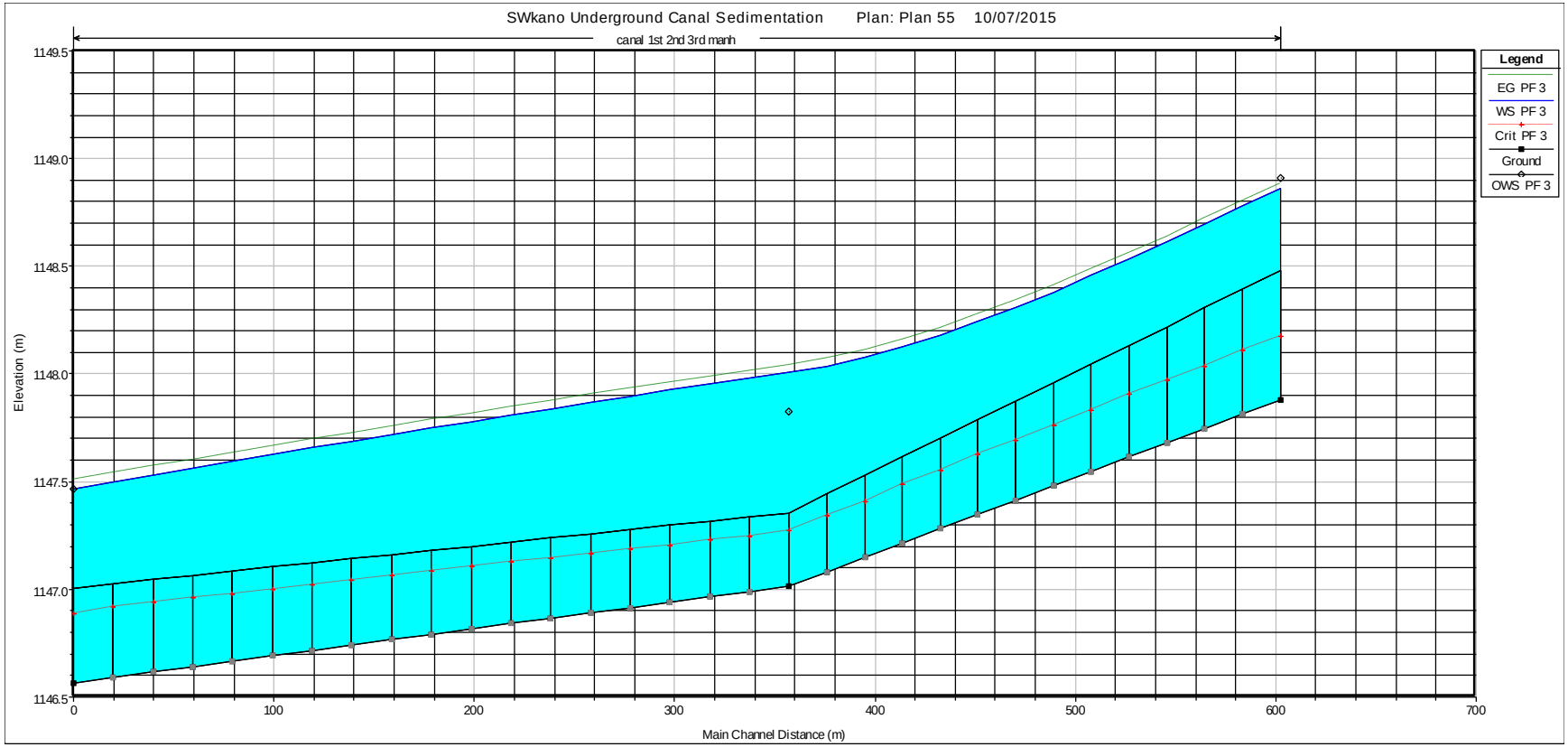

Appendix 3: HEC-RAS calibration water profile output for profile PF3

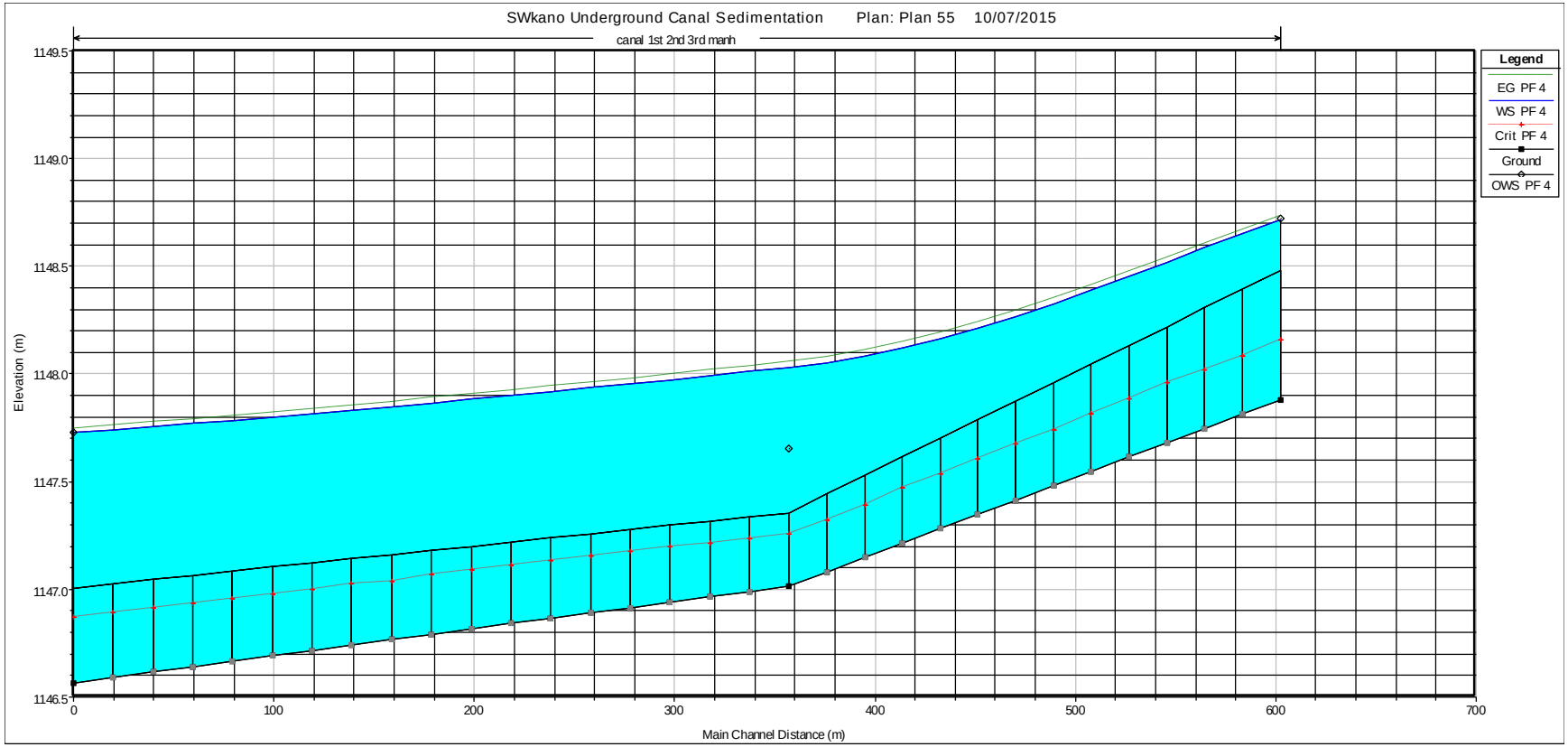

Appendix 4: HEC-RAS calibration water profile output for profile PF4

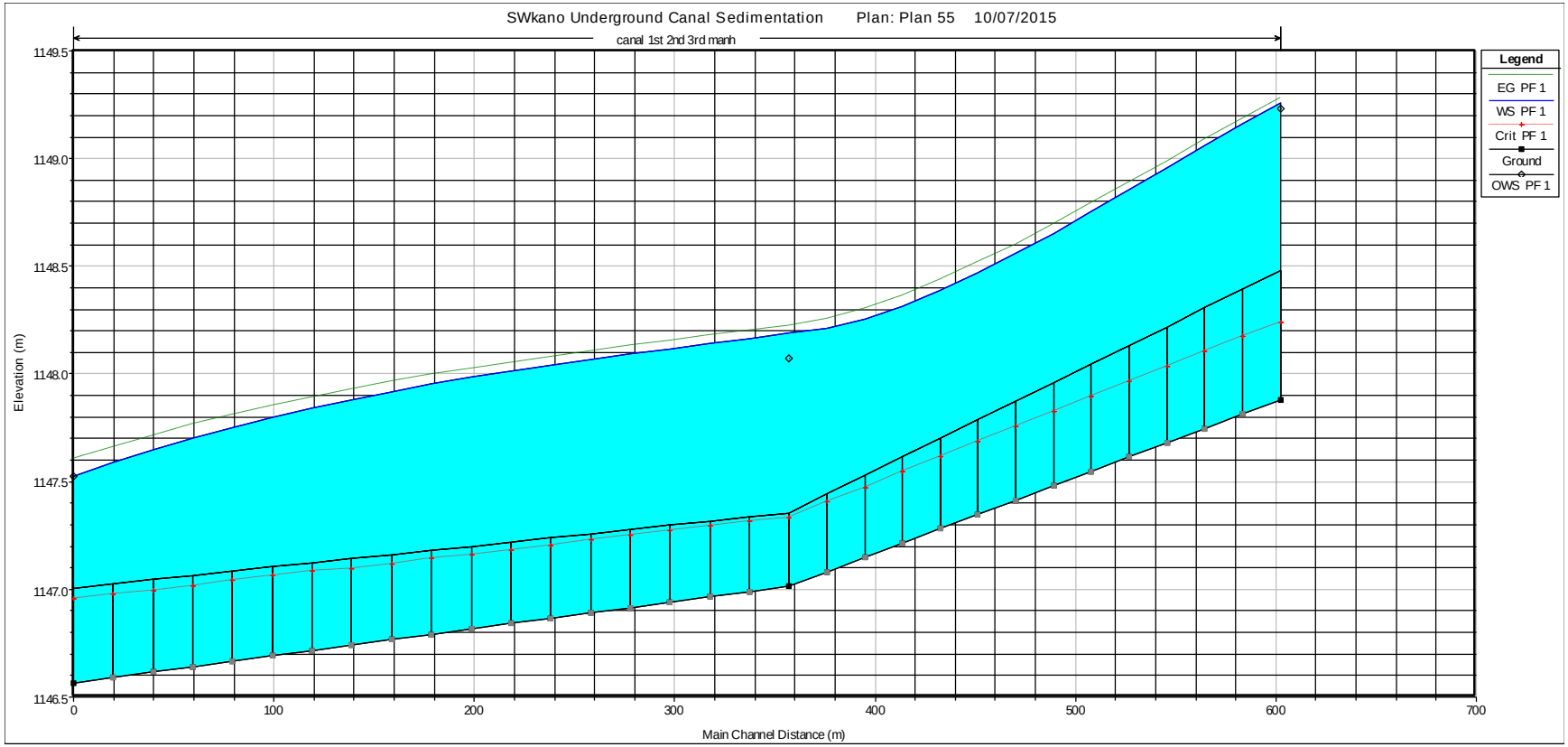

Appendix 5: HEC-RAS validation water profile output for profile PF1

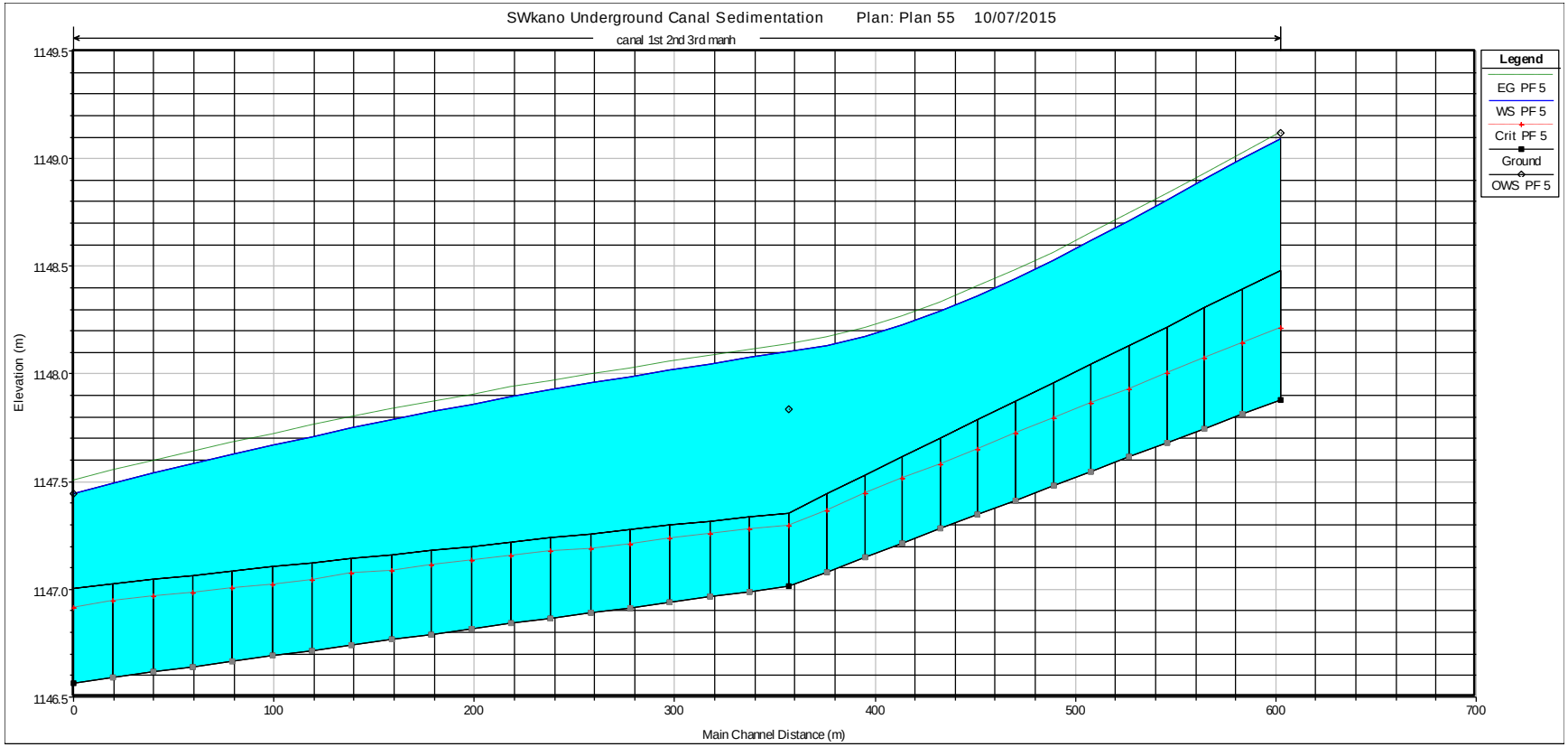

Appendix 6: HEC-RAS validation water profile output for profile PF5

Appendix 7: Table of simulated transport capacity for discharge of 0.366 m^3/s at Manhole 1 (Mh1)

	Time	Mass Capacity: All (tons/day)	Mass Capacity: 5 (tons/day)	Mass Capacity: 6 (tons/day)	Mass Capacity: 7 (tons/day)	Mass Capacity: 8 (tons/day)	Mass Capacity: 9 (tons/day)	Mass Capacity: 10 (tons/day)	Mass Capacity: 11 (tons/day)
1	9/15/2011 8:00	0	0	0	0	0	0	0	0
2	9/17/2011 10:00	2014.066	462.1588	829.0487	384.6288	308.8448	28.52779	0.7935575	6.34E-02
3	9/19/2011 12:00	2014.066	462.1588	829.0487	384.6288	308.8448	28.52779	0.7935575	6.34E-02
4	9/21/2011 14:00	2014.066	462.1588	829.0487	384.6288	308.8448	28.52779	0.7935575	6.34E-02
5	9/23/2011 16:00	2014.066	462.1588	829.0487	384.6288	308.8448	28.52779	0.7935575	6.34E-02
6	9/25/2011 18:00	2014.066	462.1588	829.0487	384.6288	308.8448	28.52779	0.7935575	6.34E-02
7	9/27/2011 20:00	2014.066	462.1588	829.0487	384.6288	308.8448	28.52779	0.7935575	6.34E-02
8	9/29/2011 22:00	1648.55	382.6646	682.0452	313.2545	247.6309	22.31414	0.5960171	4.44E-02
9	10/2/2011 0:00	1648.55	382.6646	682.0452	313.2545	247.6309	22.31414	0.5960171	4.44E-02
10	10/4/2011 2:00	1387.699	325.4353	576.6932	262.4746	204.5768	18.02322	0.4636644	0.0322996
11	10/6/2011 4:00	1619.627	376.3417	670.384	307.617	242.8286	21.83195	0.5809593	4.30E-02
12	10/8/2011 6:00	1737.49	402.0761	717.8765	330.6006	262.439	23.8062	0.642877	4.88E-02
13	10/10/2011 8:00	1573.163	366.1729	651.6404	298.5639	235.128	21.06051	0.556961	4.08E-02
14	10/12/2011 10:00	1514.868	353.3944	628.1058	287.2119	225.492	20.09839	0.5271957	0.0380234

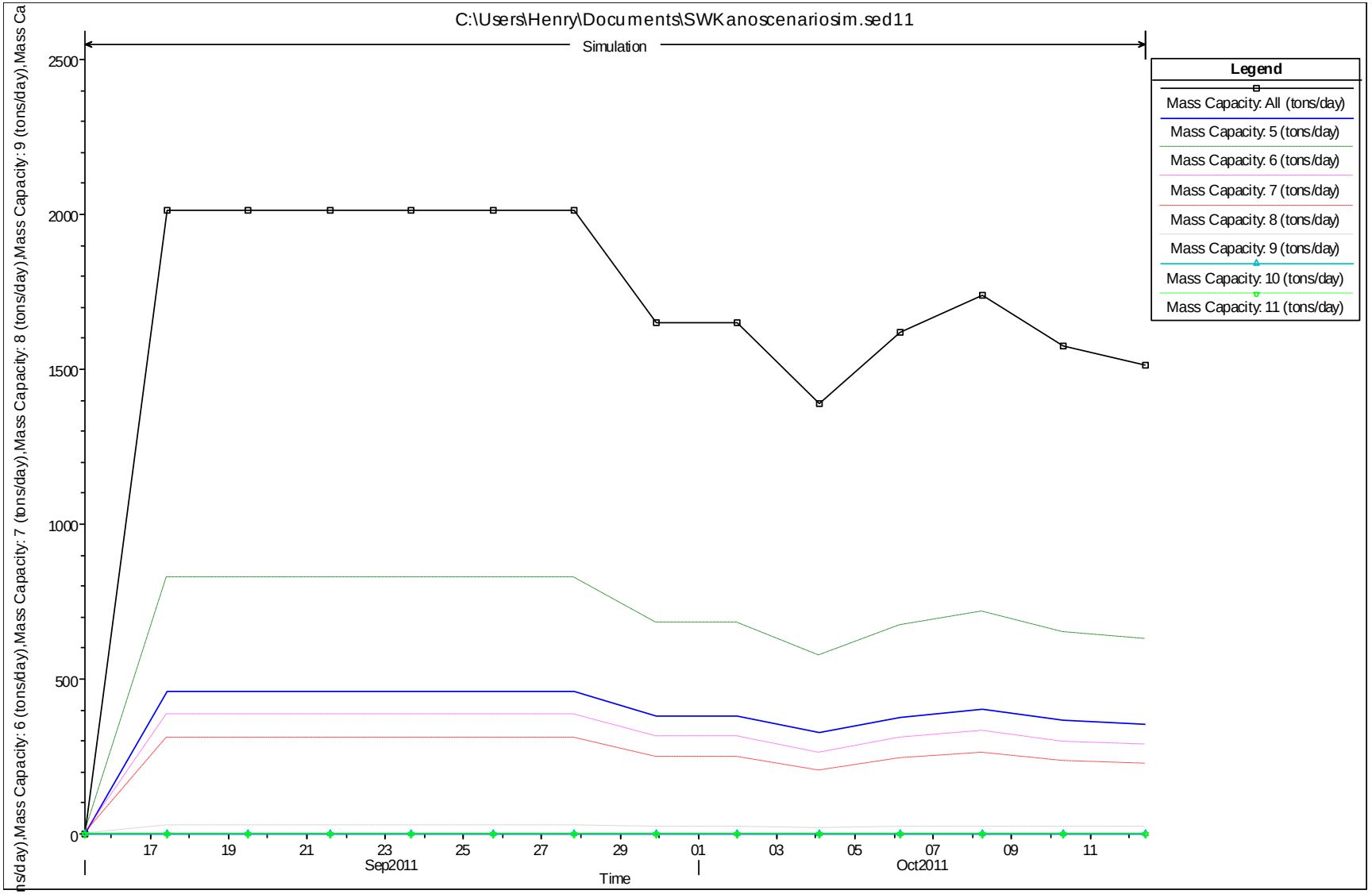

Appendix 8: Graph of simulated transport capacity for discharge of 0.366 m^3/s at Manhole 1 (Mh1)

Appendix 9: Table of simulated transport capacity for discharge of 0.366 m^3/s at Manhole 3 (Mh3)

	Time	Mass Capacity: All (tons/day)	Mass Capacity: 5 (tons/day)	Mass Capacity: 6 (tons/day)	Mass Capacity: 7 (tons/day)	Mass Capacity: 8 (tons/day)	Mass Capacity: 9 (tons/day)	Mass Capacity: 10 (tons/day)	Mass Capacity: 11 (tons/day)
1	9/15/2011 8:00	0	0	0	0	0	0	0	0
2	9/17/2011 10:00	1570.281	428.8797	753.7504	302.0037	80.14597	5.501064	0	0
3	9/19/2011 12:00	1585.33	422.7845	744.6591	316.0244	94.26225	7.599769	0	0
4	9/21/2011 14:00	1646.828	454.3027	779.6046	310.3549	94.02036	8.545716	0	0
5	9/23/2011 16:00	1593.799	454.8495	771.3417	280.902	78.94469	7.760629	0	0
6	9/25/2011 18:00	1487.196	429.5066	724.8381	257.6715	68.09079	7.088956	0	0
7	9/27/2011 20:00	1412.339	419.5119	693.9781	234.1966	58.23083	6.421957	0	0
8	9/29/2011 22:00	1436.845	433.105	728.6648	219.6819	49.67813	5.715606	0	0
9	10/2/2011 0:00	1467.145	378.6503	715.5833	299.1482	65.62934	8.134238	0	0
10	10/4/2011 2:00	3943.696	575.645	2048.092	1079.107	217.0344	23.81798	0	0
11	10/6/2011 4:00	3331.847	552.4276	1590.881	946.7685	217.2214	24.54901	0	0
12	10/8/2011 6:00	1215.429	321.1095	490.7484	295.7507	94.65681	13.16309	0	0
13	10/10/2011 8:00	2756.595	471.8898	1329.215	705.4293	223.882	26.17939	0	0
14	10/12/2011 10:00	1403.982	320.8918	531.7789	380.6232	153.0354	17.6529	0	0

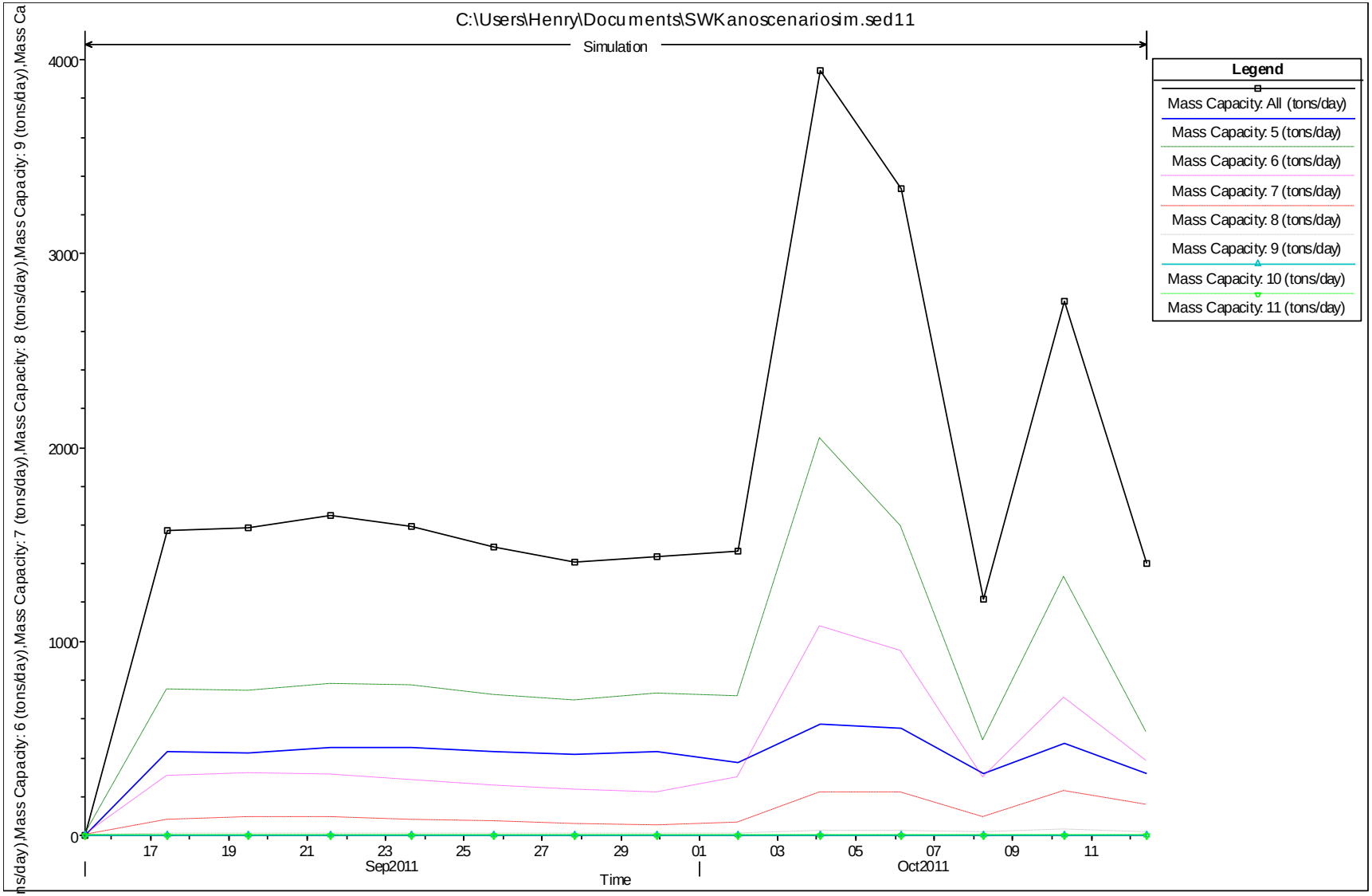

Appendix 10: Graph of simulated transport capacity for discharge of 0.366 m^3/s at Manhole 3 (Mh3)

Appendix 11: Table of simulated transport capacity for discharge of 0.366 m3/s at Manhole 5 (Mh5)

	Time	Mass Capacity: All (tons/day)	Mass Capacity: 5 (tons/day)	Mass Capacity: 6 (tons/day)	Mass Capacity: 7 (tons/day)	Mass Capacity: 8 (tons/day)	Mass Capacity: 9 (tons/day)	Mass Capacity: 10 (tons/day)	Mass Capacity: 11 (tons/day)
1	9/15/2011 8:00	0	0	0	0	0	0	0	0
2	9/17/2011 10:00	1083.007	430.9559	628.2578	22.57834	1.93E-03	0.1686126	1.044081	0
3	9/19/2011 12:00	1080.649	431.8842	611.9162	35.58055	0	0	1.268227	0
4	9/21/2011 14:00	1073.12	403.5039	619.9155	47.92252	0	0	1.777607	0
5	9/23/2011 16:00	1075.753	422.713	598.3983	52.68799	0	0	1.953935	0
6	9/25/2011 18:00	1096.396	435.2913	603.3383	55.82153	0	0	1.944631	0
7	9/27/2011 20:00	1086.258	420.3632	606.1831	58.50731	0	0	1.204827	0
8	9/29/2011 22:00	1112.598	432.7151	613.2441	65.30616	0	0	1.332618	0
9	10/2/2011 0:00	1046.466	370.6122	611.8354	63.08952	0	0	0.9289371	0
10	10/4/2011 2:00	1128.252	391.5533	666.3432	69.54992	0	0	0.805276	0
11	10/6/2011 4:00	1110.665	319.416	719.8208	70.87731	0	0	0.5513542	0
12	10/8/2011 6:00	952.5446	286.6221	598.2731	67.23045	0	0	0.4189065	0
13	10/10/2011 8:00	965.9603	314.4725	573.5031	77.56407	0	0	0.4206265	0
14	10/12/2011 10:00	970.2493	294.562	586.1919	89.12323	0	0	0.3722236	0

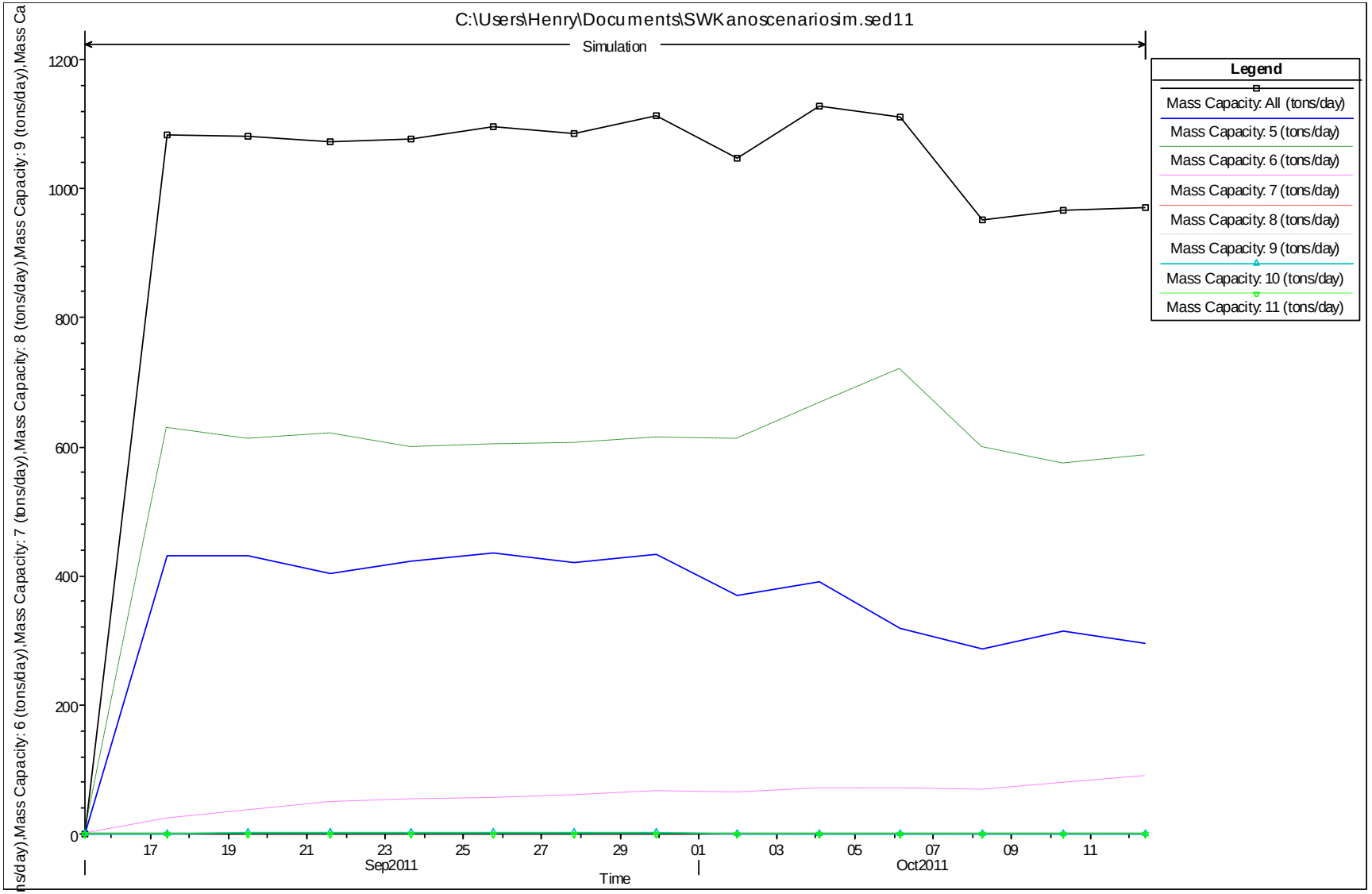

Appendix 12: Graph of simulated transport capacity for discharge of 0.366 m3/s at Manhole 5 (Mh5)

Appendix 13: Table of simulated transport capacity for discharge of 1.337 m3/s at Manhole 1 (Mh1)

	Time	Mass Capacity: All (tons/day)	Mass Capacity: 5 (tons/day)	Mass Capacity: 6 (tons/day)	Mass Capacity: 7 (tons/day)	Mass Capacity: 8 (tons/day)	Mass Capacity: 9 (tons/day)	Mass Capacity: 10 (tons/day)	Mass Capacity: 11 (tons/day)
1	9/15/2011 8:00	0	0	0	0	0	0	0	0
2	9/17/2011 10:00	9426.434	2906.101	4099.835	1470.099	890.7014	58.64427	1.01637	3.67E-02
3	9/19/2011 12:00	9068.903	2805.616	3946.907	1410.023	849.8724	55.50335	0.9480279	0.033129
4	9/21/2011 14:00	8836.045	2739.446	3847.157	1371.217	823.7696	53.51937	0.9055561	3.10E-02
5	9/23/2011 16:00	8588.99	2669.21	3741.278	1330.054	796.1306	51.42627	0.8610783	2.88E-02
6	9/25/2011 18:00	8404.78	2617.856	3662.432	1298.903	774.9316	49.8041	0.8263987	2.71E-02
7	9/27/2011 20:00	8330.139	2596.895	3630.456	1286.348	766.4417	49.15902	0.8127337	2.64E-02
8	9/29/2011 22:00	8133.436	2541.318	3546.121	1253.413	744.2939	47.48697	0.7776189	2.47E-02
9	10/2/2011 0:00	7996.604	2502.412	3487.406	1230.612	729.0522	46.34447	0.7538632	2.36E-02
10	10/4/2011 2:00	7949.09	2488.862	3467.009	1222.712	723.787	45.95122	0.7457289	2.32E-02
11	10/6/2011 4:00	7791.311	2443.735	3399.248	1196.537	706.3936	44.65697	0.7191054	0.0220117
12	10/8/2011 6:00	7813.783	2450.174	3408.902	1200.26	708.8629	44.84027	0.7228626	2.22E-02
13	10/10/2011 8:00	7662.625	2408.395	3344.136	1174.526	691.3432	43.50954	0.6950326	0.0208909
14	10/12/2011 10:00	7608.283	2393.571	3320.867	1165.185	684.9341	43.02002	0.6847692	2.04E-02

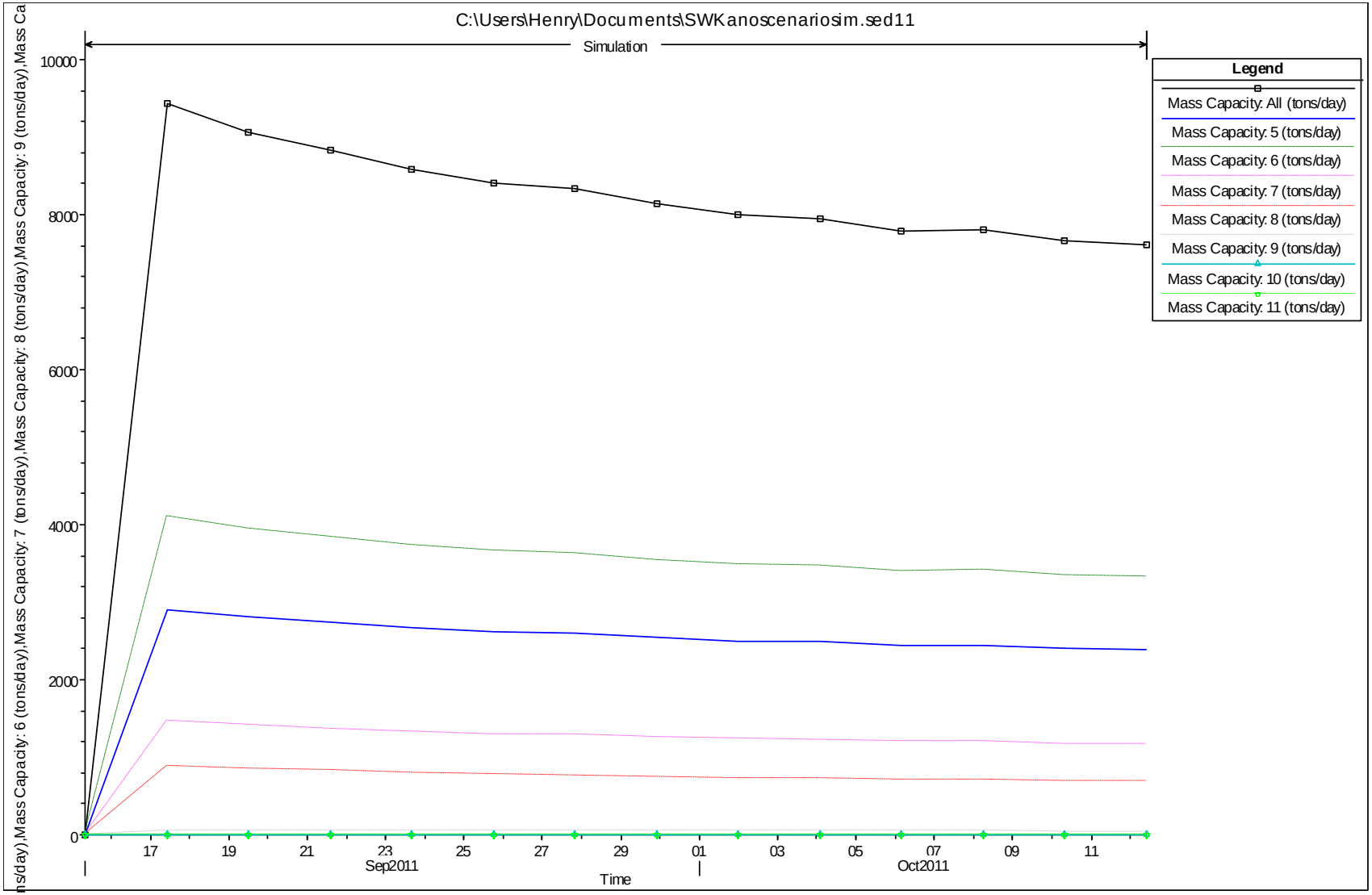

Appendix 14: Graph of simulated transport capacity for discharge of 1.337 m3/s at Manhole 1 (Mh1)

Appendix 15: Table of simulated transport capacity for discharge of 1.337 m3/s at Manhole 3 (Mh3)

	Time	Mass Capacity: All (tons/day)	Mass Capacity: 5 (tons/day)	Mass Capacity: 6 (tons/day)	Mass Capacity: 7 (tons/day)	Mass Capacity: 8 (tons/day)	Mass Capacity: 9 (tons/day)	Mass Capacity: 10 (tons/day)	Mass Capacity: 11 (tons/day)
1	9/15/2011 8:00	0	0	0	0	0	0	0	0
2	9/17/2011 10:00	8831.233	2809.128	4031.531	1440.369	533.5693	16.63599	0	0
3	9/19/2011 12:00	8794.363	2787.403	3906.19	1395.927	679.7969	25.04696	0	0
4	9/21/2011 14:00	8685.34	2727.824	3825.876	1385.859	712.093	33.6883	0	0
5	9/23/2011 16:00	8493.51	2625.042	3740.565	1360.24	726.7177	40.94504	0	0
6	9/25/2011 18:00	8412.148	2604.321	3666.624	1338.498	753.5125	49.19266	0	0
7	9/27/2011 20:00	8229.204	2576.506	3584.688	1283.655	730.3517	54.00383	0	0
8	9/29/2011 22:00	7524.527	2354.52	3227.171	1182.708	702.076	58.05338	0	0
9	10/2/2011 0:00	7991.468	2490.144	3459.445	1241.775	735.3394	64.76465	0	0
10	10/4/2011 2:00	7975.25	2485.928	3459.891	1251.982	709.6753	67.77395	0	0
11	10/6/2011 4:00	7857.433	2432.737	3414.097	1237.458	702.5366	70.6048	0	0
12	10/8/2011 6:00	7878.539	2449.148	3406.398	1229.07	717.9818	75.94043	0	0
13	10/10/2011 8:00	7751.074	2392.419	3359.065	1222.181	699.4973	77.91171	0	0
14	10/12/2011 10:00	7699.711	2392.428	3324.036	1209.436	693.5449	80.26659	0	0

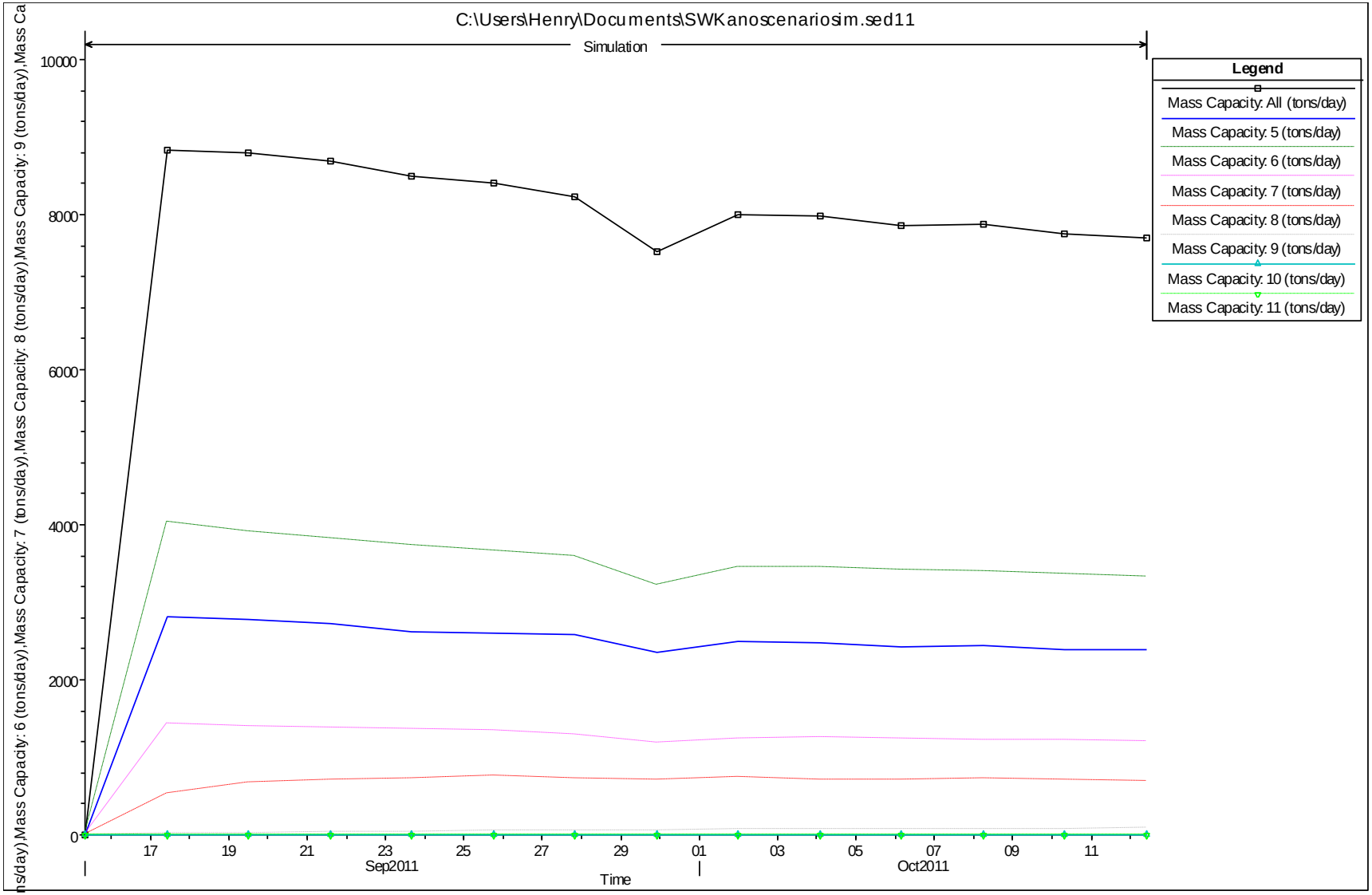

Appendix 16: Graph of simulated transport capacity for discharge of 1.337 m3/s at Manhole 3 (Mh3)

Appendix 17: Table of simulated transport capacity for discharge of 1.337 m3/s at Manhole 5 (Mh5)

	Time	Mass Capacity: All (tons/day)	Mass Capacity: 5 (tons/day)	Mass Capacity: 6 (tons/day)	Mass Capacity: 7 (tons/day)	Mass Capacity: 8 (tons/day)	Mass Capacity: 9 (tons/day)	Mass Capacity: 10 (tons/day)	Mass Capacity: 11 (tons/day)
1	9/15/2011 8:00	0	0	0	0	0	0	0	0
2	9/17/2011 10:00	34972.45	14373.71	13770.03	6336.413	431.4355	34.20267	26.10996	0.5469546
3	9/19/2011 12:00	32882.13	13425.26	12861.41	5918.302	620.3162	31.94579	24.38708	0.5108633
4	9/21/2011 14:00	32372.49	13194.02	12639.88	5816.363	666.3667	31.39555	23.96703	0.502064
5	9/23/2011 16:00	31776.89	12923.02	12376.53	5693.713	728.5545	30.72532	23.85619	0.4915352
6	9/25/2011 18:00	31743.13	12909.24	12363.33	5687.644	727.7778	30.69256	23.94763	0.4910112
7	9/27/2011 20:00	31739.05	12907.57	12361.74	5686.911	727.684	30.68861	23.95867	0.4909479
8	9/29/2011 22:00	31532.37	12819.93	12277.8	5648.296	728.8104	33.17624	23.86317	0.4876143
9	10/2/2011 0:00	30654.25	12440.67	11914.58	5481.199	755.5211	38.02868	23.77183	0.473189
10	10/4/2011 2:00	30262.51	12279.11	11759.85	5410.016	745.7093	43.52851	23.82772	0.4670438
11	10/6/2011 4:00	29890.6	12125.64	11612.88	5342.401	736.3894	48.98939	23.83896	0.4612066
12	10/8/2011 6:00	29665.93	12033.01	11524.16	5301.587	730.7635	52.07692	23.88266	0.4576831
13	10/10/2011 8:00	29479.3	11956.05	11450.46	5267.681	726.09	54.65392	23.91681	0.4547561
14	10/12/2011 10:00	29154.6	11822	11322.07	5208.619	717.949	59.61702	23.89254	0.4496573

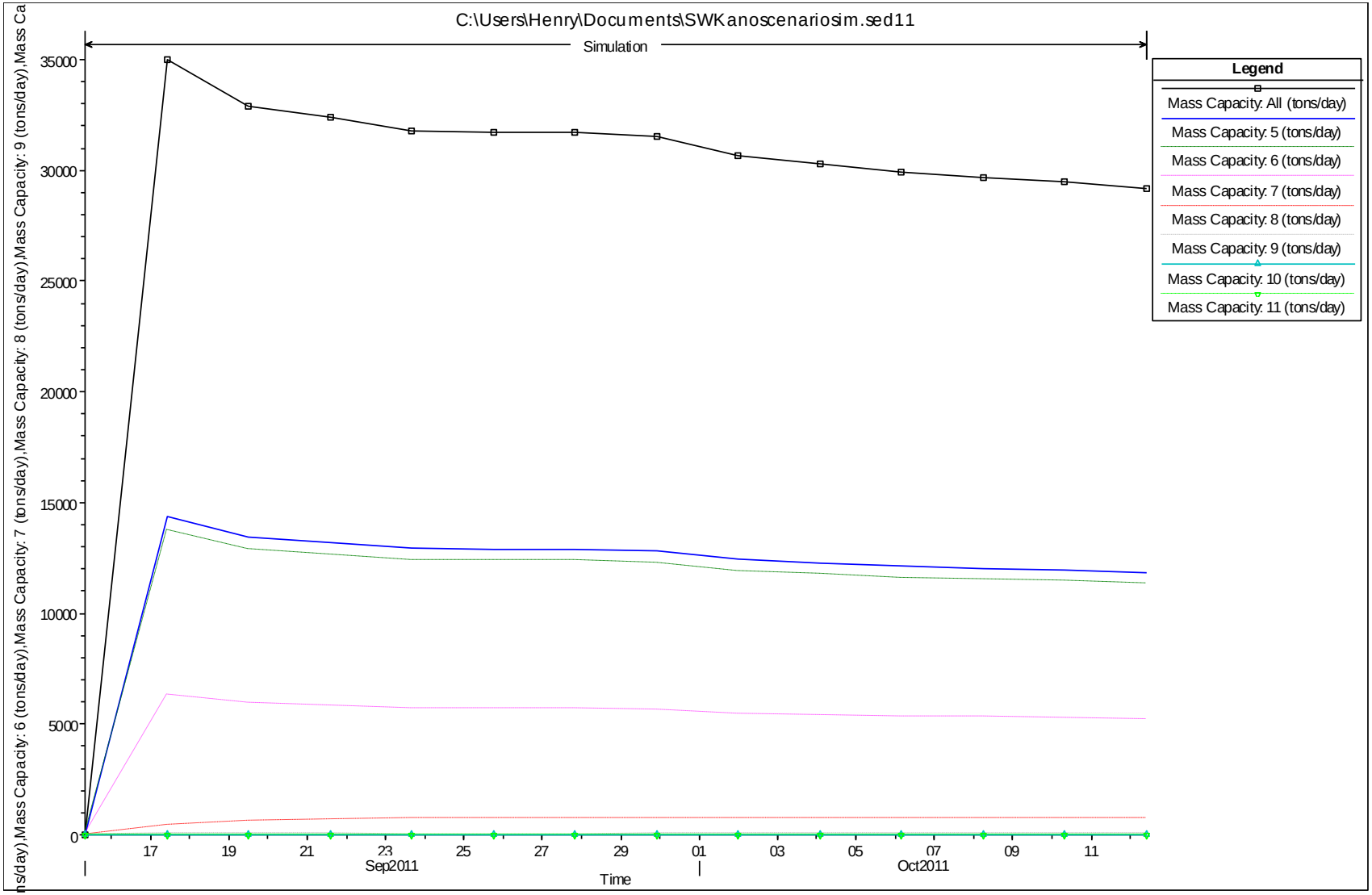

Appendix 18: Graph of simulated transport capacity for discharge of 1.337 m3/s at Manhole 5 (Mh5)

Appendix 19: Table of simulated transport capacity for discharge of 2.438 m3/s at Manhole 1 (Mh1)

	Time	Mass Capacity: All (tons/day)	Mass Capacity: 5 (tons/day)	Mass Capacity: 6 (tons/day)	Mass Capacity: 7 (tons/day)	Mass Capacity: 8 (tons/day)	Mass Capacity: 9 (tons/day)	Mass Capacity: 10 (tons/day)	Mass Capacity: 11 (tons/day)
1	9/15/2011 8:00	0	0	0	0	0	0	0	0
2	9/17/2011 10:00	28444.81	9097.674	12347.76	4285.205	2543.574	167.4587	3.015006	0.1238468
3	9/19/2011 12:00	21887.81	7039.062	9520.792	3280.695	1921.623	123.4443	2.11902	0.0783291
4	9/21/2011 14:00	21239.06	6834.866	9240.796	3181.523	1860.594	119.1742	2.033997	7.42E-02
5	9/23/2011 16:00	17519.1	5661.805	7634.063	2613.785	1512.793	95.04301	1.561348	5.22E-02
6	9/25/2011 18:00	17145.03	5543.615	7472.364	2556.79	1478.041	92.65295	1.515341	5.01E-02
7	9/27/2011 20:00	16398.31	5307.546	7149.507	2443.076	1408.805	87.90396	1.424411	4.61E-02
8	9/29/2011 22:00	16329.03	5285.634	7119.547	2432.53	1402.39	87.46487	1.416037	4.57E-02
9	10/2/2011 0:00	16013.24	5185.733	6982.973	2384.467	1373.173	85.46684	1.378007	4.41E-02
10	10/4/2011 2:00	16583.72	5366.182	7229.685	2471.304	1425.979	89.08037	1.446874	4.71E-02
11	10/6/2011 4:00	16854.38	5451.753	7346.711	2512.52	1451.071	90.80096	1.479803	4.85E-02
12	10/8/2011 6:00	15473.67	5014.96	6749.577	2302.382	1323.333	82.06608	1.313563	0.0412867
13	10/10/2011 8:00	14911.55	4836.931	6506.359	2216.914	1271.522	78.54128	1.247165	3.85E-02
14	10/12/2011 10:00	16228.33	5253.784	7076.001	2417.203	1393.07	86.82718	1.403886	4.52E-02

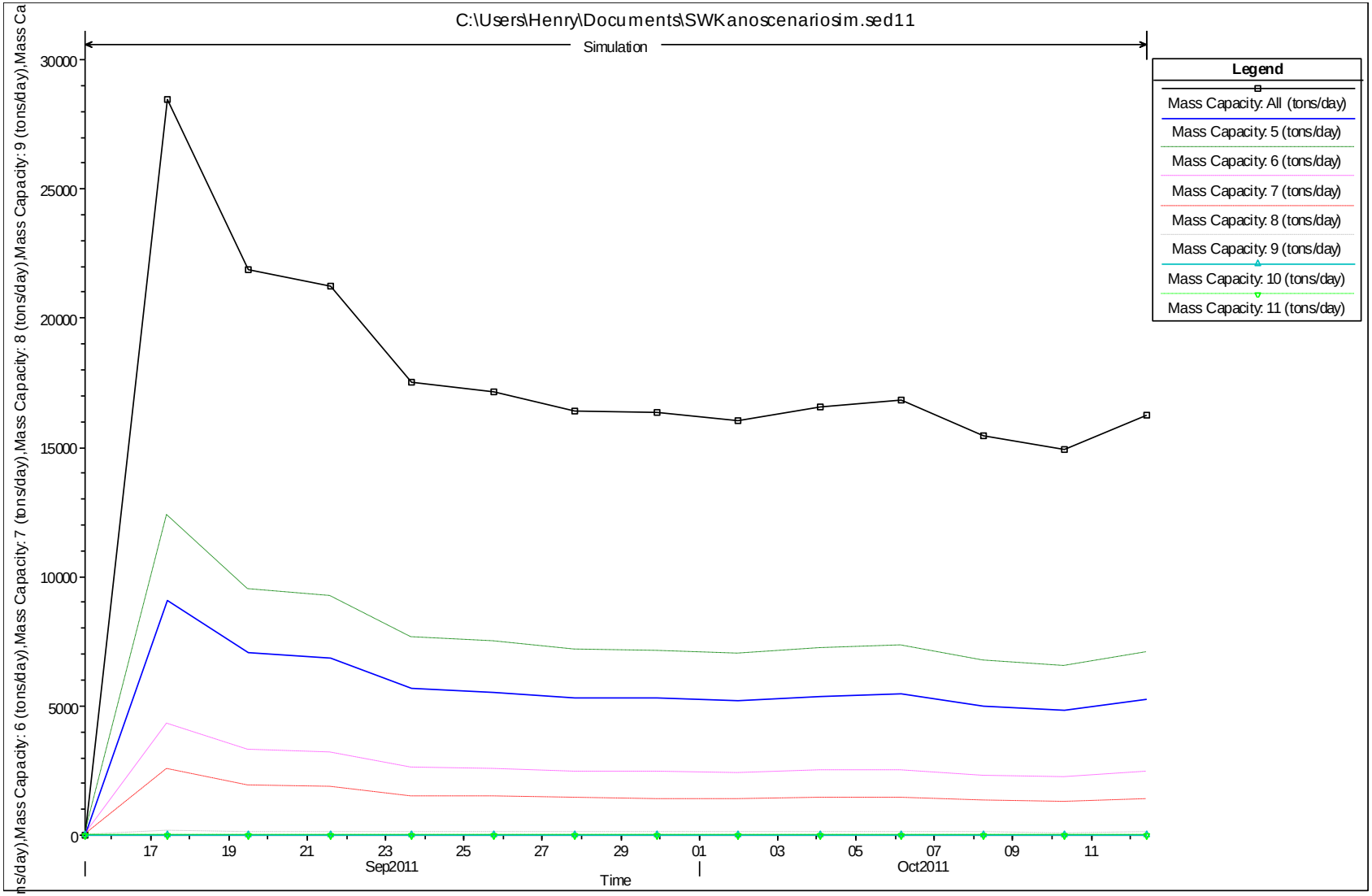

Appendix 20: Graph of simulated transport capacity for discharge of 2.438 m3/s at Manhole 1 (Mh1)

Appendix 21: Table of simulated transport capacity for discharge of 2.438 m3/s at Manhole 3 (Mh3)

	Time	Mass Capacity: All (tons/day)	Mass Capacity: 5 (tons/day)	Mass Capacity: 6 (tons/day)	Mass Capacity: 7 (tons/day)	Mass Capacity: 8 (tons/day)	Mass Capacity: 9 (tons/day)	Mass Capacity: 10 (tons/day)	Mass Capacity: 11 (tons/day)
1	9/15/2011 8:00	0	0	0	0	0	0	0	0
2	9/17/2011 10:00	25547.01	6745.535	12573.89	4747.75	1462.465	17.37702	0	0
3	9/19/2011 12:00	19633.03	4979.621	9637.172	3446.051	1546.187	24.00322	0	0
4	9/21/2011 14:00	20558.79	6497.22	8988.161	3291.634	1744.668	37.10107	0	0
5	9/23/2011 16:00	17827.62	4114.201	8545.078	3301.91	1819.266	47.15996	0	0
6	9/25/2011 18:00	17073.67	3979.213	8006.374	3175.676	1854.528	57.87519	0	0
7	9/27/2011 20:00	15627.97	3556.207	7522.119	2840.808	1649.729	59.10649	0	0
8	9/29/2011 22:00	15456.58	3529.891	7448.212	2774.941	1635.795	67.74065	0	0
9	10/2/2011 0:00	15315.5	3522.443	7268.347	2790.711	1655.709	78.28677	0	0
10	10/4/2011 2:00	16447.43	4705.528	7426.857	2667.177	1562.835	85.03586	0	0
11	10/6/2011 4:00	16682.2	4825.557	7547.492	2680.522	1536.141	92.48853	0	0
12	10/8/2011 6:00	15147.26	3521.431	7116.535	2773.828	1630.393	105.0703	0	0
13	10/10/2011 8:00	14525.74	3352.601	6836.98	2652.965	1573.171	110.0187	0	0
14	10/12/2011 10:00	16023.01	4624.464	7222.978	2576.877	1484.648	114.0437	0	0

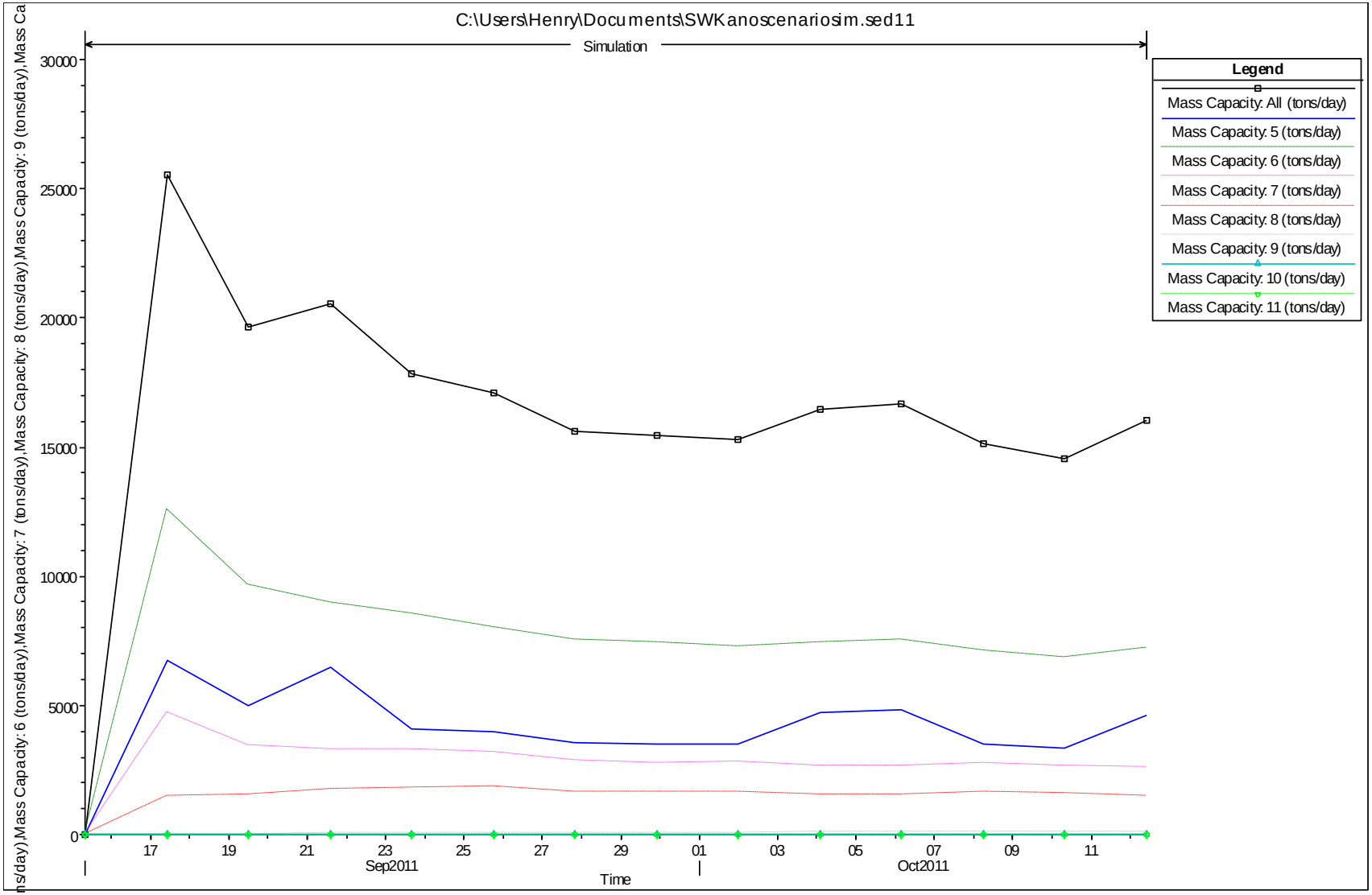

Appendix 22: Graph of simulated transport capacity for discharge of 2.438 m3/s at Manhole 3 (Mh3)

Appendix 23: Table of simulated transport capacity for discharge of 2.438 m3/s at Manhole 5 (Mh5)

	Time	Mass Capacity: All (tons/day)	Mass Capacity: 5 (tons/day)	Mass Capacity: 6 (tons/day)	Mass Capacity: 7 (tons/day)	Mass Capacity: 8 (tons/day)	Mass Capacity: 9 (tons/day)	Mass Capacity: 10 (tons/day)	Mass Capacity: 11 (tons/day)
1	9/15/2011 8:00	0	0	0	0	0	0	0	0
2	9/17/2011 10:00	803108.8	429503.3	313937.7	58862.86	756.2013	9.963507	36.99573	1.723332
3	9/19/2011 12:00	803112.4	429505.2	313939.2	58863.19	756.2061	9.963579	36.99605	1.723351
4	9/21/2011 14:00	787596.3	420967.6	307699	57693.19	1188.752	9.765553	36.2608	1.689106
5	9/23/2011 16:00	777251.7	415275.8	303538.6	56913.12	1477.021	9.633506	35.77047	1.666264
6	9/25/2011 18:00	777252.8	415276.4	303539.1	56913.21	1477.024	9.633526	35.77056	1.666269
7	9/27/2011 20:00	776612.4	414924	303281.5	56864.92	1494.874	9.625353	35.74022	1.664855
8	9/29/2011 22:00	771778.6	412264.3	301337.5	56500.41	1629.6	9.563655	35.51112	1.654184
9	10/2/2011 0:00	771778.6	412264.3	301337.5	56500.41	1629.6	9.563656	35.51113	1.654184
10	10/4/2011 2:00	771778.6	412264.4	301337.5	56500.42	1629.6	9.563657	35.51113	1.654184
11	10/6/2011 4:00	771778.7	412264.4	301337.5	56500.43	1629.601	9.563658	35.51114	1.654185
12	10/8/2011 6:00	771421.4	412072.6	301197.3	56474.14	1628.843	11.28737	35.49462	1.653415
13	10/10/2011 8:00	770625.1	411645.2	300884.9	56415.57	1627.153	15.12744	35.45781	1.651701
14	10/12/2011 10:00	769601	411095.5	300483.2	56340.23	1624.98	20.06638	35.41046	1.649495

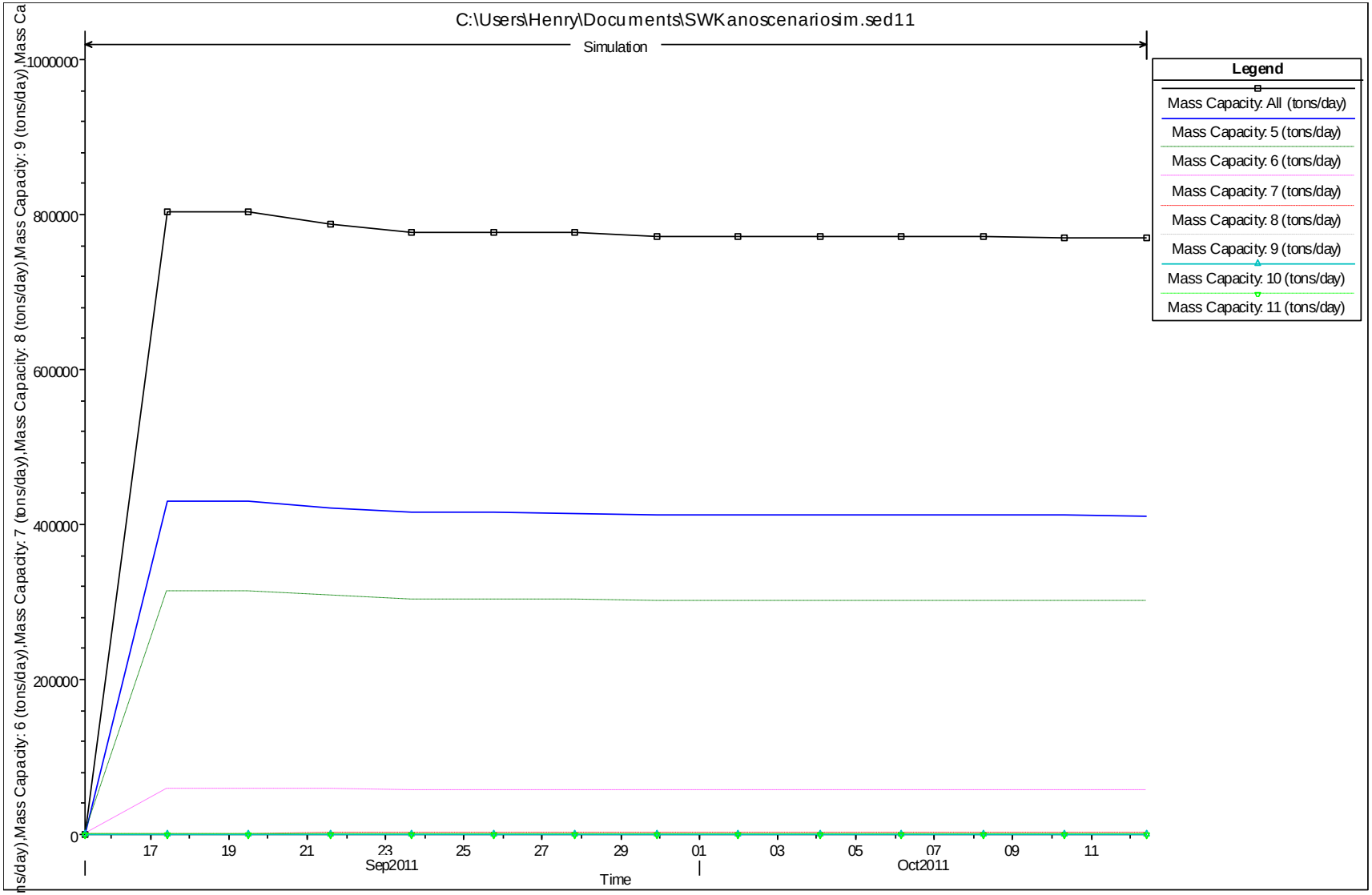

Appendix 24: Graph of simulated transport capacity for discharge of 2.438 m3/s at Manhole 5 (Mh5)

Appendix 25: Table of simulated transport capacity for discharge of 2.674 m3/s at Manhole 1 (Mh1)

	Time	Mass Capacity: All (tons/day)	Mass Capacity: 5 (tons/day)	Mass Capacity: 6 (tons/day)	Mass Capacity: 7 (tons/day)	Mass Capacity: 8 (tons/day)	Mass Capacity: 9 (tons/day)	Mass Capacity: 10 (tons/day)	Mass Capacity: 11 (tons/day)
1	9/15/2011 8:00	0	0	0	0	0	0	0	0
2	9/17/2011 10:00	30821.45	9826.02	13374.69	4657.101	2776.204	183.9492	3.349144	0.140791
3	9/19/2011 12:00	25461.41	8149.006	11065.01	3833.476	2263.798	147.4171	2.595574	0.1014271
4	9/21/2011 14:00	23124.99	7416.267	10057.23	3475.184	2042.164	131.7823	2.279608	8.56E-02
5	9/23/2011 16:00	20513.77	6595.863	8930.07	3075.365	1795.917	114.5514	1.936819	6.91E-02
6	9/25/2011 18:00	19828.55	6380.289	8634.124	2970.567	1731.58	110.0764	1.848835	0.0649707
7	9/27/2011 20:00	19267.67	6203.739	8391.828	2884.826	1679.012	106.429	1.777465	6.17E-02
8	9/29/2011 22:00	19142.99	6164.479	8337.959	2865.771	1667.338	105.6201	1.761681	6.09E-02
9	10/2/2011 0:00	18957.83	6106.168	8257.954	2837.476	1650.009	104.4202	1.738295	5.98E-02
10	10/4/2011 2:00	18728.49	6033.933	8158.856	2802.437	1628.559	102.9362	1.709424	5.85E-02
11	10/6/2011 4:00	18032.94	5814.755	7858.25	2696.208	1563.599	98.45084	1.622498	5.46E-02
12	10/8/2011 6:00	18174.1	5859.248	7919.263	2717.761	1576.771	99.35921	1.64006	5.54E-02
13	10/10/2011 8:00	17917.58	5778.39	7808.386	2678.596	1552.839	97.70922	1.608176	5.39E-02
14	10/12/2011 10:00	16035.2	5184.378	6994.378	2391.46	1377.857	85.70476	1.378476	4.38E-02

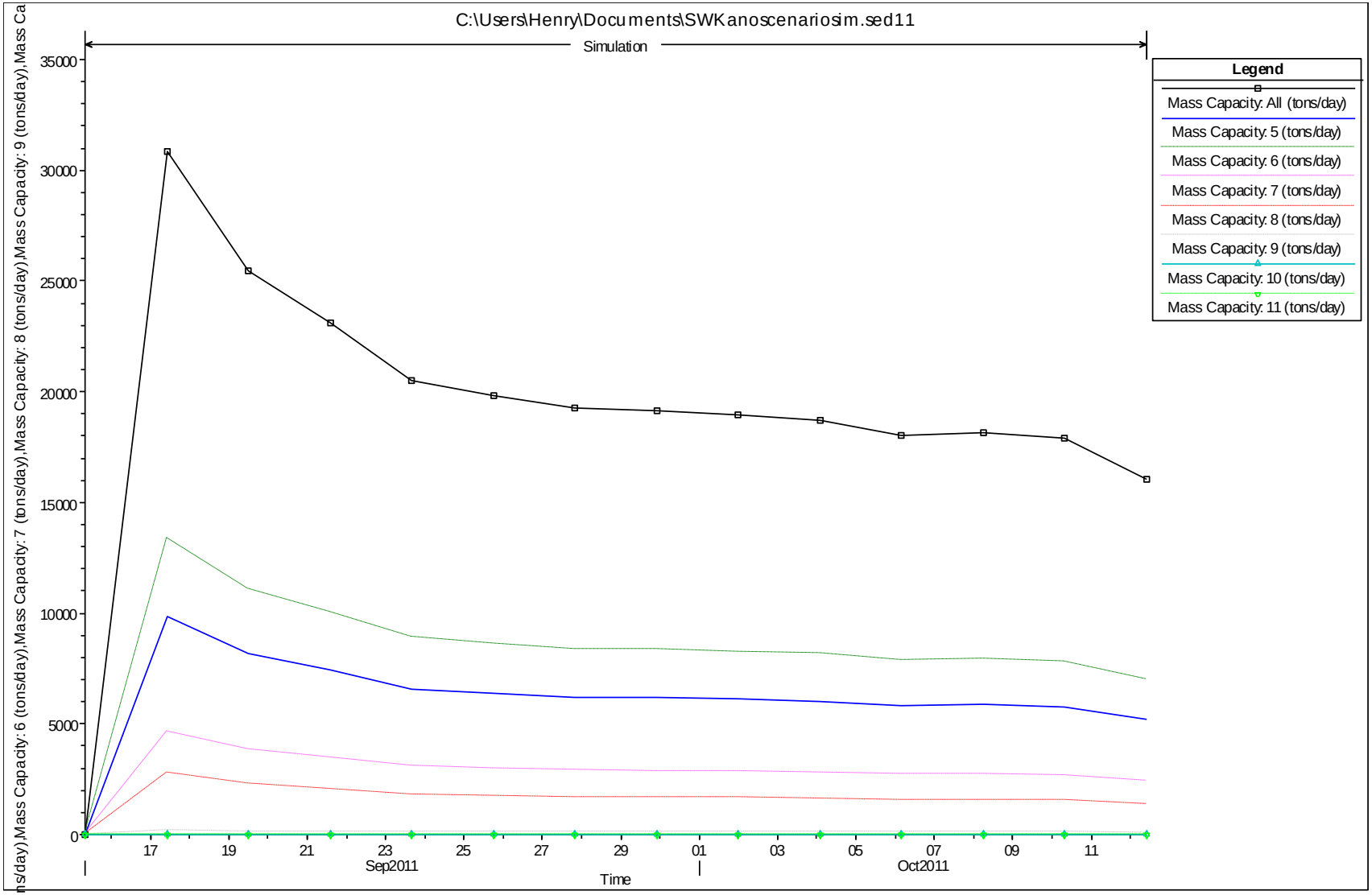

Appendix 26: Graph of simulated transport capacity for discharge of 2.674 m3/s at Manhole 1 (Mh1)

Appendix 27: Table of simulated transport capacity for discharge of 2.674 m3/s at Manhole 3 (Mh3)

	Time	Mass Capacity: All (tons/day)	Mass Capacity: 5 (tons/day)	Mass Capacity: 6 (tons/day)	Mass Capacity: 7 (tons/day)	Mass Capacity: 8 (tons/day)	Mass Capacity: 9 (tons/day)	Mass Capacity: 10 (tons/day)	Mass Capacity: 11 (tons/day)
1	9/15/2011 8:00	0	0	0	0	0	0	0	0
2	9/17/2011 10:00	28596.93	9539.08	12940.67	4482.76	1616.488	17.93199	0	0
3	9/19/2011 12:00	22327.56	7452.234	9858.26	3374.362	1618.112	24.59054	0	0
4	9/21/2011 14:00	17821.35	6027.505	7698.839	2647.537	1420.255	27.21429	0	0
5	9/23/2011 16:00	16549.7	5418.716	7106.711	2597.095	1393.123	34.05836	0	0
6	9/25/2011 18:00	15733.84	5216.688	6680.588	2362.634	1431.746	42.18105	0	0
7	9/27/2011 20:00	16562.94	5372.042	7154.663	2512.433	1471.323	52.47665	0	0
8	9/29/2011 22:00	16365.74	5321.351	7088.877	2465.05	1430.316	60.14898	0	0
9	10/2/2011 0:00	16247.67	5286.755	7017.174	2450.927	1424.292	68.52009	0	0
10	10/4/2011 2:00	15868.11	5194.451	6827.325	2368.737	1401.818	75.77477	0	0
11	10/6/2011 4:00	16264.48	5203.332	7112.711	2457.591	1406.426	84.42017	0	0
12	10/8/2011 6:00	16225.93	5214.941	7032.884	2491.07	1395.377	91.65812	0	0
13	10/10/2011 8:00	16090.4	5163.476	6956.55	2471.653	1399.992	98.73489	0	0
14	10/12/2011 10:00	16142.95	5062.063	7006.939	2512.032	1454.905	107.0124	0	0

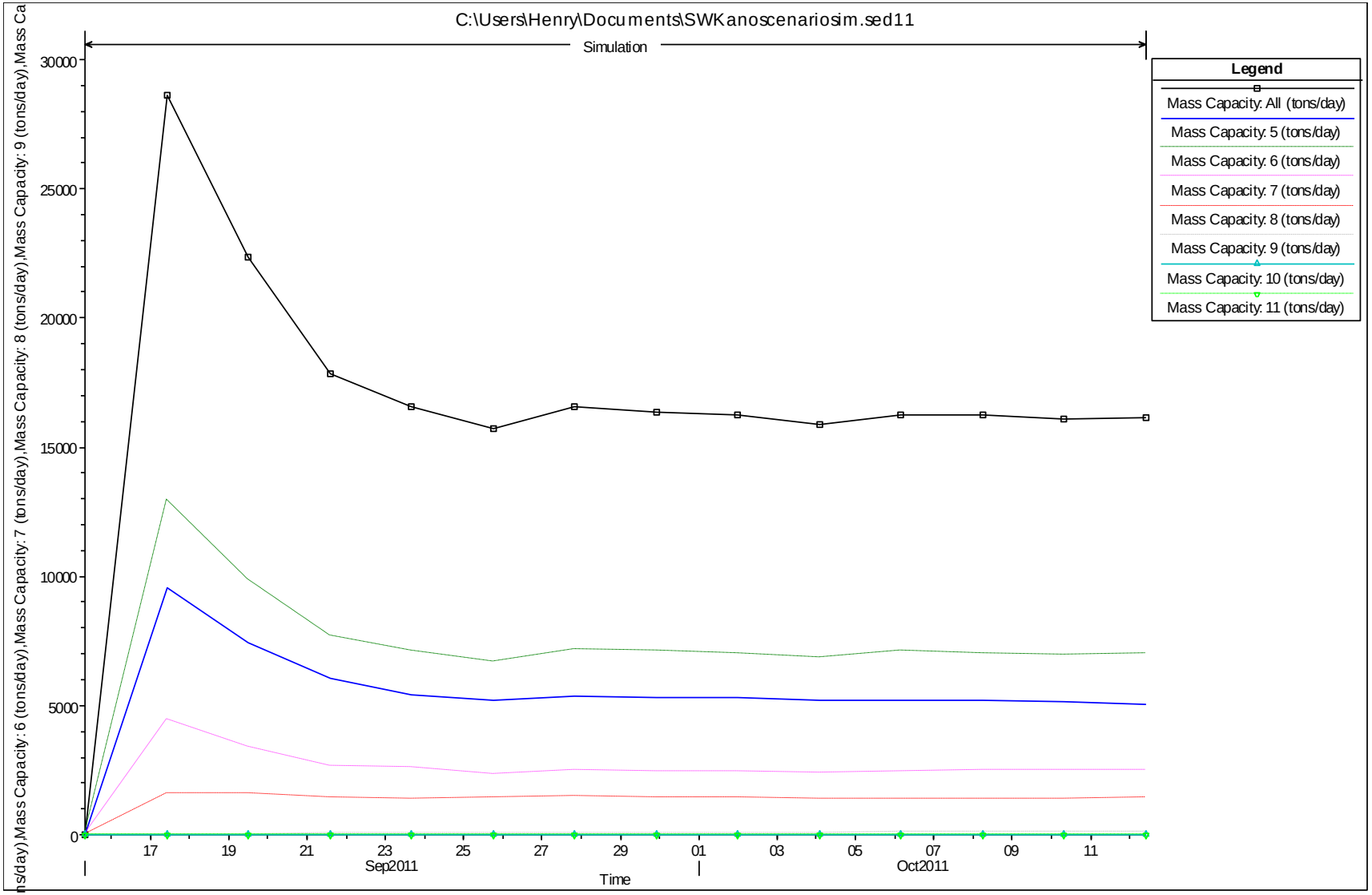

Appendix 28: Graph of simulated transport capacity for discharge of 2.674 m3/s at Manhole 3 (Mh3)

Appendix 29: Table of simulated transport capacity for discharge of 2.674 m3/s at Manhole 5 (Mh5)

	Time	Mass Capacity: All (tons/day)	Mass Capacity: 5 (tons/day)	Mass Capacity: 6 (tons/day)	Mass Capacity: 7 (tons/day)	Mass Capacity: 8 (tons/day)	Mass Capacity: 9 (tons/day)	Mass Capacity: 10 (tons/day)	Mass Capacity: 11 (tons/day)
1	9/15/2011 8:00	0	0	0	0	0	0	0	0
2	9/17/2011 10:00	451293.1	247645.4	173327.5	29976.69	310.2981	6.495492	26.12498	0.5818288
3	9/19/2011 12:00	424327.4	232533.4	162751.3	28147.7	861.3396	6.099262	27.01542	0.5463552
4	9/21/2011 14:00	390857.5	213685.8	149560.3	25866.45	1713.962	5.605011	24.8265	0.5020965
5	9/23/2011 16:00	390859.7	213686.9	149561.3	25866.63	1713.976	5.605068	24.82682	0.502105
6	9/25/2011 18:00	390858.1	213686.1	149560.6	25866.5	1713.966	5.605026	24.82659	0.5020987
7	9/27/2011 20:00	390859.2	213686.6	149561	25866.59	1713.973	5.605053	24.82674	0.5021028
8	9/29/2011 22:00	390860	213687.1	149561.4	25866.66	1713.978	5.605074	24.82685	0.502106
9	10/2/2011 0:00	390860.3	213687.2	149561.5	25866.69	1713.98	5.605083	24.8269	0.5021073
10	10/4/2011 2:00	390860.9	213687.5	149561.8	25866.73	1713.984	5.605099	24.82698	0.5021096
11	10/6/2011 4:00	390863.8	213689	149562.9	25866.97	1714.002	5.60517	24.82738	0.5021203
12	10/8/2011 6:00	390022	213226.7	149239.4	25811.02	1710.295	9.251351	24.77367	0.5010341
13	10/10/2011 8:00	389022.1	212677.7	148855.2	25744.57	1705.892	13.58459	24.70993	0.4997455
14	10/12/2011 10:00	390394.3	213280.8	149464.4	25886.71	1718.183	18.78194	25.02319	0.5089864

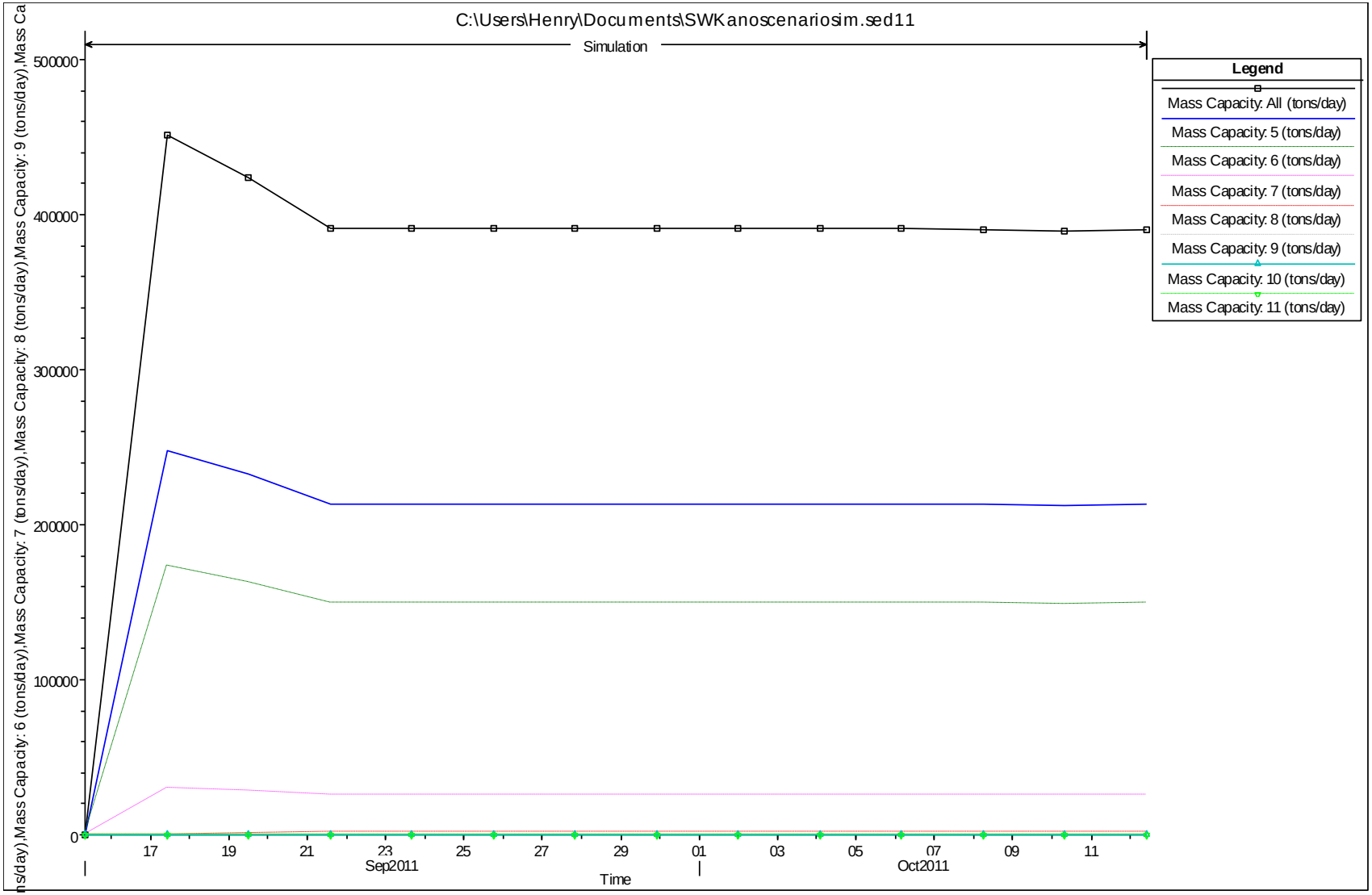

Appendix 30: Graph of simulated transport capacity for discharge of 2.674 m3/s at Manhole 5 (Mh5)

Appendix 31: Data Collected

V=kn + D
where D= current meter constant (0.025m/s)
n= prop. Rev/s
k=hydraulic pitch (0.30m)
v = flow velocity m/s

No.	Section		Distance (m)	Depth of flow (m)	Revolution /30s	Depth of deposit (m)	Water temp (deg C)	Velocity (m/s)	Sample Volume (cm^3)	Wt. of sediment (g)	Sediment flux kg/m^3	X-section area (m^2)	Discharge (m^3/s)	Water Discharge (m^3/s)	Average water discharge (m^3/s)	Sediment discharge (kg/s)	Total sediment discharge (kg/s)	TSS (ppm) or mg/lt	TQS (ppm) or mg/lt	TQS (ton/h)
1	1st Manhole	11.28 am	0.25	1.42	24	0.15	23	0.265	390	0.65	1.667	0.4849	0.128	0.585	0.711	0.214	0.879	1501.860	1839.779	4.70910
2		11.30 am	0.75	1.35	48			0.505	400	0.61	1.525	0.6592	0.333			0.508				
3		11.33 am	1.25	1.42	23			0.255	410	0.52	1.268	0.4849	0.124			0.157				
4	3rd Manhole	2.28 pm	0.25	1.06	65	0.44	23	0.675	275	0.71	2.582	0.4051	0.273	0.782		0.706	2.206	2819.796	3454.250	8.84150
5		2.31 pm	0.75	1.03	68			0.705	415	1.23	2.964	0.5164	0.364			1.079				
6		2.35 pm	1.25	1.06	34			0.365	430	1.25	2.907	0.3968	0.145			0.421				
7	5th Manhole	3.30 pm	0.25	0.99	43	0.47	23	0.455	275	0.73	2.655	0.3994	0.182	0.766		0.482	2.062	2691.736	3297.376	8.43996
8		3.31 pm	0.75	0.80	69			0.715	435	1.16	2.667	0.4175	0.299			0.796				
9		3.33 pm	1.25	0.92	71			0.735	445	1.22	2.742	0.3888	0.286			0.783				
10	1st Manhole	9.23 am	0.25	0.84	48	0.50	22	0.505	415	0.39	0.940	0.3598	0.182	0.490	0.507	0.171	0.415	845.778	1585.834	2.89446
11		9.28 am	0.75	0.68	52			0.545	260	0.20	0.769	0.3396	0.185			0.142				
12		9.31 am	1.25	0.48	50			0.525	450	0.37	0.822	0.2352	0.123			0.102				
13	3rd Manhole	10.09 am	0.25	0.82	40	0.45	22	0.425	440	0.35	0.795	0.3585	0.152	0.521		0.121	0.452	867.984	1627.470	2.97046
14		10.12 am	0.75	0.86	45			0.475	445	0.37	0.831	0.4223	0.201			0.167				
15		10.15 am	1.25	0.78	47			0.495	440	0.43	0.977	0.3397	0.168			0.164				
16	5th Manhole	11.00 am	0.25	0.74	47	0.43	22	0.495	425	0.57	1.341	0.3357	0.166	0.510		0.223	0.514	1006.997	1233.571	2.25151
17		11.02 am	0.75	0.69	52			0.545	310	0.26	0.839	0.3483	0.190			0.159				
18		11.04 am	1.25	0.67	47			0.495	445	0.38	0.854	0.3113	0.154			0.132				
19	1st Manhole	12.45 pm	0.25	0.80	53	0.60	22	0.555	375	0.25	0.667	0.3352	0.186	0.494	0.499	0.124	0.330	667.121	1250.851	2.24703
20		12.48 pm	0.75	0.58	61			0.635	365	0.25	0.685	0.3006	0.191			0.131				
21		12.52 pm	1.25	0.40	51			0.535	360	0.23	0.639	0.2195	0.117			0.075				
22	3rd Manhole	1.35 pm	0.25	0.78	52	0.45	22	0.545	435	0.27	0.621	0.3515	0.192	0.557		0.119	0.391	703.203	1318.506	2.36856
23		1.40 pm	0.75	0.77	61			0.635	445	0.34	0.764	0.3844	0.244			0.186				
24		1.41 pm	1.25	0.75	33			0.355	450	0.32	0.711	0.3405	0.121			0.086				

25	5th Manhole	2.10 pm	0.25	0.72	47	0.57	22	0.495	440	0.30	0.682	0.3157	0.156	0.446		0.107	0.263	589.943	1106.143	1.98707
26		2.12 pm	0.75	0.64	47			0.495	285	0.15	0.526	0.3275	0.162			0.085				
27		2.15 pm	1.25	0.68	40			0.425	430	0.24	0.558	0.2991	0.127			0.071				
28	1st Manhole	11.09 am	0.25	0.58	37	0.49	25	0.395	455	0.10	0.220	0.2624	0.104	0.302	0.445	0.023	0.080	266.198	499.122	0.79959
29		11.12 am	0.75	0.50	40			0.425	450	0.13	0.289	0.2475	0.105			0.030				
30		11.19 am	1.25	0.38	48			0.505	445	0.13	0.292	0.1851	0.093			0.027				
31	3rd Manhole	12.02 pm	0.25	0.60	33	0.45	25	0.355	430	0.13	0.302	0.2840	0.101	0.336		0.030	0.105	310.887	582.913	0.93383
32		12.07 pm	0.75	0.60	37			0.395	440	0.11	0.250	0.3025	0.119			0.030				
33		12.10 pm	1.25	0.61	38			0.405	420	0.16	0.381	0.2868	0.116			0.044				
34	5th Manhole	12.59 pm	0.25	0.80	58	0.57	26	0.605	450	0.44	0.978	0.2904	0.176	0.697		0.172	0.605	867.856	1627.230	2.60682
35		1.02 pm	0.75	0.90	72			0.745	430	0.37	0.860	0.4370	0.326			0.280				
36		1.07 pm	1.25	0.80	65			0.675	435	0.34	0.782	0.2904	0.196			0.153				
37	1st Manhole	1.47 pm	0.25	0.97	47	0.52	26	0.495	435	0.19	0.437	0.3880	0.192	0.654	0.590	0.084	0.221	338.119	633.973	1.34656
38		1.55 pm	0.75	0.87	61			0.635	430	0.13	0.302	0.4345	0.276			0.083				
39		2.01 pm	1.25	0.76	58			0.605	380	0.11	0.289	0.3083	0.187			0.054				
40	3rd Manhole	2.25 pm	0.25	0.79	40	0.41	26	0.425	430	0.14	0.326	0.3571	0.152	0.547		0.049	0.281	513.857	963.481	2.04643
41		2.28 pm	0.75	0.82	57			0.595	430	0.14	0.326	0.4033	0.240			0.078				
42		2.32 pm	1.25	0.75	43			0.455	425	0.42	0.988	0.3417	0.155			0.154				
43	5th Manhole	3.00 pm	0.25	0.83	55	0.52	27	0.575	420	0.18	0.429	0.3550	0.204	0.568		0.087	0.243	428.314	803.089	1.70576
44		3.02 pm	0.75	0.67	55			0.575	370	0.19	0.514	0.3456	0.199			0.102				
45		3.04 pm	1.25	0.68	51			0.535	430	0.14	0.326	0.3090	0.165			0.054				

Appendix 32: Publication

Simulation of Sediment Transport in the Canal Using the HEC-RAS (Hydrologic Engineering Centre - River Analysis System) in an Underground Canal in Southwest Kano Irrigation Scheme – Kenya. International Journal of Engineering Science Invention, Volume 4, Issue 9, September 2015, PP.15-31